Yale University
Feb. 17, 2011

Satellite Estimation of Land Surface Radiation and Energy Budgets

Dr. Shunlin Liang, Professor
Department of Geography
301-405-4556, sliang@umd.edu
http://www.glue.umd.edu/~sliang

Energy budget

$R_n = H + ET + G$

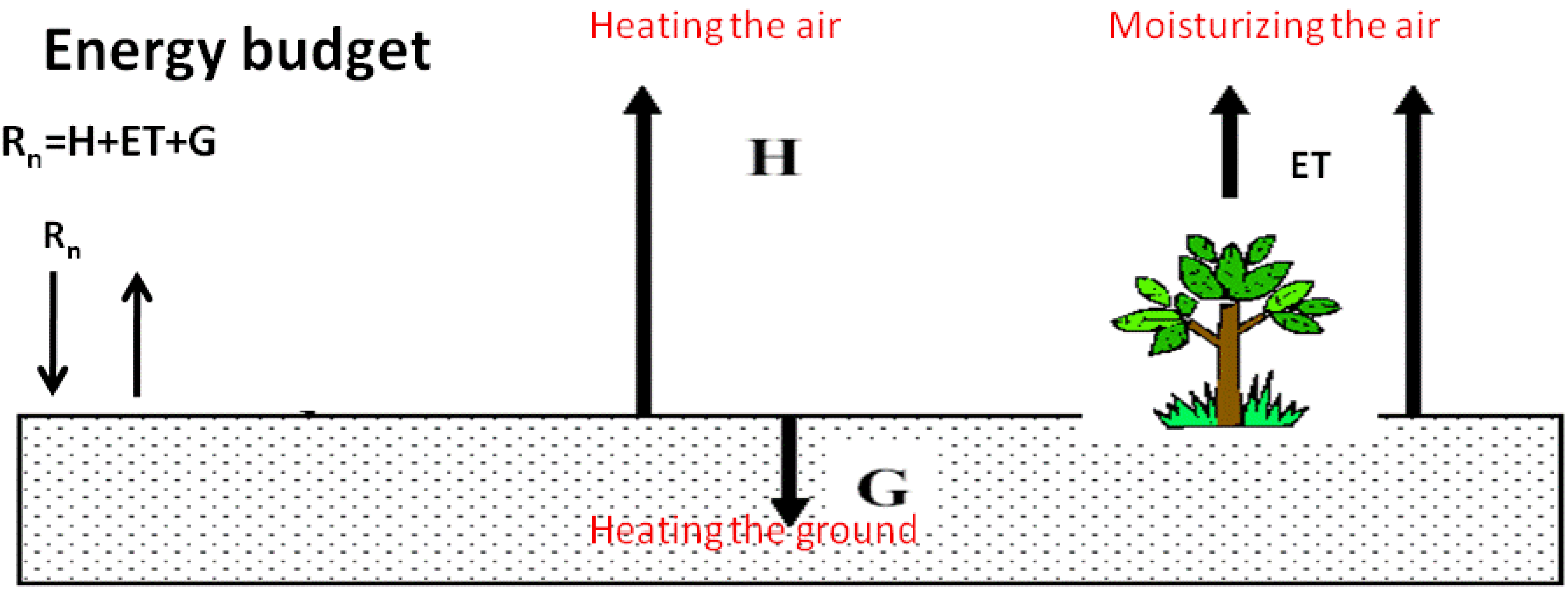

$$R_n = R_n^s + R_n^l = (1-\alpha)F_d^s + \varepsilon F_d^l - \sigma\varepsilon T^4$$

Net radiation

albedo

Insolation

Emissivity

Longwave downward radiation

Skin temperature

Radiation budget

Outlines

- Background
- Insolation/PAR
- Albedo
- Longwave net radiation
- Evapotranpiration
- Summary

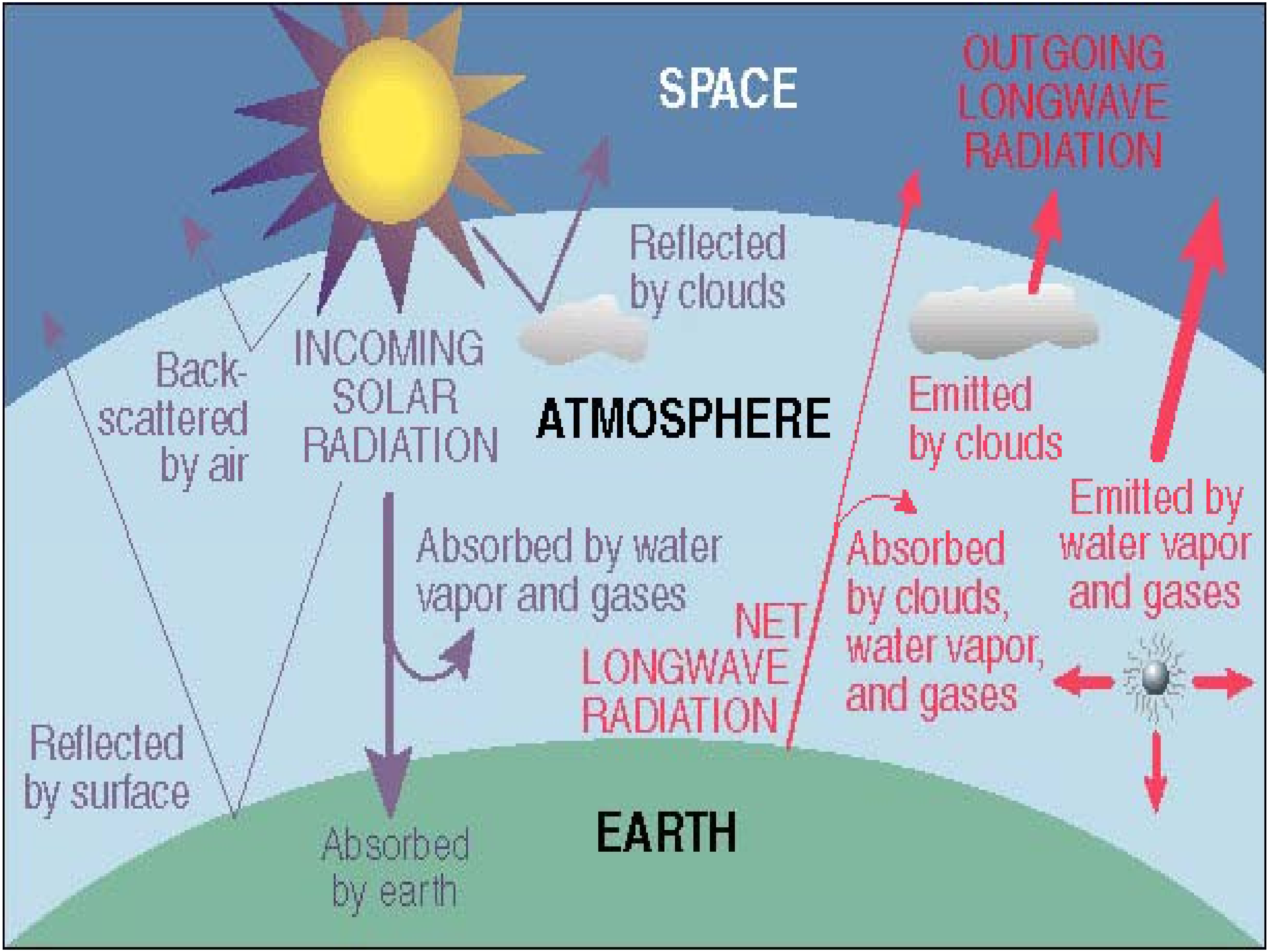
SPACE
OUTGOING LONGWAVE RADIATION
Reflected by clouds
Back-scattered by air
INCOMING SOLAR RADIATION
ATMOSPHERE
Emitted by clouds
Emitted by water vapor and gases
Absorbed by water vapor and gases
NET LONGWAVE RADIATION
Absorbed by clouds, water vapor, and gases
Reflected by surface
EARTH
Absorbed by earth

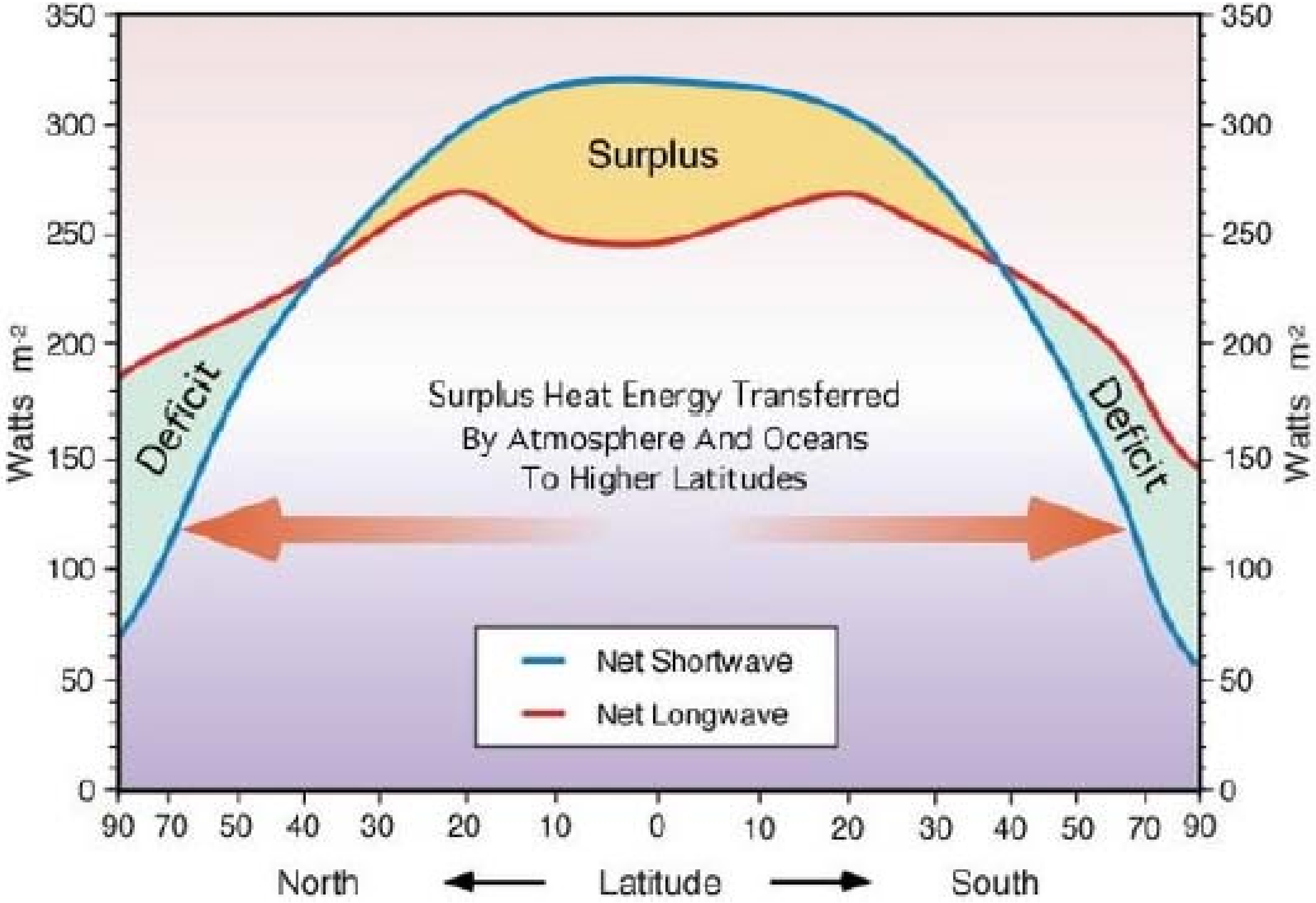

350
300
250
200
150
100
50
0
Watts m-2
Surplus
Deficit
Deficit
Surplus Heat Energy Transferred
By Atmosphere And Oceans
To Higher Latitudes
Net Shortwave
Net Longwave
90 70 50 40 30 20 10 0 10 20 30 40 50 70 90
North
Latitude
South

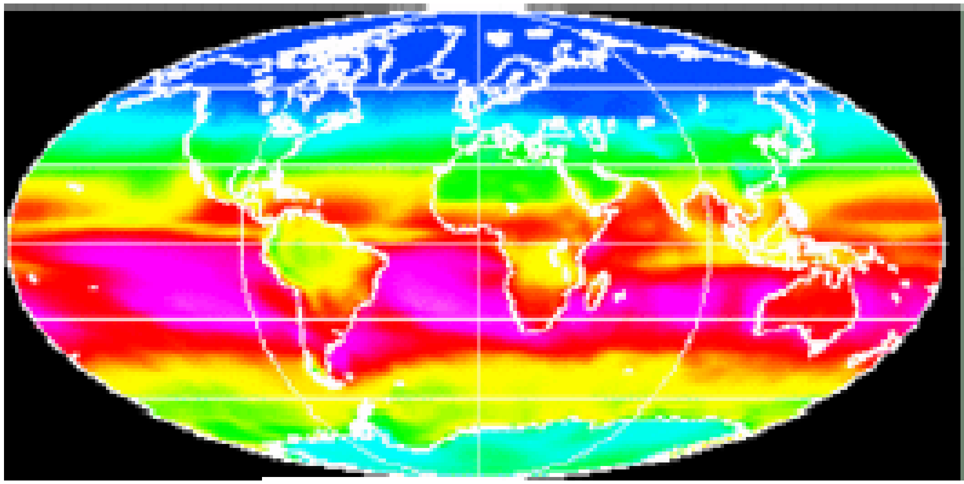

Average Net Shortwave Radiation at the Earth's Surface:
January 1984-1991 (K)

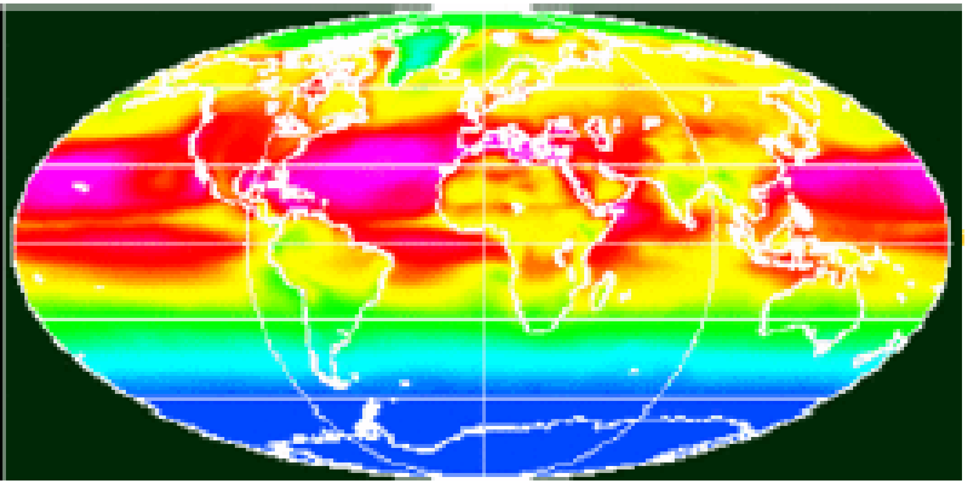

Average Net Shortwave Radiation at the Earth's Surface:
July 1984-1991 (K)

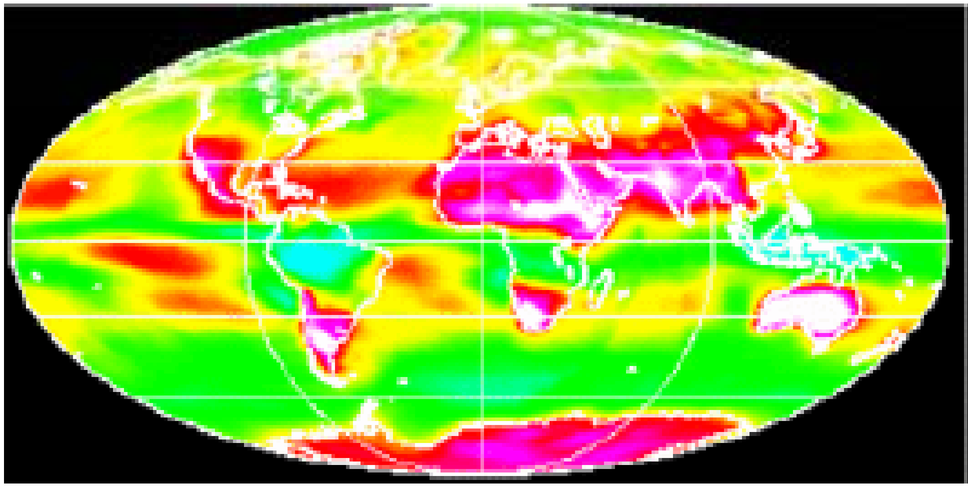

Average Net longwave Radiation at the Earth's Surface:
January 1984-1991 (K)

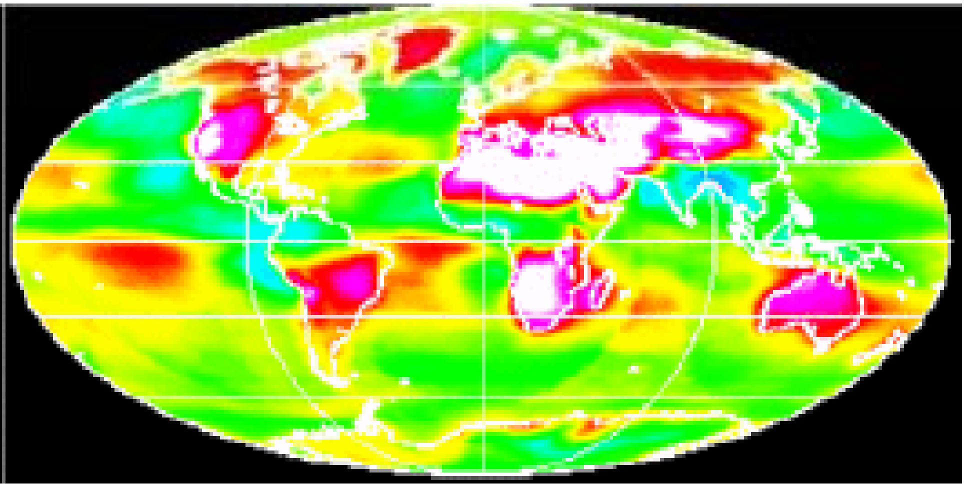

Average Net longwave Radiation at the Earth's Surface:
July 1983-1990 (K)

radiation and energy budgets in the climate models

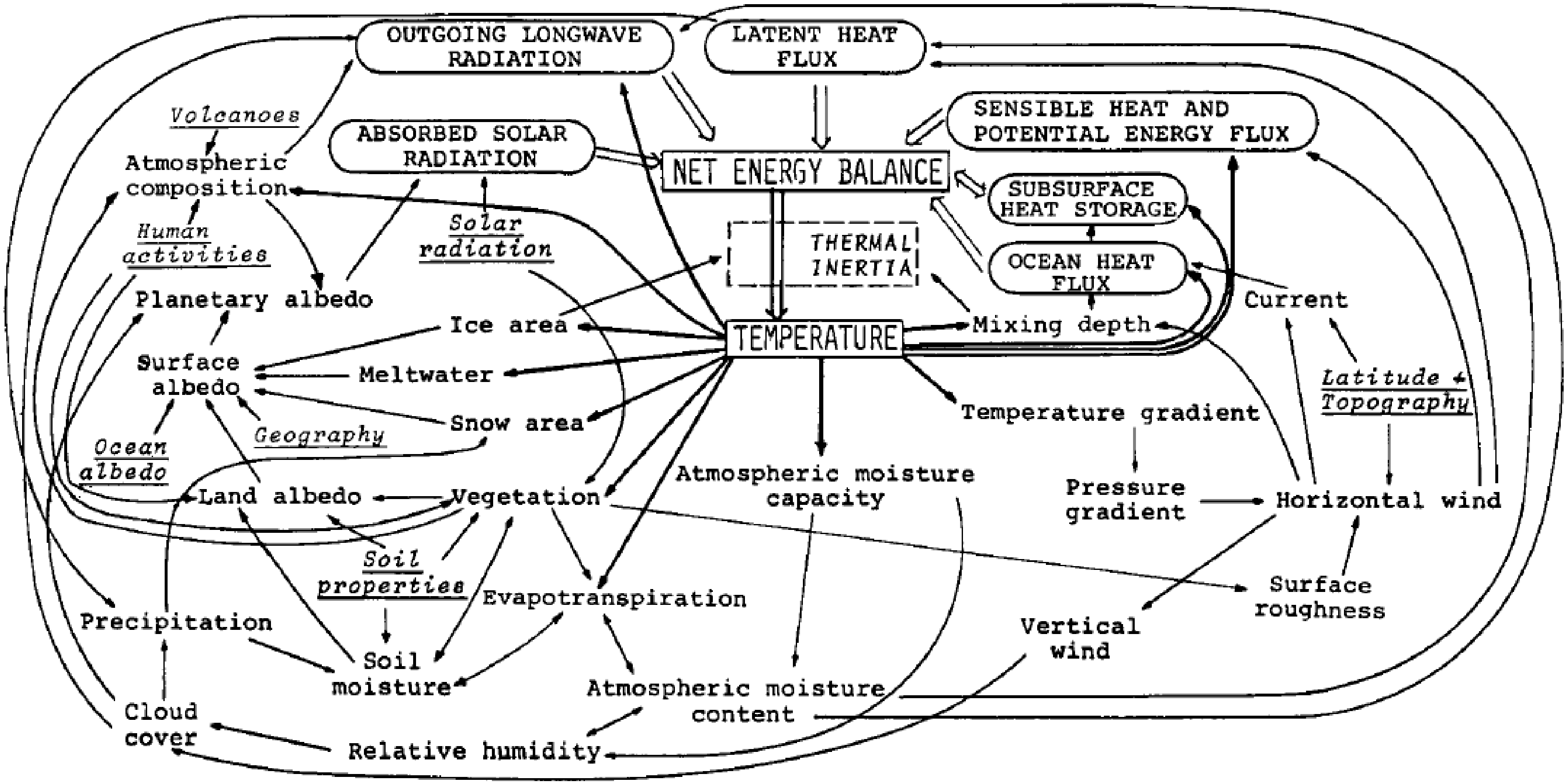

FIG. 1. Climate feedback diagram.

(Robock, 1985)

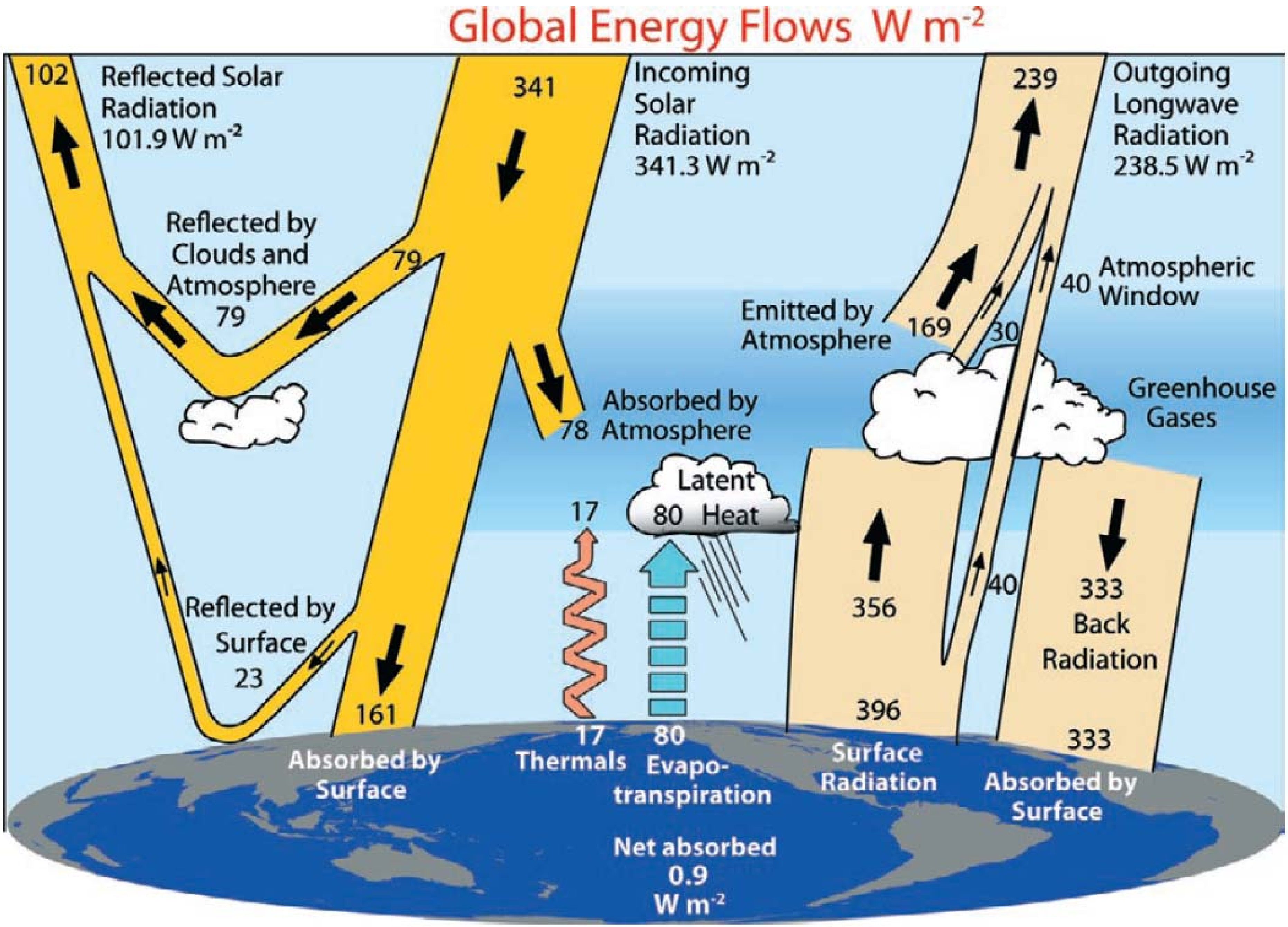

Trenberth et al. (2009)

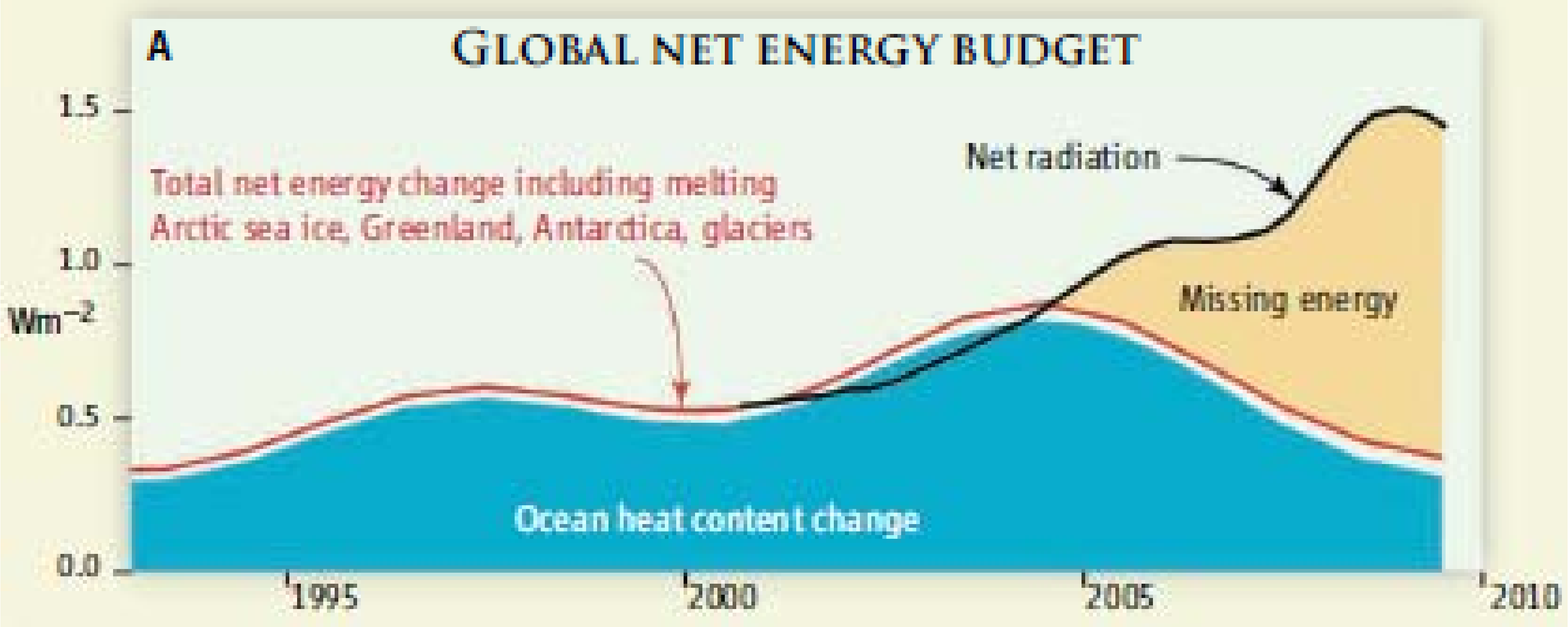

Trenberth , Science, 2010

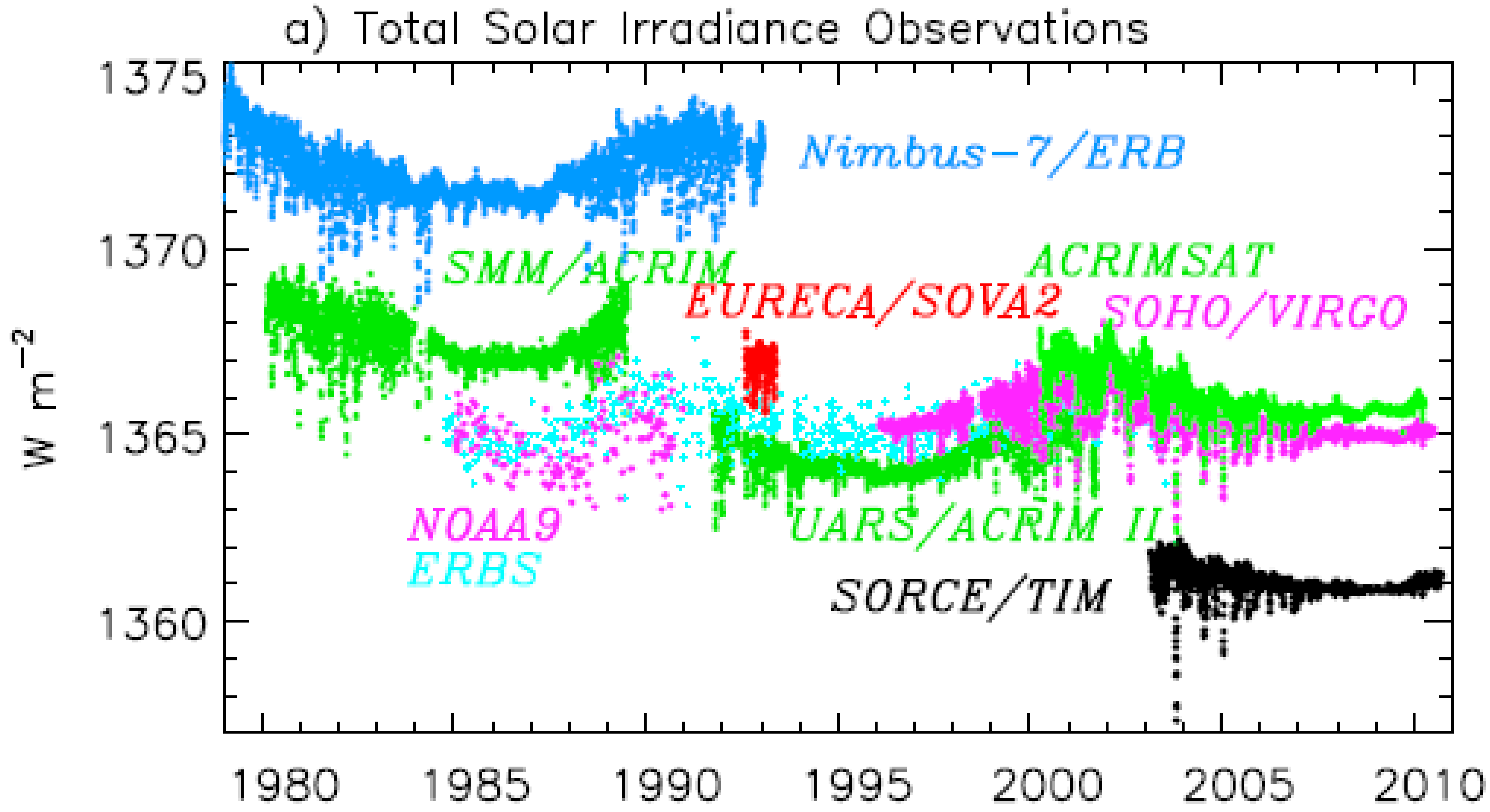

Figure Space-borne total solar irradiance (TSI) measurements are shown on "native" scales with offsets attributable to calibration errors. Instrument overlap allows corrections for offsets and the creation of a composite TSI record.

Kopp & Lean, 2011

TABLE 1. Global mean clear- and all-sky SW, LW, and net TOA radiative fluxes, solar irradiance, and CRE for satellite-based data products (units in W m^{-2}).

		CERES				
Product name	ERBE S-4	ES-4 Ed2_rev1	SRBAVG-nonGEO Ed2D_rev1	SRBAVG-GEO Ed2D_rev1	GEWEX SRB Version 2.86	ISCCP FD
Time period	02/85 – 01/89			03/00 – 02/2005		
Solar irradiance	341.3	341.3	341.3	341.3	341.8	341.5
LW (All sky)	235.2	239.0	237.7	237.1	240.4	235.8
SW (All Sky)	101.2	98.3	96.6	97.7	101.7	105.2
Net (All Sky)	4.9	4.0	7.0	6.5	−0.3	0.5
LW (Clear Sky)	264.9	266.6	266.4	264.1	268.1	262.3
SW (Clear Sky)	53.6	49.3	51.2	51.1	54.5	54.2
Net (Clear Sky)	22.8	25.4	23.7	26.2	19.2	25.0
LW CRE	29.7	27.6	28.7	27.0	27.7	26.5
SW CRE	−47.6	−49.0	−45.4	−46.6	−47.2	−51.0
NET CRE	−17.9	−21.4	−16.7	−19.7	−19.5	−24.5

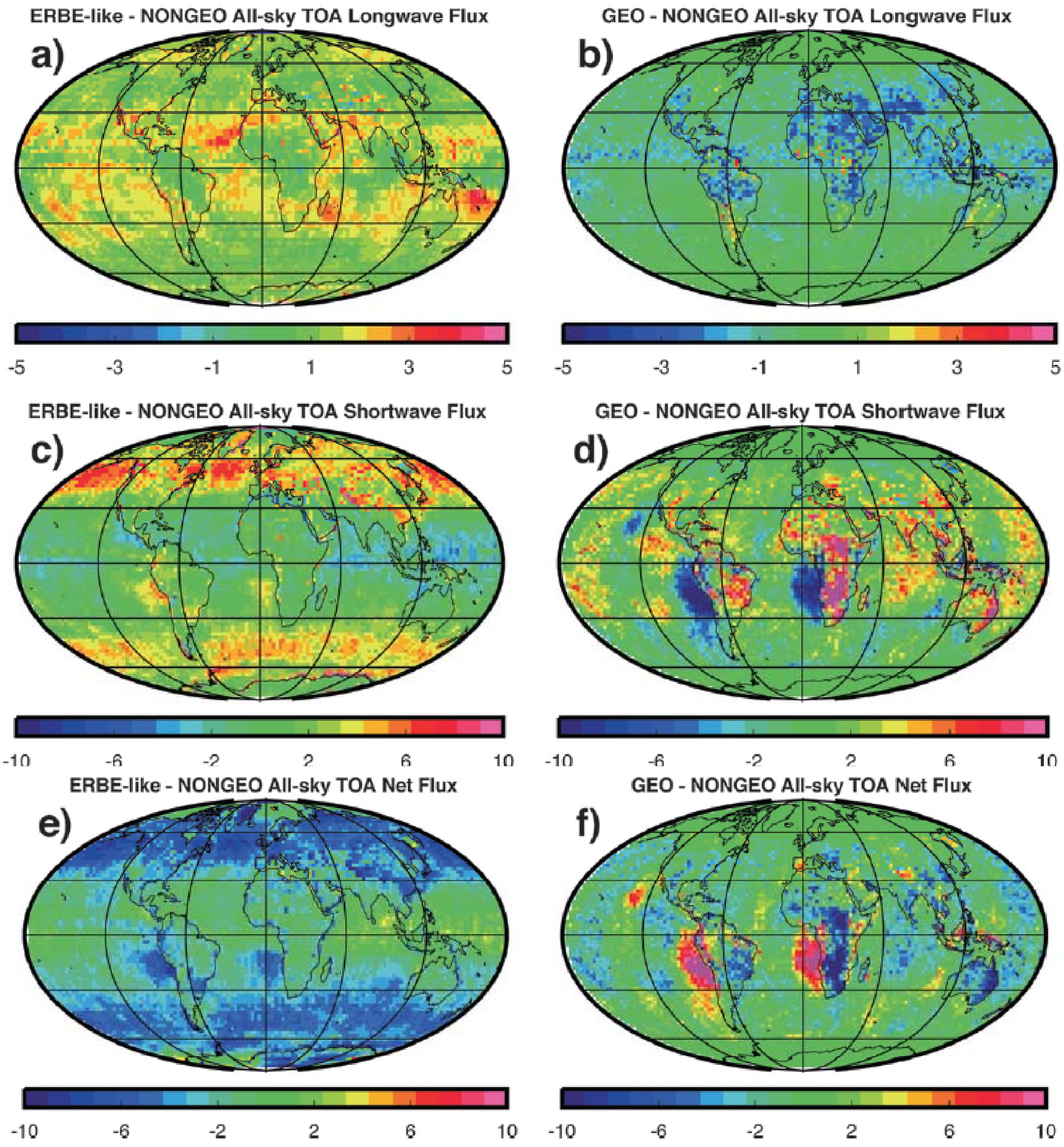

FIG. 1. Annual mean TOA flux difference between (left) CERES ERBE-like and CERES SRBAVG-nonGEO and (right) CERES SRBAVG-nonGEO and SRBAVG-GEO for (a), (b) LW; (c), (d) SW; and (e), (f) net for the year 2002.

Outlines

- Background
- Insolation/PAR
- Albedo
- Longwave net radiation
- Evapotranpiration
- Summary

Production Efficiency Principles:

$$GPP = \varepsilon_g \bullet fPAR \bullet PAR$$

$$NPP = \varepsilon_n \bullet fPAR \bullet PAR$$

where PAR (MJ m-2) is in a time period (day, month), FAPAR is the fraction of PAR absorbed by vegetation canopy, and ε_g is the light use efficiency (LUE, g C MJ-1 PAR) in GPP calculation, and is ε_n the light use efficiency in NPP calculation.

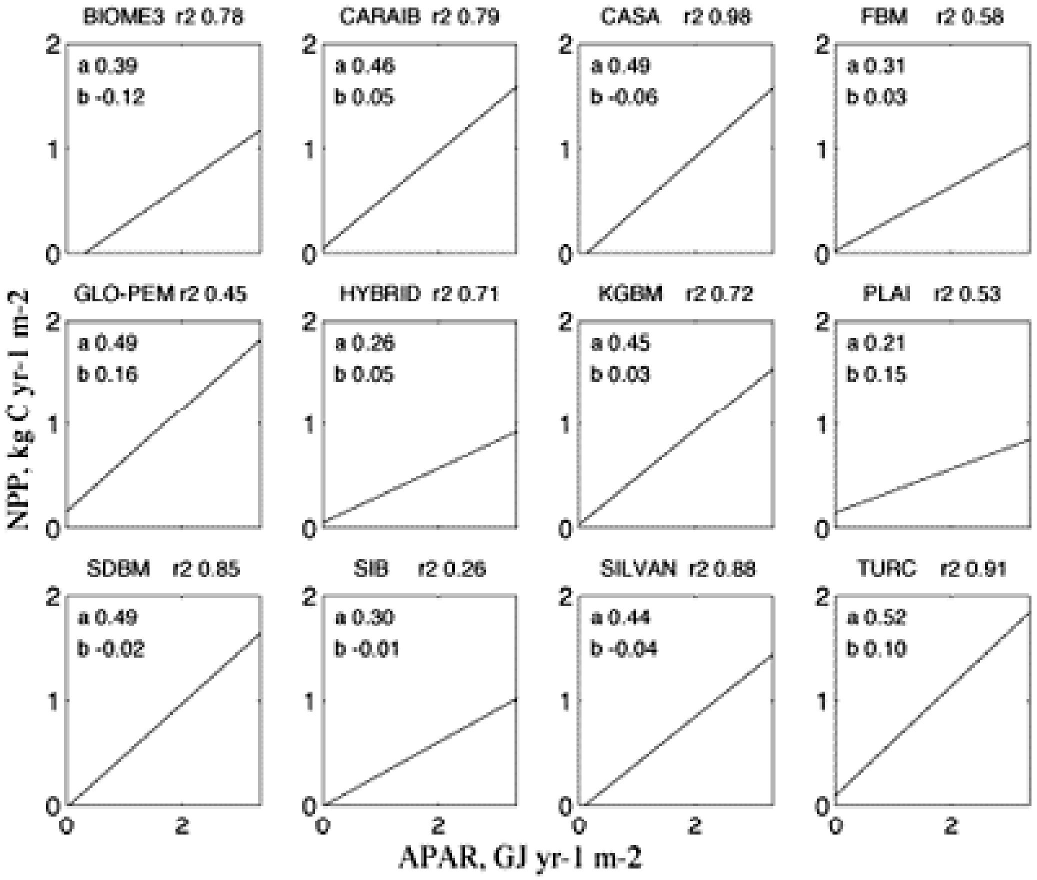

Grid cell level regression of net primary production (NPP) (kg C yr -1 m-2) against absorbed photosynthetically active radiation (APAR) (GJ yr -1 m-2)

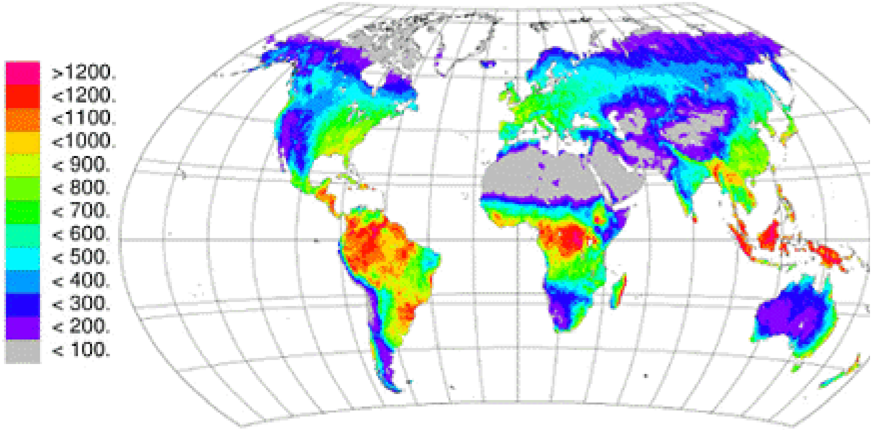

Annual net primary production (g C m -2 yr-1) estimated as the average of all model NPP estimates.

Cramer, et al., 1995, Net primary productivity model inter-comparison activity, IGBP/GAIM report series 5

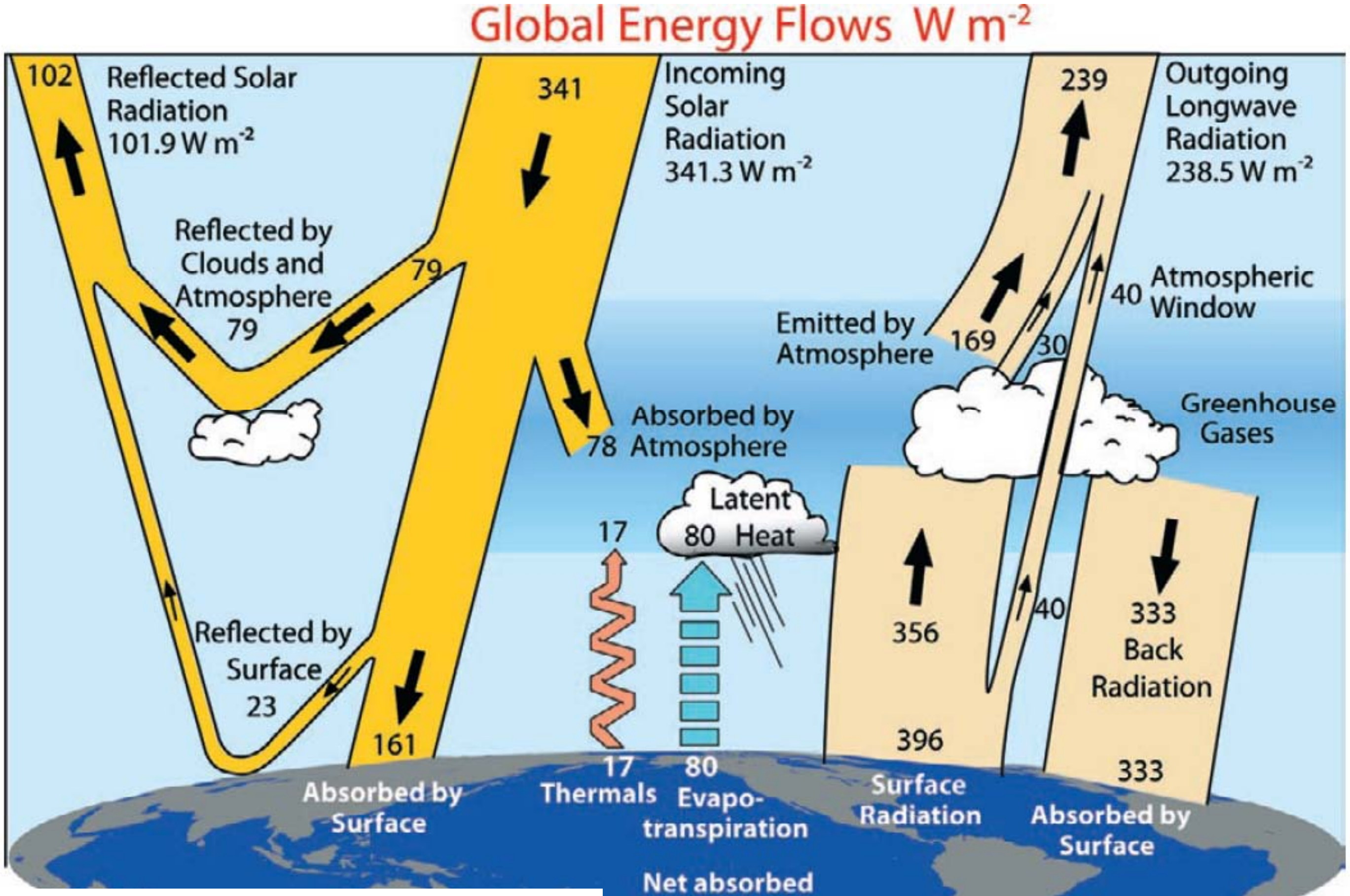

Model range: 24
Standard dev.: 5.5

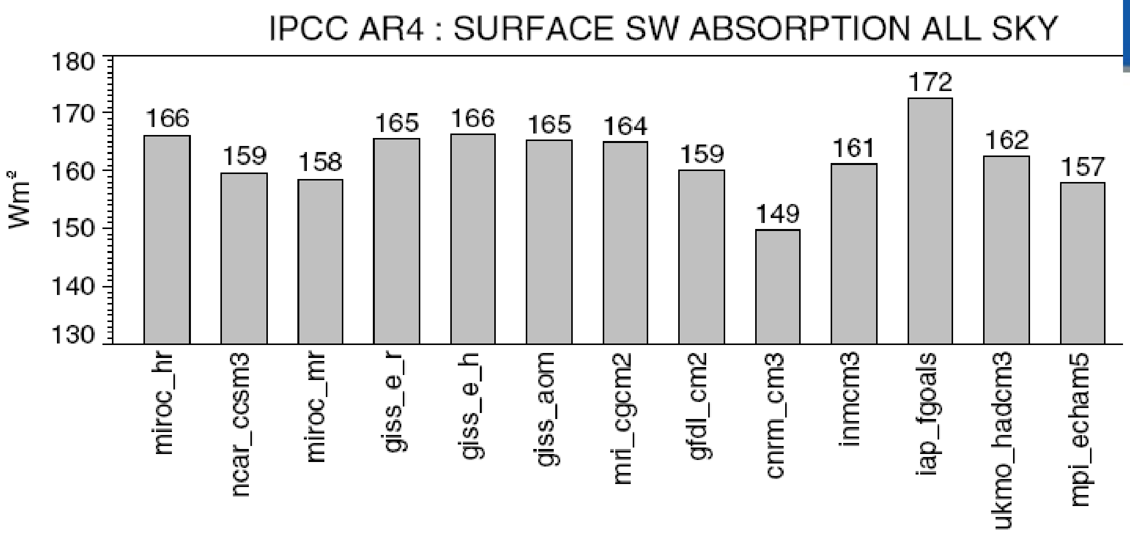

Radiation budgets in IPCC AR4 GCMs

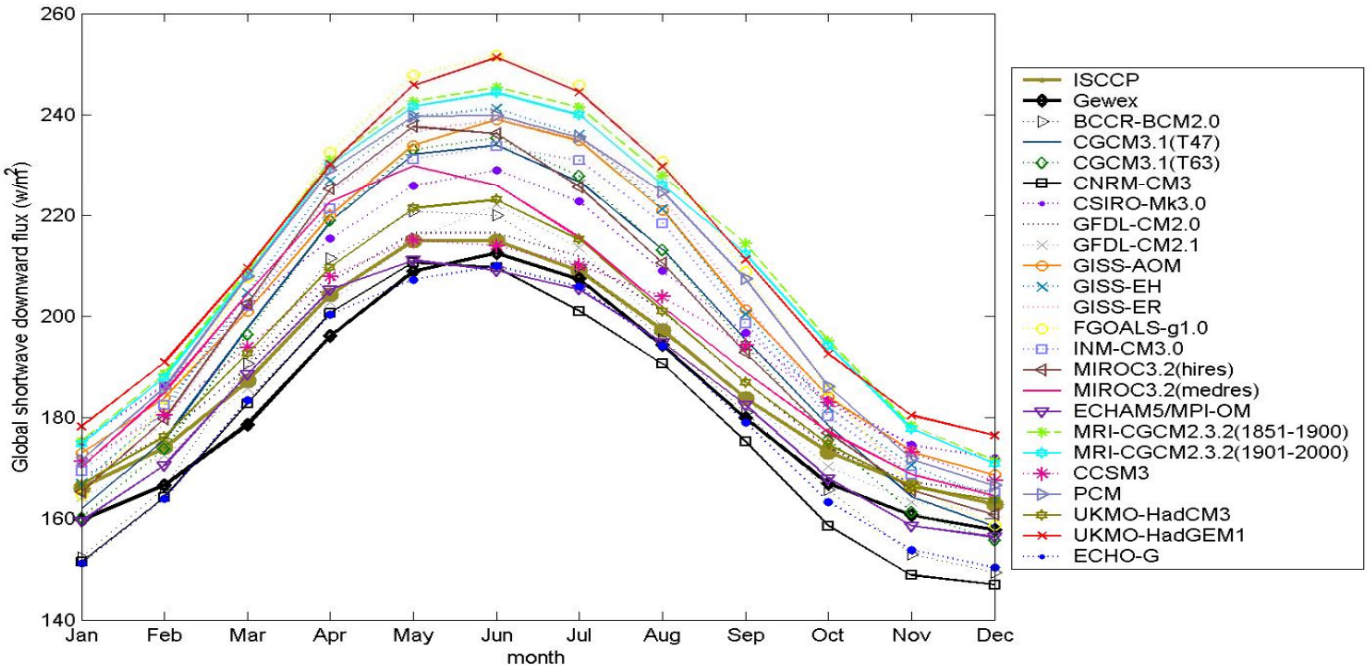

IPCC AR4 GCM model simulations and two satellite products

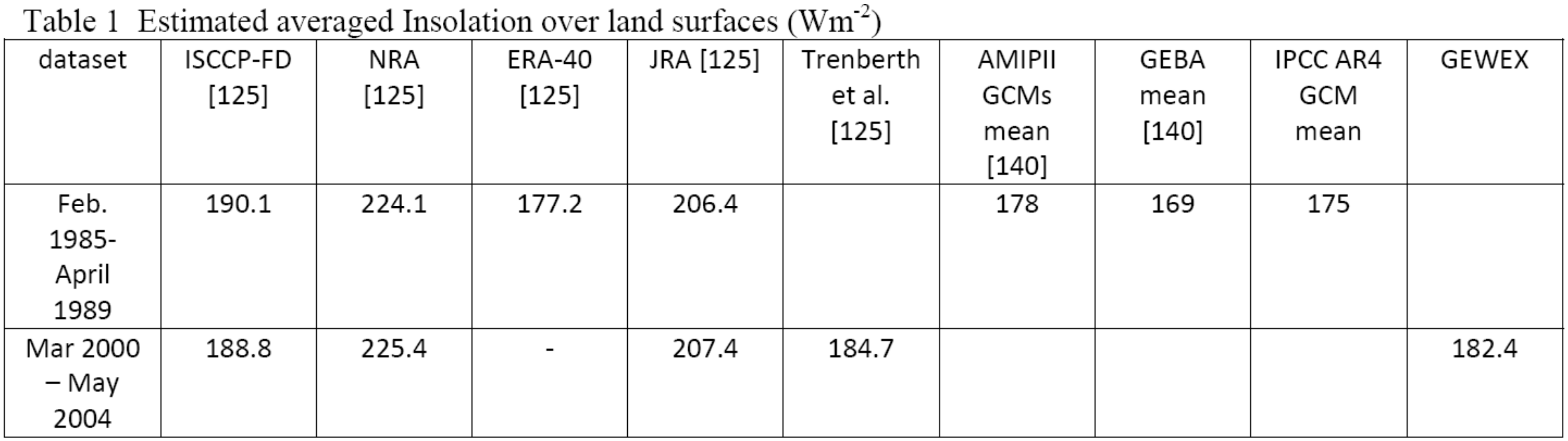

Table 1 Estimated averaged Insolation over land surfaces (Wm^{-2})

dataset	ISCCP-FD [125]	NRA [125]	ERA-40 [125]	JRA [125]	Trenberth et al. [125]	AMIPII GCMs mean [140]	GEBA mean [140]	IPCC AR4 GCM mean	GEWEX
Feb. 1985-April 1989	190.1	224.1	177.2	206.4		178	169	175	
Mar 2000 – May 2004	188.8	225.4	-	207.4	184.7				182.4

Liang, et al., *IEEE JSTARS*, 2010

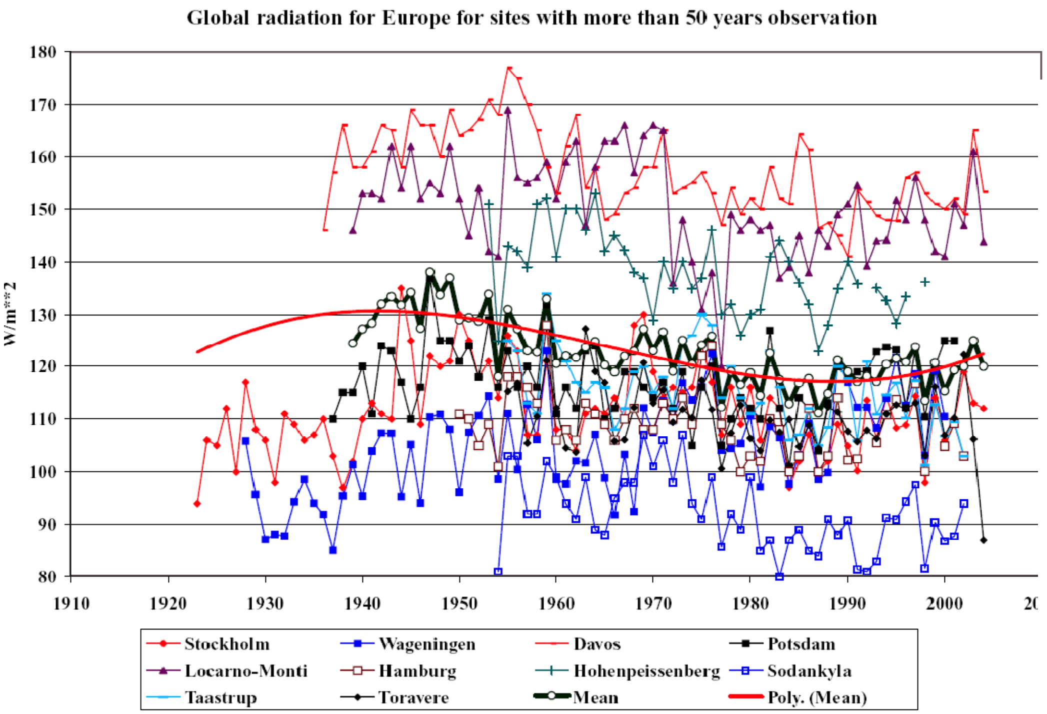
Global radiation for Europe for sites with more than 50 years observation

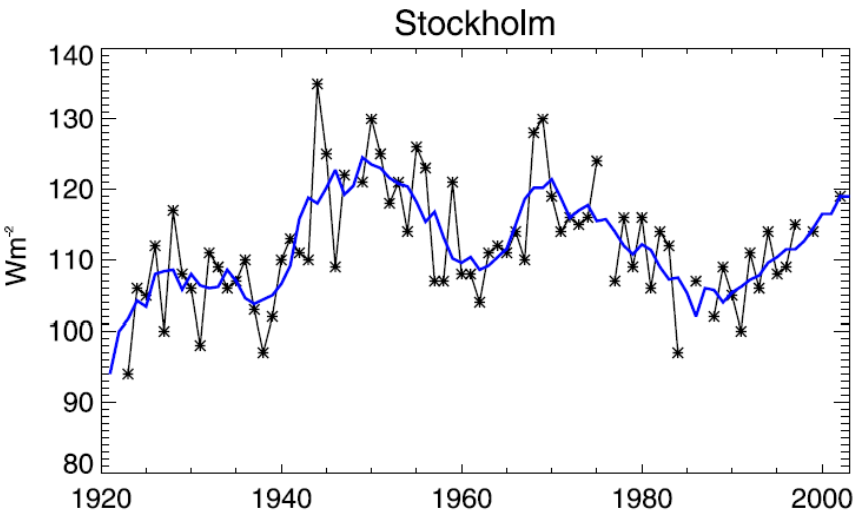
Stockholm

“**global dimming**” **:**Substantial decline in solar radiation the surface

“**global brightening**”**:**Substantial increase in solar radiation the surface

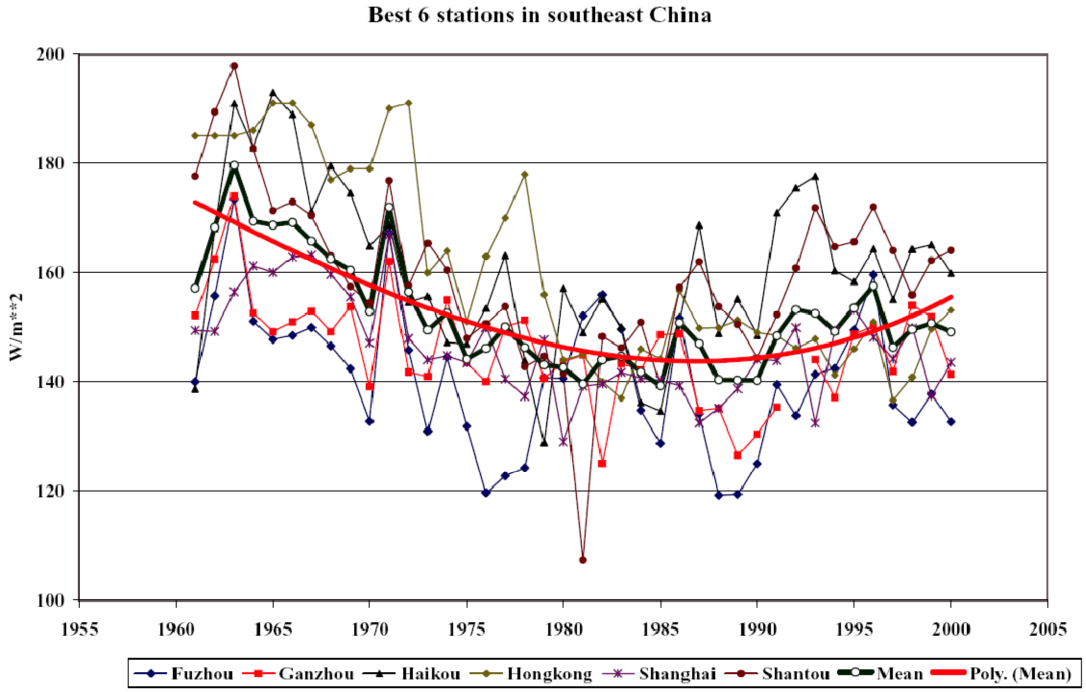
Best 6 stations in southeast China

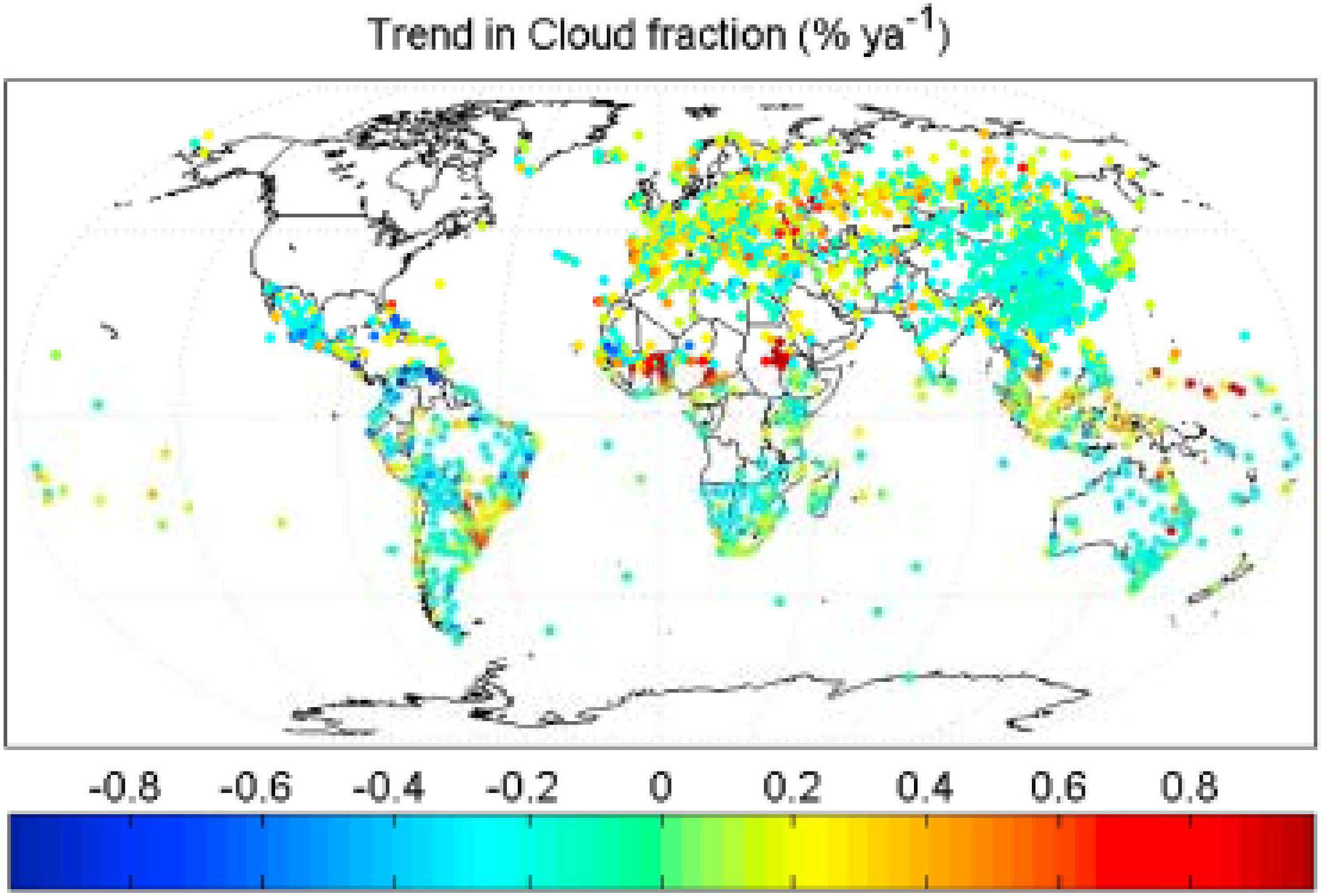

Figure 6. Linear trend of daily total cloud coverage from 1973 to 2008. The monthly total cloud cover fraction anomaly is derived and used to calculate the linear trend using the Mann-Kendall trend test method, and only stations that pass the 95% significance level in the Mann-Kendall trend test are shown. Some sites over North America and some European countries changed the observational method from human visual observations to instrument observations during the 1990s and are excluded because they show obvious discontinuities in total cloud coverage.

Wang, et al., 2010

Wang, K., R. Dickinson and **S. Liang**, (2009), Clear sky visibility has decreased over land globally from 1973 to 2007,*Science*, 323, 1468-1470

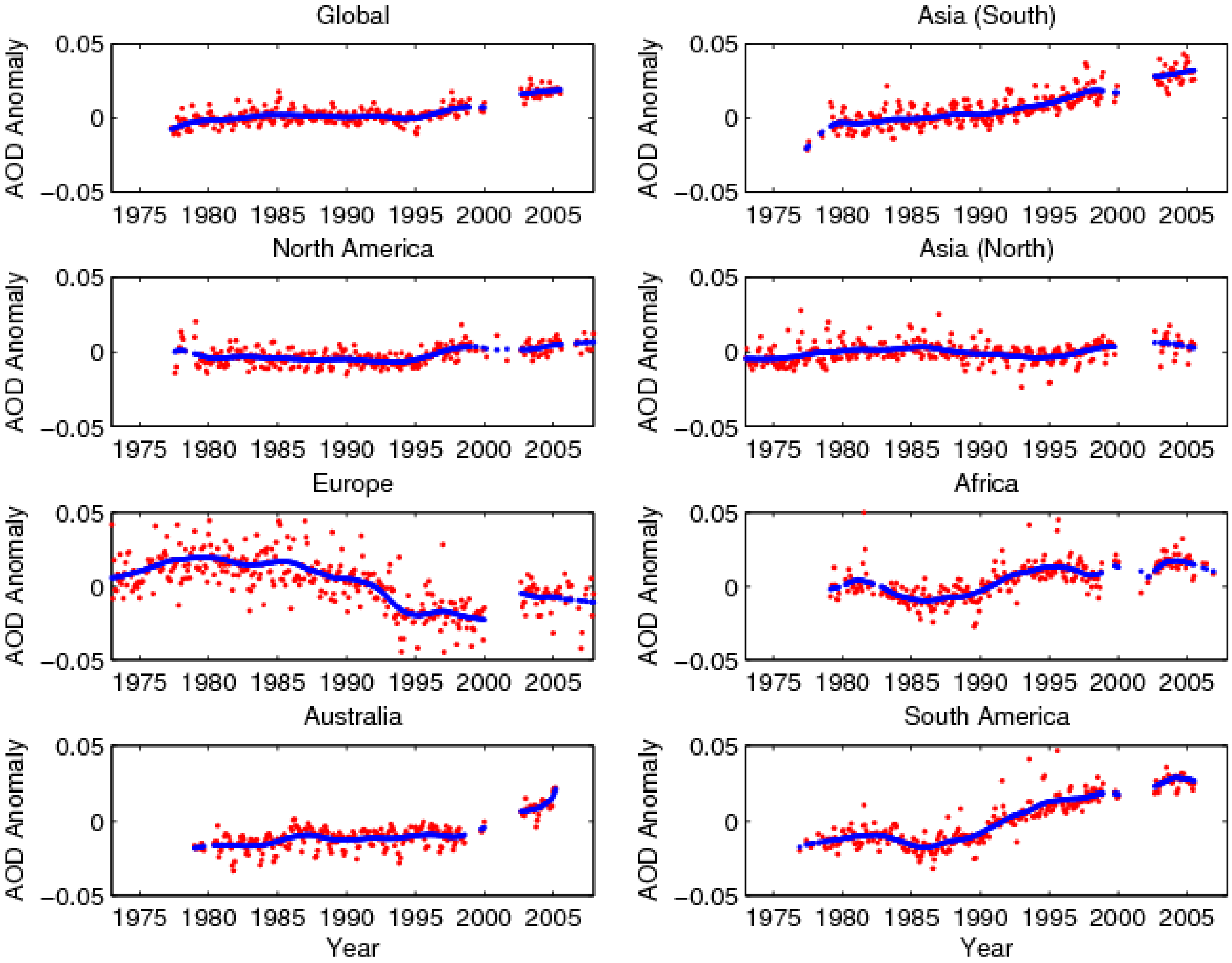

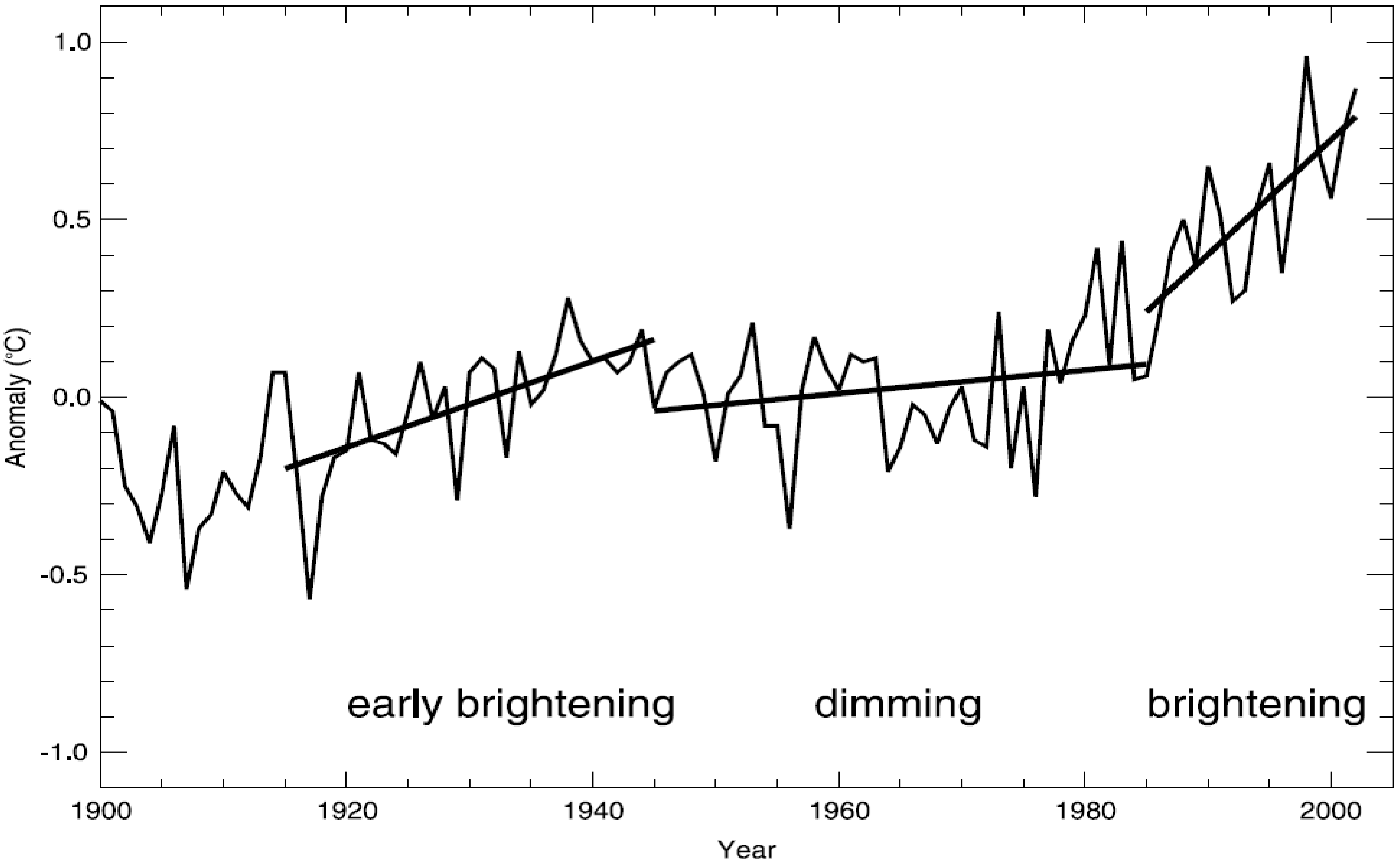

Figure 9. Observed 2-m temperature anomalies over global land surfaces during the 20th century. There is indication for a suppression of greenhouse-induced warming through "global dimming" between the 1950s and 1980s, and an enhancement through "brightening" between the 1920s and 1940s as well as from the 1980s onward. Anomalies with respect to the 20th century average. Units are °C. Adapted from *Wild et al.* [2007].

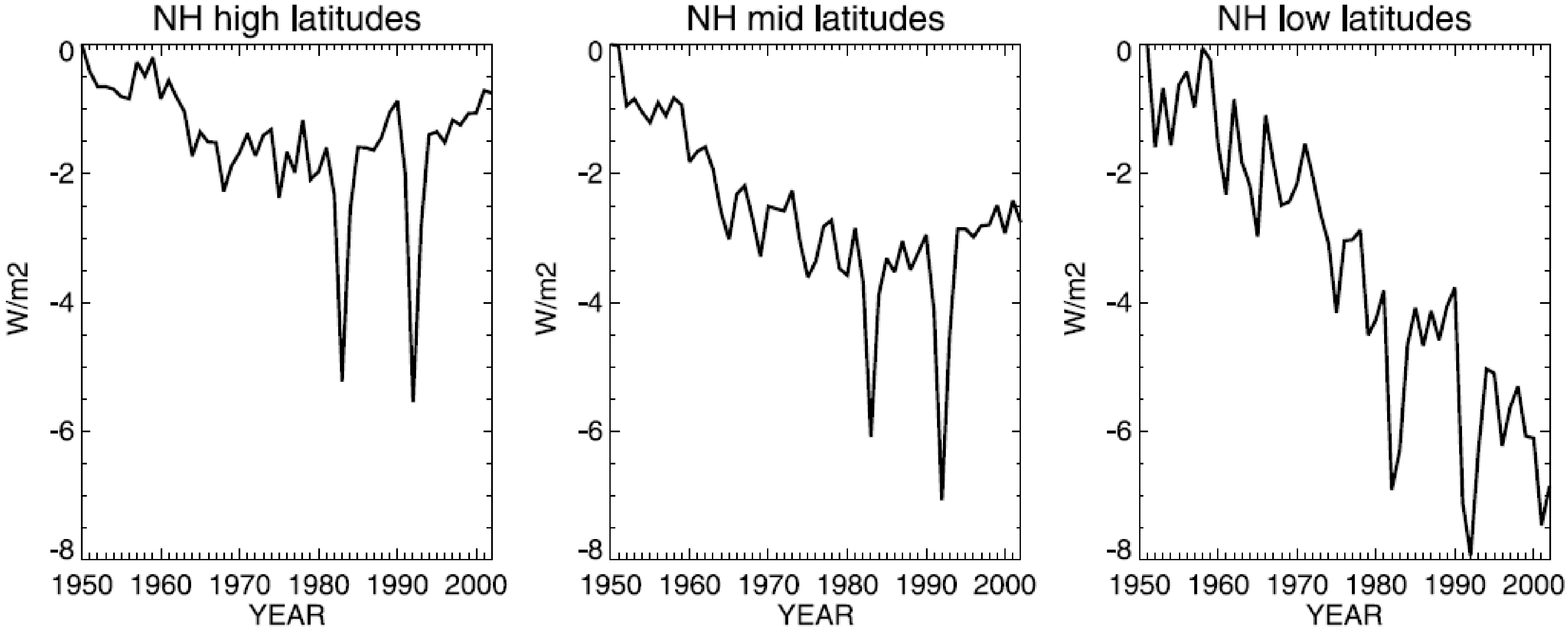

Figure 5. Simulated annual clear-sky surface solar radiation anomalies over the period 1950–2000 in different latitude belts of the Northern Hemisphere: High latitudes (60°N–90°N), middle latitudes (30°N–60°N), and low latitudes (0°–30°N). Simulations done with the aerosol-climate modeling system ECHAM5 HAM [*Stier et al.*, 2005, 2006]. Reference value is 1950. Units are W m^{-2}.

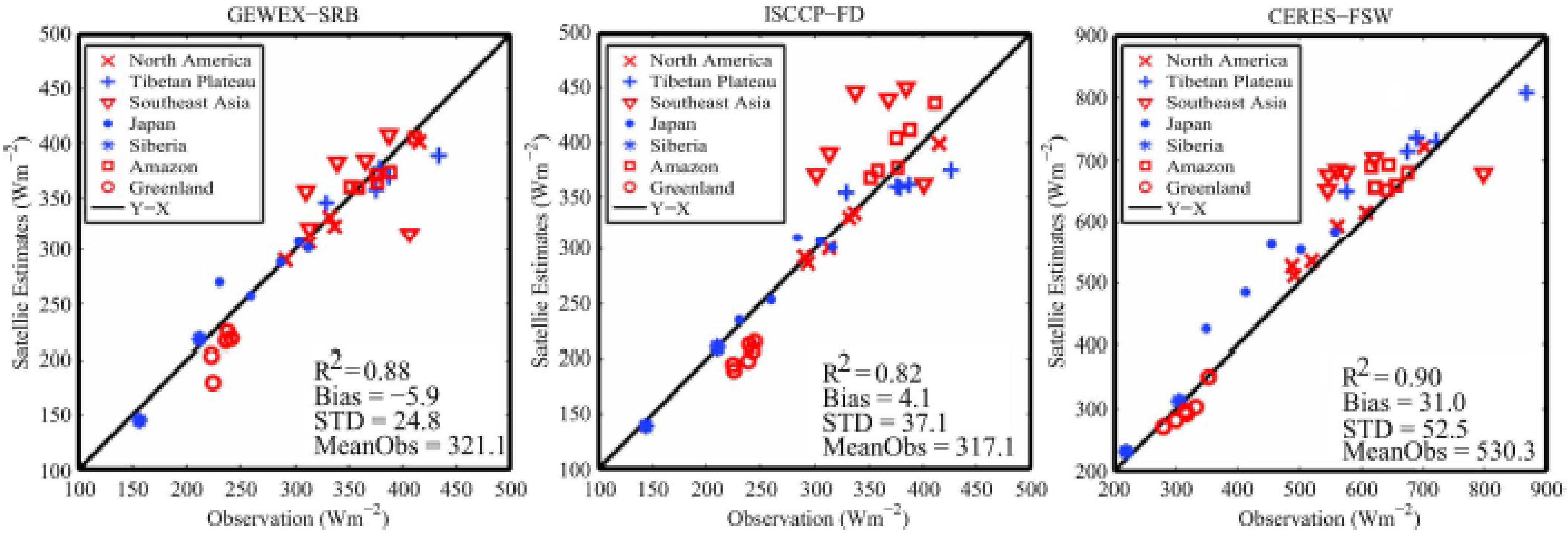

Fig. 2. Comparison of three-year mean DSSR between satellite estimates and ground measurements at 36 sites in seven regions, averaged from three hourly or hourly values over 2000–2002.

Gui, et al., *IEEE GRSL*, 2010

Estimating incident solar radiation

- **Liang, S.,** Zheng, T., Liu, R., Fang, H., Tsay, S.C., & Running, S. (2006). Mapping incident Photosynthetically Active Radiation (PAR) from MODIS Data. *Journal of Geophysical Research-Atmospheres, 111*, Art. No. D15208, doi:15210.11029/12005JD006730.

- **Liang, S.L**., Zheng, T., Wang, D.D., Wang, K.C., Liu, R.G., Tsay, S.C., Running, S., & Townshend, J. (2007). Mapping high-resolution incident photosynthetically active radiation over land from polar-orbiting and geostationary satellite data. *Photogrammetric Engineering and Remote Sensing*, *73*, 1085-1089

- Liu, R., **Liang, S.,** He, H., Liu, J., & Zheng, T. (2008). Mapping photosynthetically active radiation from MODIS data in China. *Remote Sensing of Environment*, *112*, 998-1009

- Wang, D., **Liang, S.,** & Zheng, T. (2010). Estimation of daily-integrated PAR from MODIS data. *International Journal of Remote Sensing*, 31(6), 1661, doi:10.1080/01431160903475407

- Zheng, T., **Liang, S.,** & Wang, K.C. (2008). Estimation of incident PAR from GOES imagery. *Journal of Applied Meteorology and Climatology, 47*, 853-868

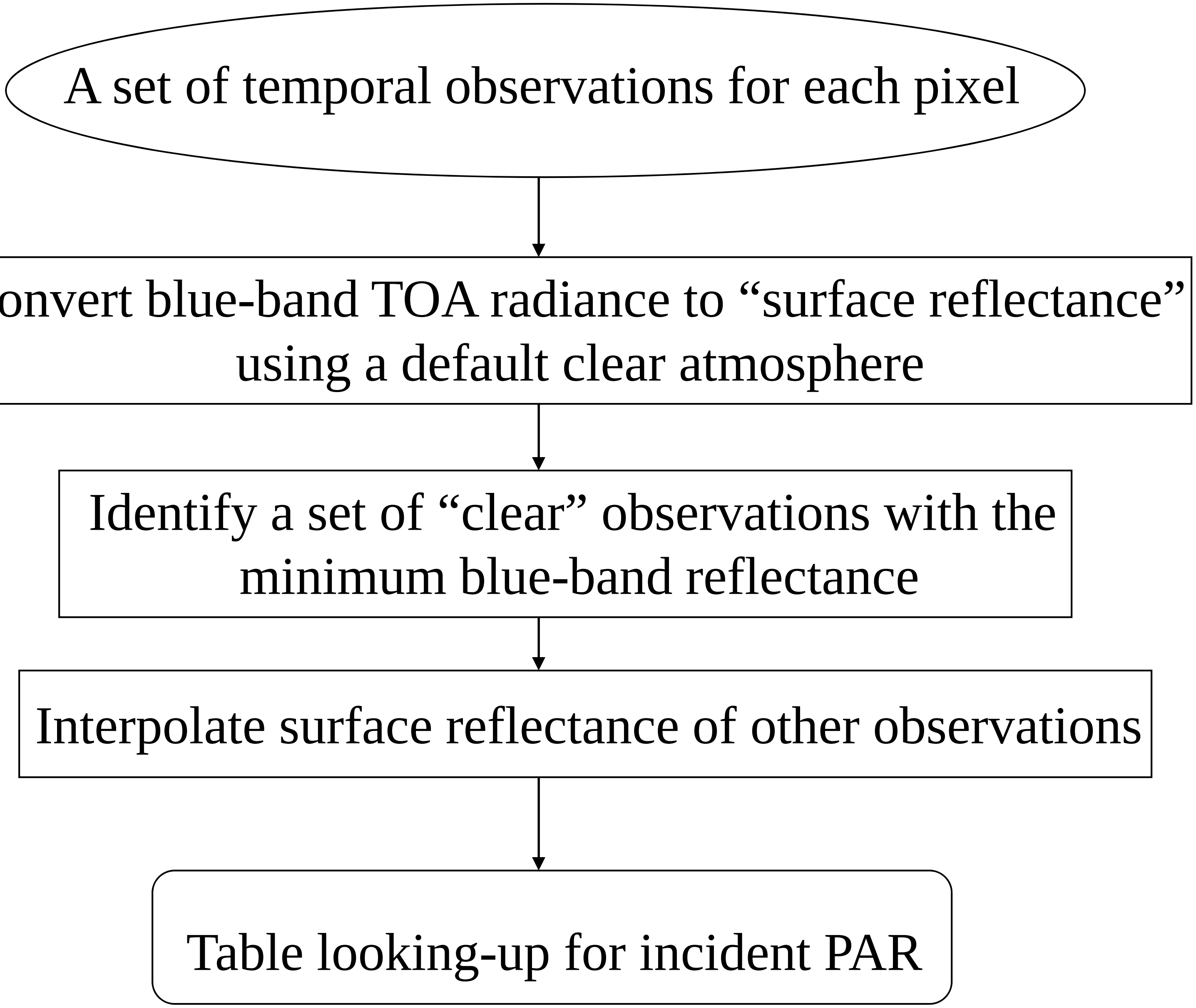

A set of temporal observations for each pixel

Convert blue-band TOA radiance to “surface reflectance” using a default clear atmosphere

Identify a set of “clear” observations with the minimum blue-band reflectance

Interpolate surface reflectance of other observations

Table looking-up for incident PAR

Flowchart of the algorithm using the temporal signatures

(Liang, et al., 2006)

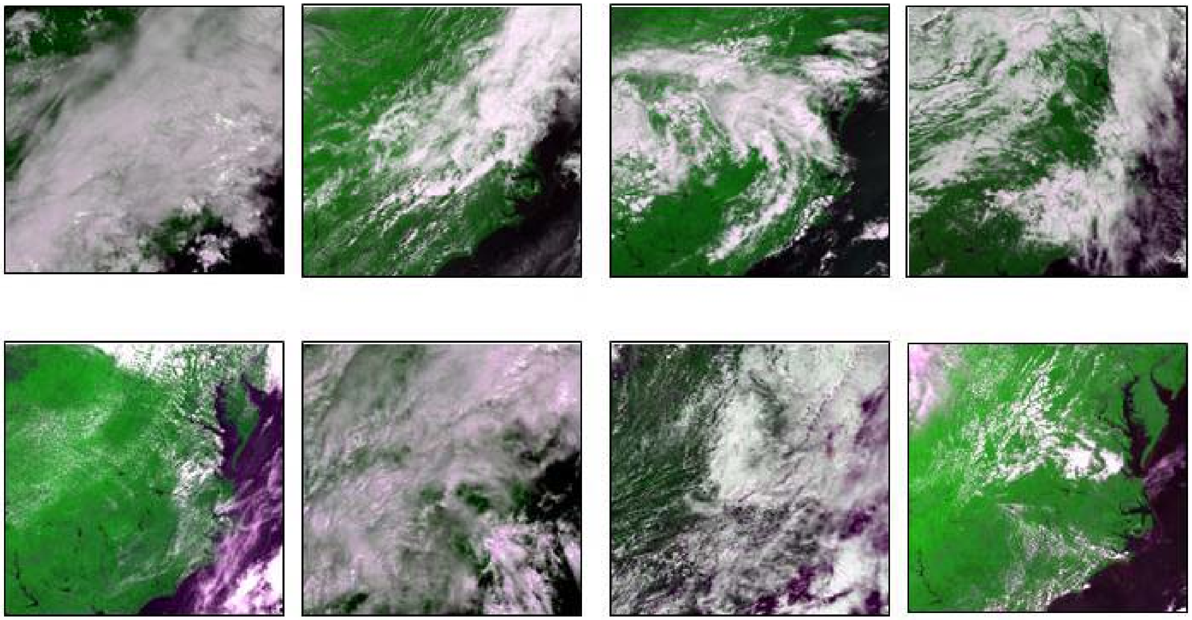

MODIS TOA radiance on 8 days in 2003:May 22, May 25, May 29, May 31, June 5, June 7, June 8, and June 10

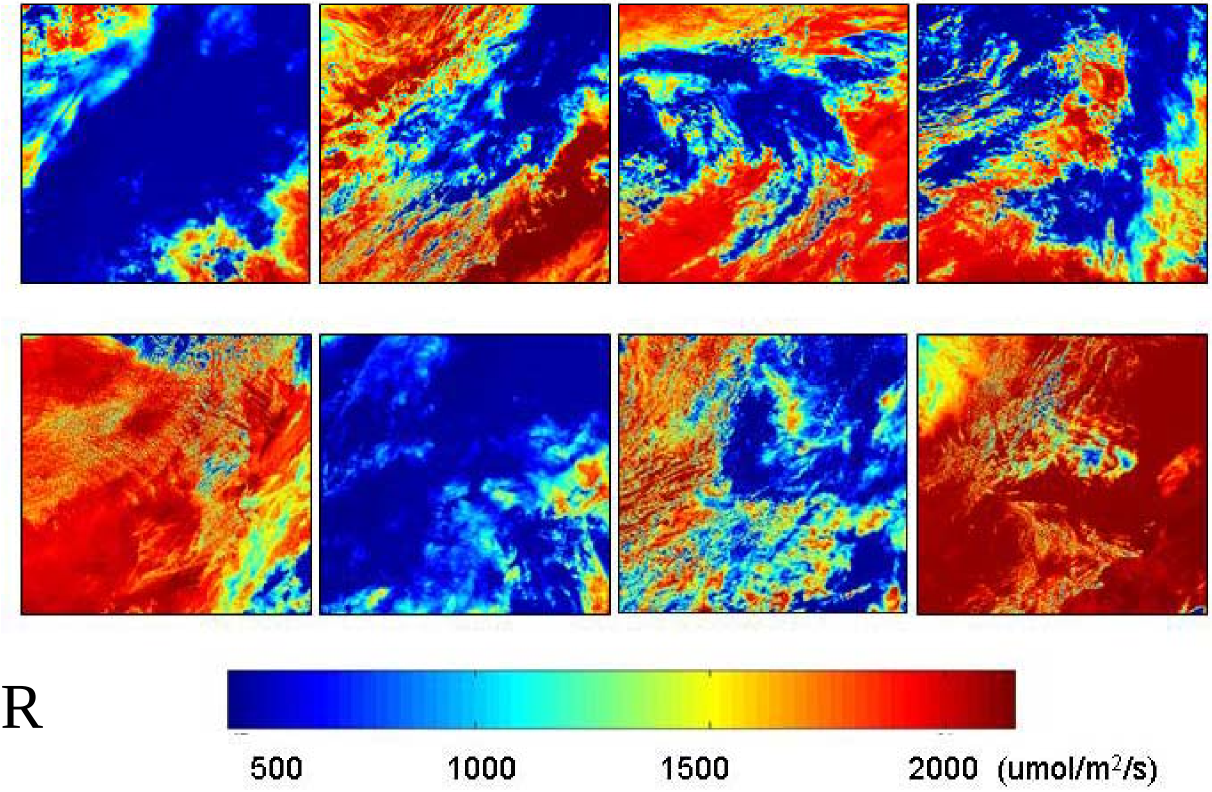

Estimated incident PAR

Monthly PAR from MODIS

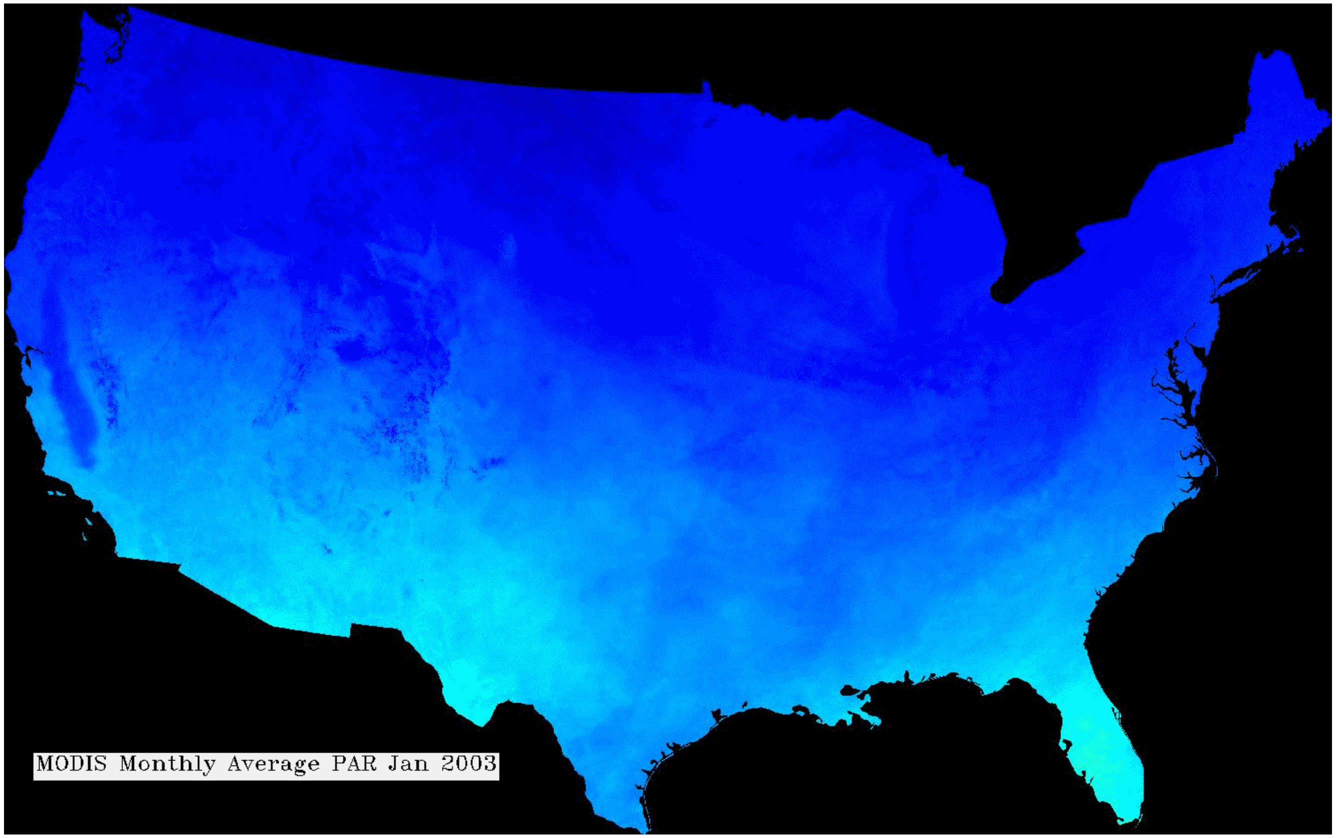

Three years (2003-2005) daily incident PAR at 4km over North America available now; Bob Cook has kindly agreed to distribute them at ORNL DAAC.

Downwelling Shortwave Radiation

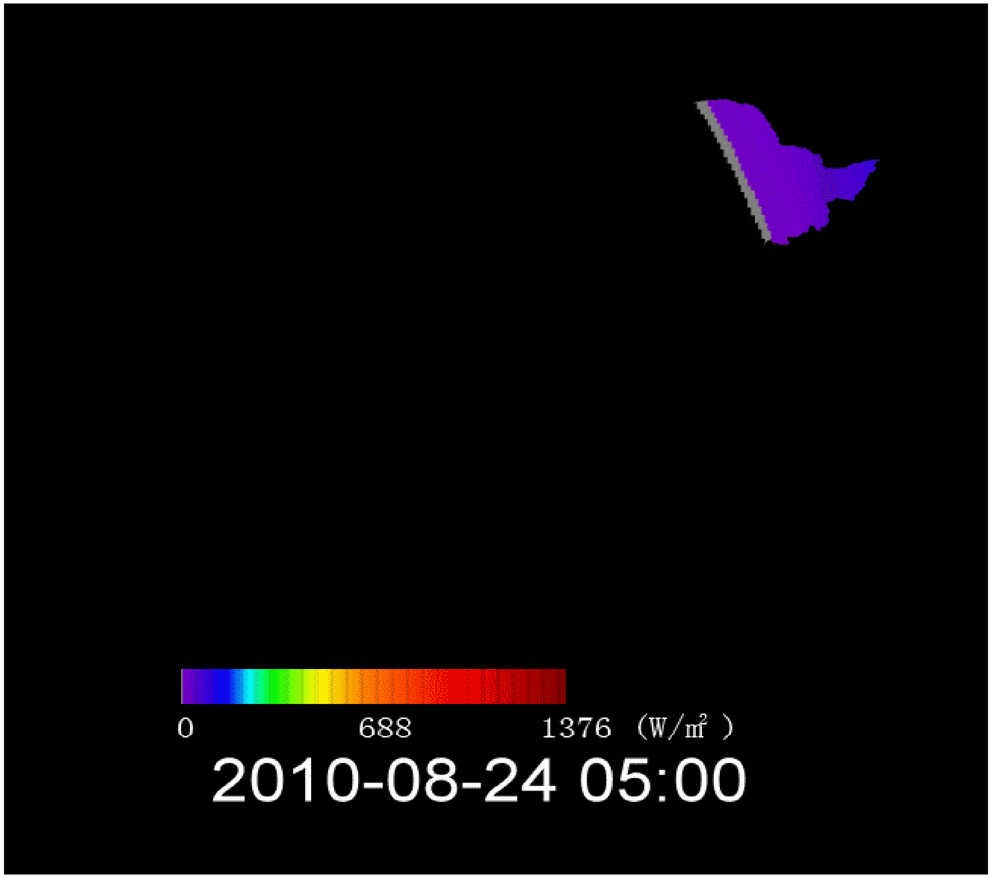

Downward Surface Shortwave Radiation of China from MTSAT images.

3 hours ,5km, (2008-2010, global)

Photosynthetically Active Radiation

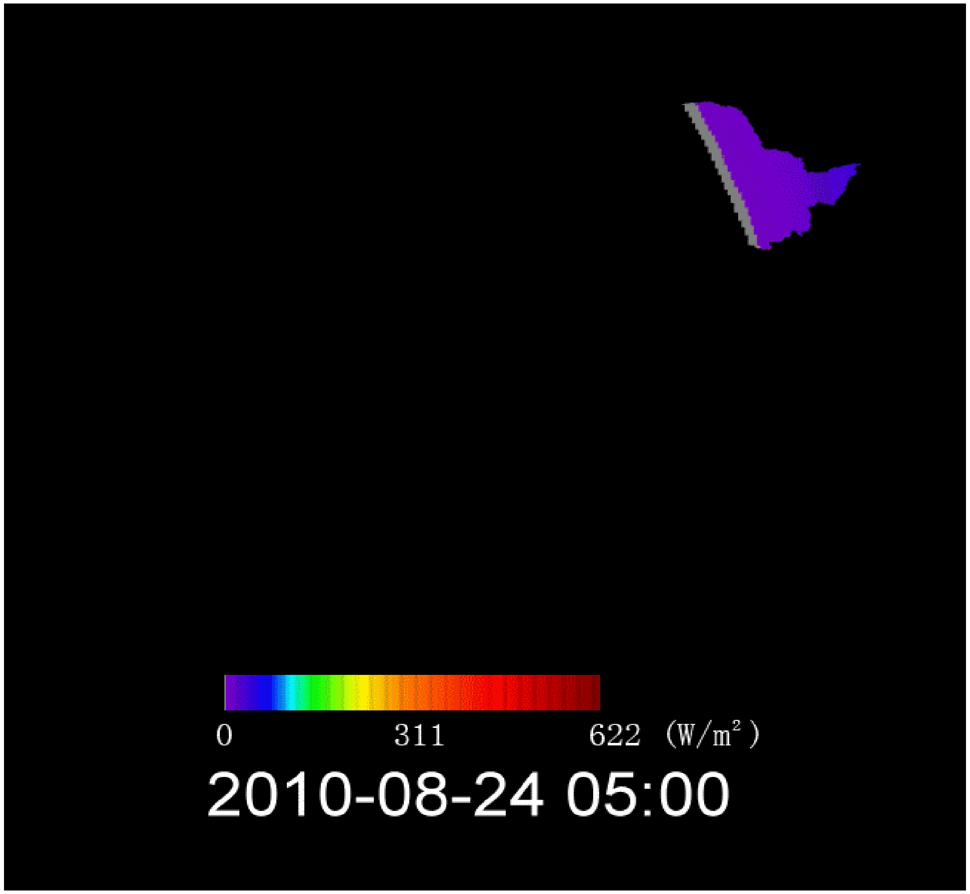

Photosynthetically Active Radiation of China from MTSAT images.

3hours, 5km. (2008-2010, global)

Outlines

- Background
- Insolation/PAR
- Albedo
- Longwave net radiation
- Evapotranpiration
- Summary

Albedo effect after deforestation

Davin, E. L. & N. de Noblet-Ducoudre (2010) Climatic Impact of Global-Scale Deforestation: Radiative versus Nonradiative Processes. *Journal of Climate, 23*, ***97-112.***

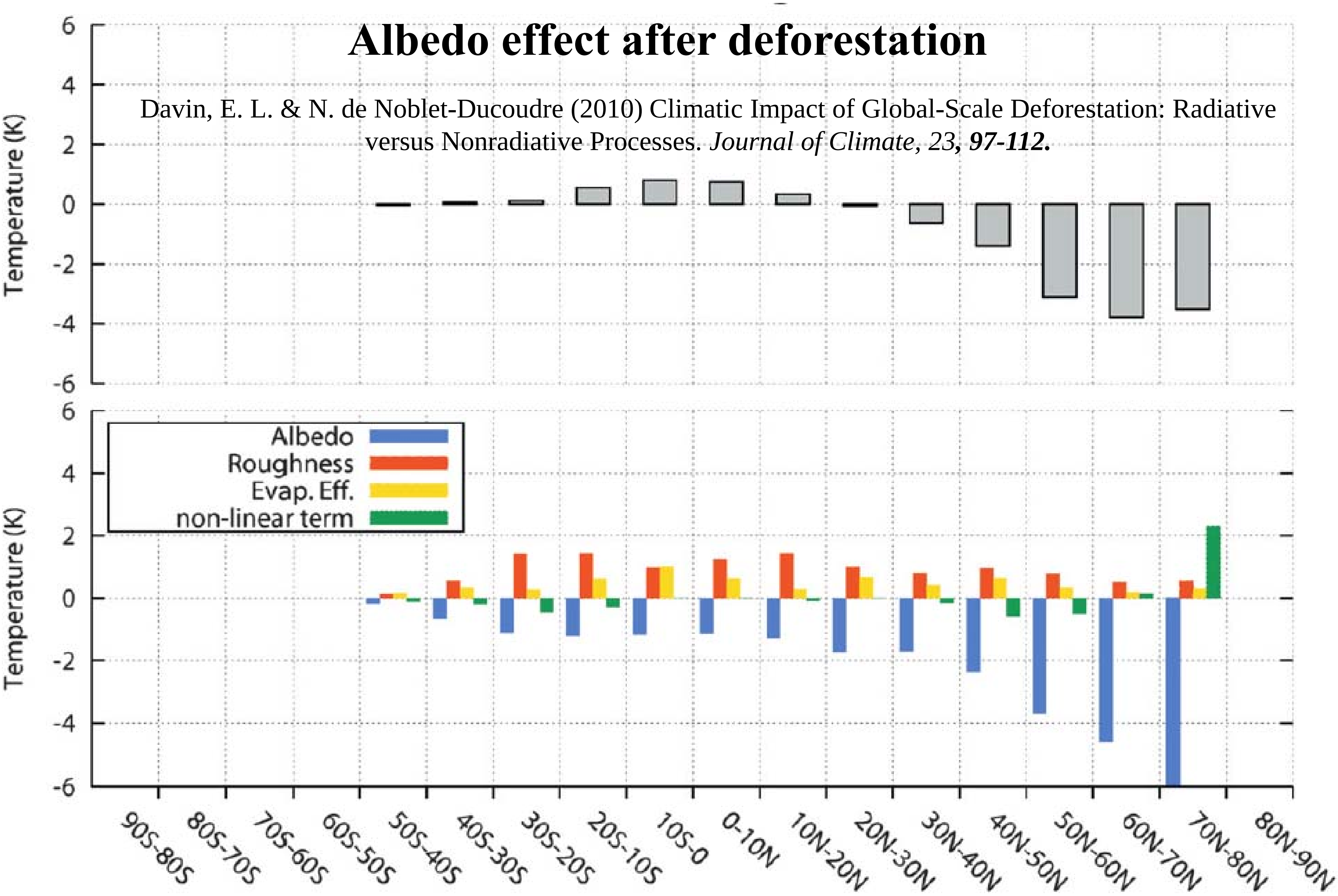

Annual mean change in surface temperature zonally averaged over deforested areas only. The bottom panel of each figure indicates the relative contribution of change

Albedo-based geoengineering solutions to offset CO2

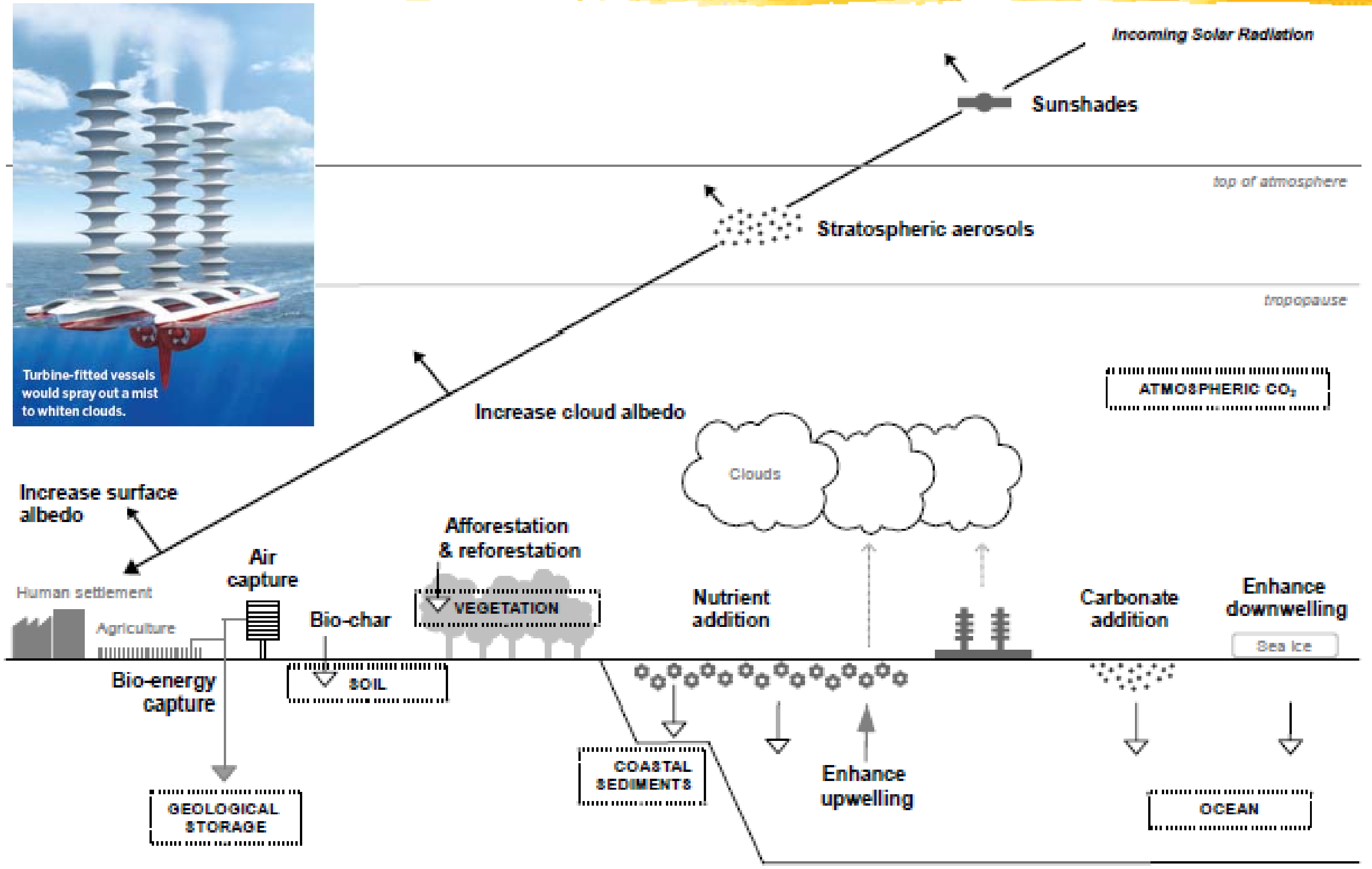

Turbine-fitted vessels would spray out a mist to whiten clouds.

Fig. 1. Schematic overview of the climate geoengineering proposals considered. Black arrowheads indicate shortwave radiation, white arrowheads indicate enhancement of natural flows of carbon, grey downward arrow indicates engineered flow of carbon, grey upward arrow indicates engineered flow of water, dotted vertical arrows illustrate sources of cloud condensation nuclei, and dashed boxes indicate carbon stores. From Vaughan and Lenton (2009), not to scale.

Table 1. Estimated radiative forcing potential of geoengineering options to alter planetary albedo. In common with the literature, for the first option, a back calculation is made of the albedo change required to counteract the radiative forcing due to doubling CO_2, whereas for the remaining options, forward calculations are made of the maximum potential radiative forcing. The latter are based on upper limit albedo changes and areas suggested in the literature (see text). Calculations were done at full precision but outputs are generally given to 2 significant figures commensurate with our first order approach.

Option	Area (m^2)	Fraction of Earth f_{Earth}	Albedo change within area $\Delta\alpha$	Scaled albedo change of layer	Transmittance factor f_a	Planetary albedo change $\Delta\alpha_p$	Solar radiation at TOA S_0 ($W m^{-2}$)	Radiative forcing RF ($W m^{-2}$)
Increase marine cloud albedo				$\Delta\alpha_a$				
Mechanical	8.9×10^{13}	0.175	0.074	0.013	0.84	0.011	345	−3.71
Biological	5.1×10^{13}	0.1	0.008	0.000067*	0.84	0.000056	345	−0.019
Increase land surface albedo				$\Delta\alpha_s$				
Desert	1.0×10^{13}	0.02	0.44	0.0088	0.73	0.0064	330	−2.12
Grassland	3.85×10^{13}	0.075	0.0425	0.0032	0.48	0.0015	330	−0.51
Cropland	1.4×10^{13}	0.028	0.08	0.0022	0.48	0.0011	330	−0.35
Settlements	3.25×10^{12}	0.0064	0.15	0.00096	0.48	0.00046	330	−0.15
Urban areas	1.5×10^{12}	0.0029	0.1	0.00029	0.48	0.00014	330	−0.047

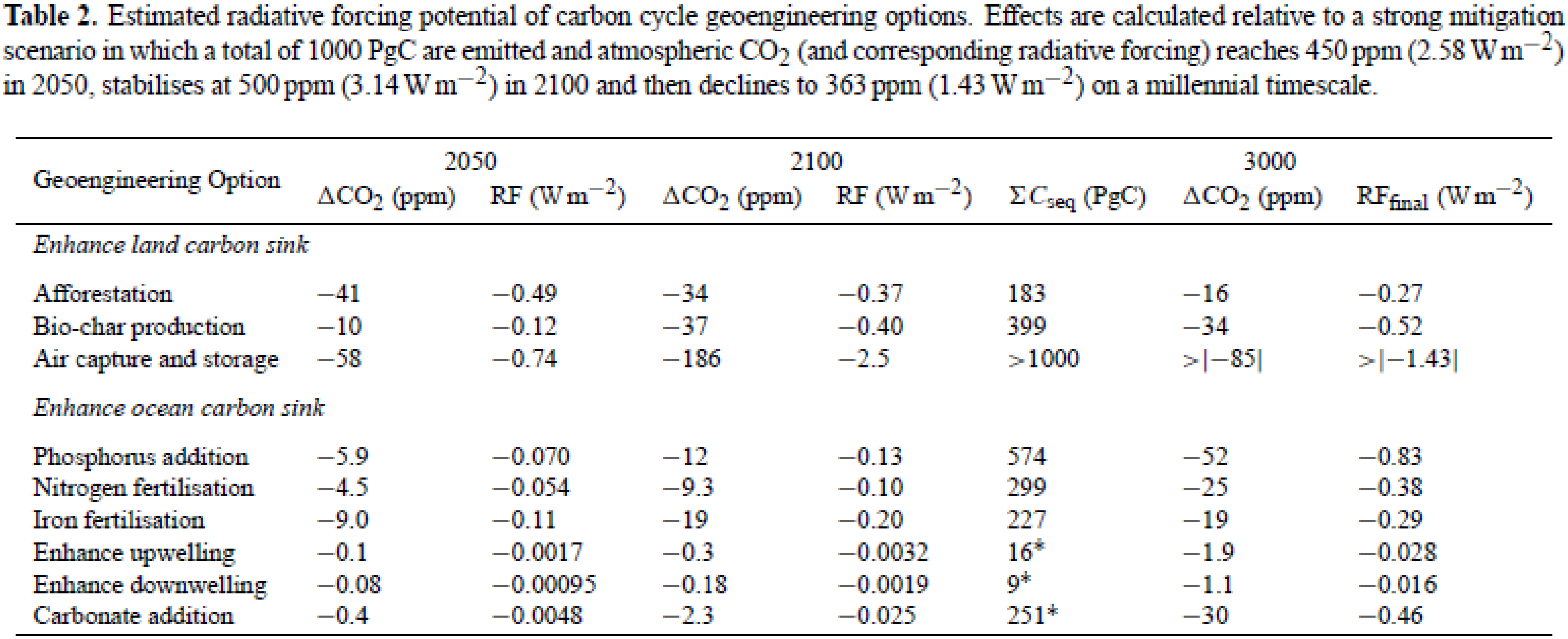

Table 2. Estimated radiative forcing potential of carbon cycle geoengineering options. Effects are calculated relative to a strong mitigation scenario in which a total of 1000 PgC are emitted and atmospheric CO_2 (and corresponding radiative forcing) reaches 450 ppm (2.58 $W m^{-2}$) in 2050, stabilises at 500 ppm (3.14 $W m^{-2}$) in 2100 and then declines to 363 ppm (1.43 $W m^{-2}$) on a millennial timescale.

Geoengineering Option	2050		2100			3000	
	ΔCO_2 (ppm)	RF ($W m^{-2}$)	ΔCO_2 (ppm)	RF ($W m^{-2}$)	ΣC_{seq} (PgC)	ΔCO_2 (ppm)	RF_{final} ($W m^{-2}$)
Enhance land carbon sink							
Afforestation	−41	−0.49	−34	−0.37	183	−16	−0.27
Bio-char production	−10	−0.12	−37	−0.40	399	−34	−0.52
Air capture and storage	−58	−0.74	−186	−2.5	>1000	>|−85|	>|−1.43|
Enhance ocean carbon sink							
Phosphorus addition	−5.9	−0.070	−12	−0.13	574	−52	−0.83
Nitrogen fertilisation	−4.5	−0.054	−9.3	−0.10	299	−25	−0.38
Iron fertilisation	−9.0	−0.11	−19	−0.20	227	−19	−0.29
Enhance upwelling	−0.1	−0.0017	−0.3	−0.0032	16*	−1.9	−0.028
Enhance downwelling	−0.08	−0.00095	−0.18	−0.0019	9*	−1.1	−0.016
Carbonate addition	−0.4	−0.0048	−2.3	−0.025	251*	−30	−0.46

Land Surface Albedo

IPCC AR4 GCM model simulations and two satellite products

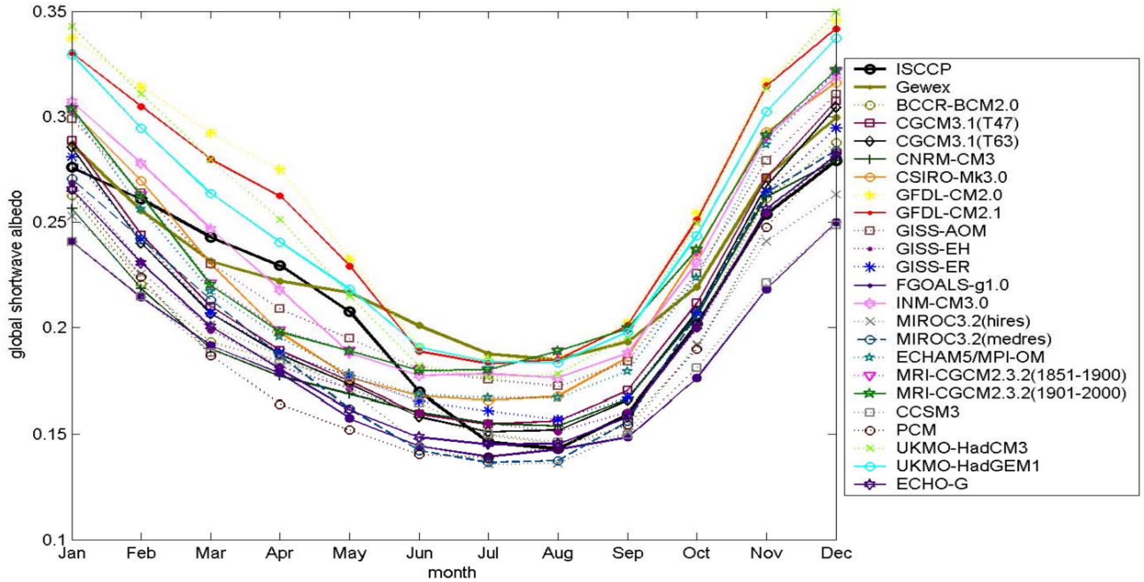

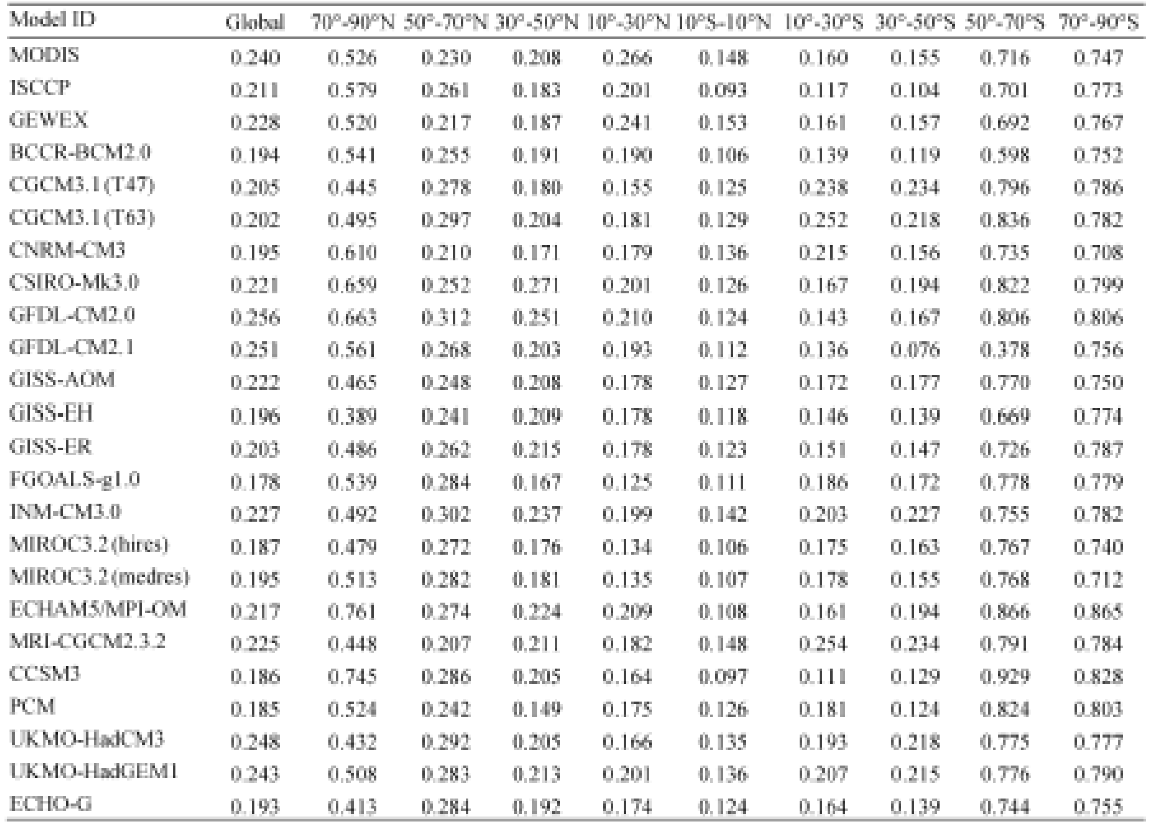

Model ID	Global	70°-90°N	50°-70°N	30°-50°N	10°-30°N	10°S-10°N	10°-30°S	30°-50°S	50°-70°S	70°-90°S
MODIS	0.240	0.526	0.230	0.208	0.266	0.148	0.160	0.155	0.716	0.747
ISCCP	0.211	0.579	0.261	0.183	0.201	0.093	0.117	0.104	0.701	0.773
GEWEX	0.228	0.520	0.217	0.187	0.241	0.153	0.161	0.157	0.692	0.767
BCCR-BCM2.0	0.194	0.541	0.255	0.191	0.190	0.106	0.139	0.119	0.598	0.752
CGCM3.1 (T47)	0.205	0.445	0.278	0.180	0.155	0.125	0.238	0.234	0.796	0.786
CGCM3.1 (T63)	0.202	0.495	0.297	0.204	0.181	0.129	0.252	0.218	0.836	0.782
CNRM-CM3	0.195	0.610	0.210	0.171	0.179	0.136	0.215	0.156	0.735	0.708
CSIRO-Mk3.0	0.221	0.659	0.252	0.271	0.201	0.126	0.167	0.194	0.822	0.799
GFDL-CM2.0	0.256	0.663	0.312	0.251	0.210	0.124	0.143	0.167	0.806	0.806
GFDL-CM2.1	0.251	0.561	0.268	0.203	0.193	0.112	0.136	0.076	0.378	0.756
GISS-AOM	0.222	0.465	0.248	0.208	0.178	0.127	0.172	0.177	0.770	0.750
GISS-EH	0.196	0.389	0.241	0.209	0.178	0.118	0.146	0.139	0.669	0.774
GISS-ER	0.203	0.486	0.262	0.215	0.178	0.123	0.151	0.147	0.726	0.787
FGOALS-g1.0	0.178	0.539	0.284	0.167	0.125	0.111	0.186	0.172	0.778	0.779
INM-CM3.0	0.227	0.492	0.302	0.237	0.199	0.142	0.203	0.227	0.755	0.782
MIROC3.2 (hires)	0.187	0.479	0.272	0.176	0.134	0.106	0.175	0.163	0.767	0.740
MIROC3.2 (medres)	0.195	0.513	0.282	0.181	0.135	0.107	0.178	0.155	0.768	0.712
ECHAM5/MPI-OM	0.217	0.761	0.274	0.224	0.209	0.108	0.161	0.194	0.866	0.865
MRI-CGCM2.3.2	0.225	0.448	0.207	0.211	0.182	0.148	0.254	0.234	0.791	0.784
CCSM3	0.186	0.745	0.286	0.205	0.164	0.097	0.111	0.129	0.929	0.828
PCM	0.185	0.524	0.242	0.149	0.175	0.126	0.181	0.124	0.824	0.803
UKMO-HadCM3	0.248	0.432	0.292	0.205	0.166	0.135	0.193	0.218	0.775	0.777
UKMO-HadGEM1	0.243	0.508	0.283	0.213	0.201	0.136	0.207	0.215	0.776	0.790
ECHO-G	0.193	0.413	0.284	0.192	0.174	0.124	0.164	0.139	0.744	0.755

Zhang, et al., *IEEE JSTARS*, 2010

Part of MODIS algorithm for global production

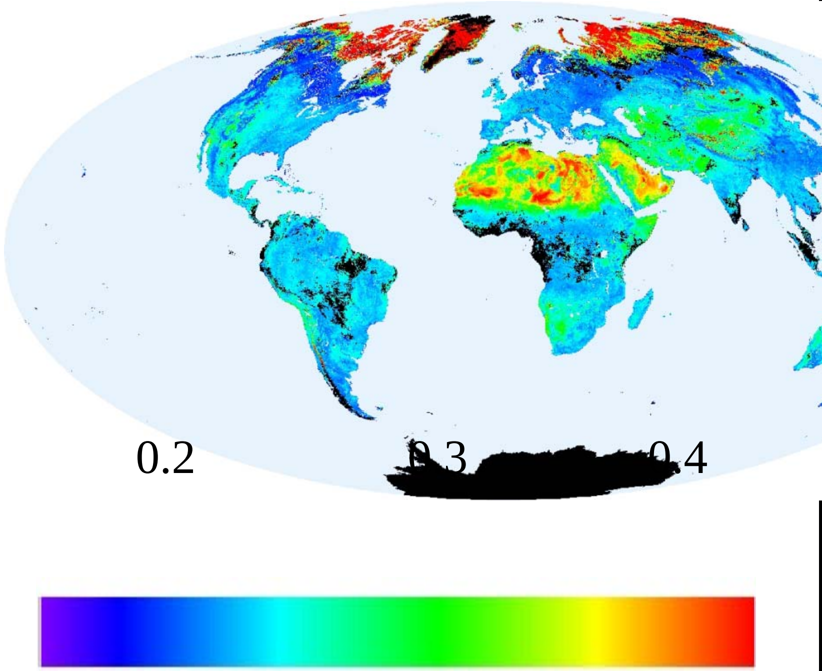

Global White-sky (bihemispherical) Albedo for the period 30 Sep - 13 Oct, 2002

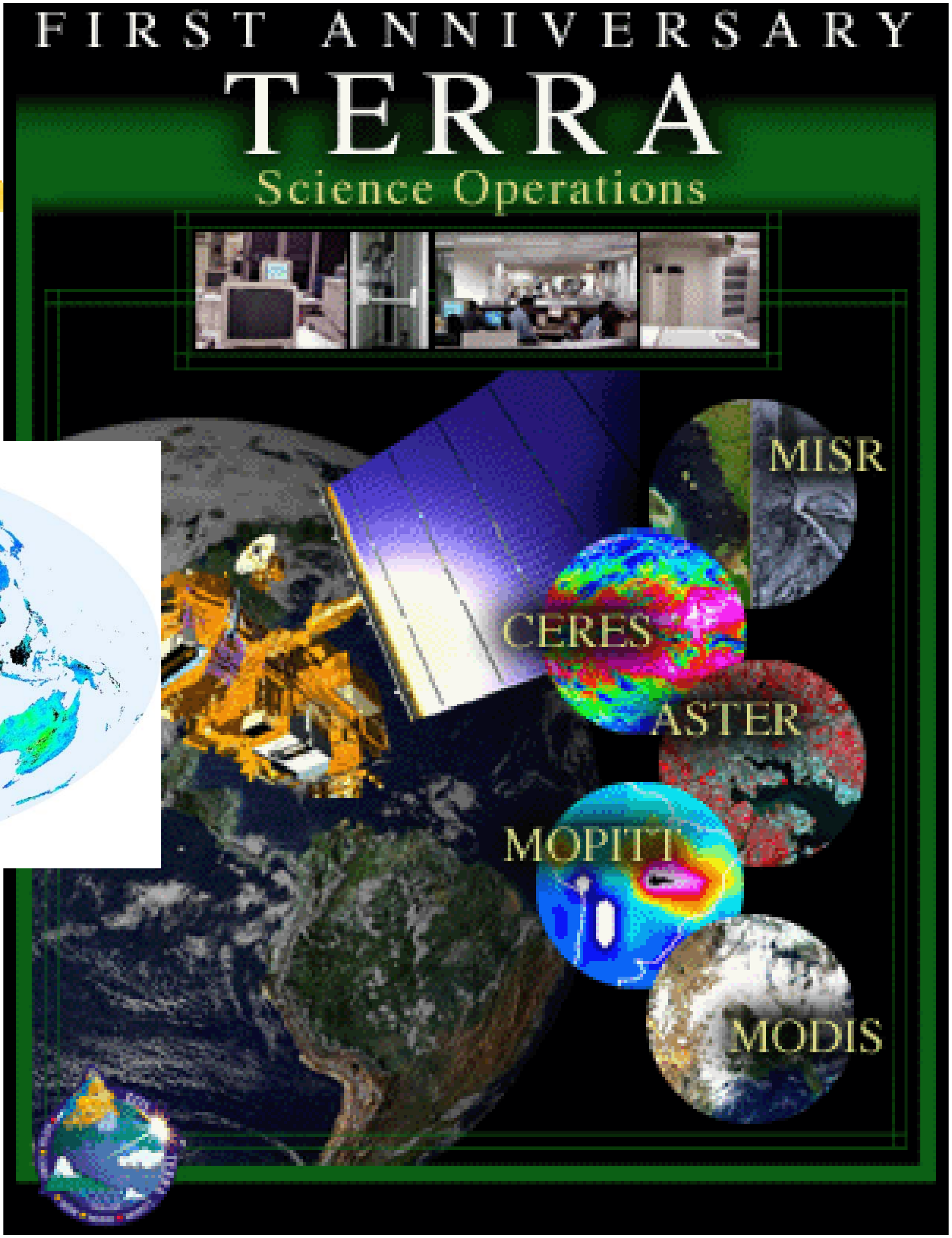

bidirectional reflectance factor (BRF) $R(\theta_i, \phi_i, \theta_v, \phi_v)$, which is numerically equivalent to BRDF multiplied by π:

$$R(\theta_i, \phi_i, \theta_v, \phi_v) = \pi f(\theta_i, \phi_i, \theta_v, \phi_v)$$ **Equation 1-9**

we need surface *directional-hemispherical reflectance (DHR)*, which can be integrated from BRF over all reflected directions:

$$r(-\mu_i, \phi_i) = \frac{1}{\pi}\int_0^{2\pi}\int_0^1 R(\mu_i, \phi_i, \mu, \phi)\mu d\mu d\phi$$ **Equation 1-10**

It is often called local or planar *albedo*, but is called black-sky albedo in the MODIS products of the NASA Earth Observing System (EOS) program. The *bihemispherical reflectance* (BHR) is a further integration of DHR over all illumination directions:

$$r_0 = 2\int_0^1 r(-\mu_i, \phi_i)\mu_i d\mu_i$$ **Equation 1-11**

which is also called global or spherical albedo, or bright-sky albedo in the MODIS

Albedometer measurements

$$\alpha_s = \frac{E_s^{\uparrow}}{E_s^{\downarrow}} = \frac{\int_0^{2\pi}\int_0^{1} I_s^{\uparrow}(\theta_s,\theta_v,\phi)\cdot\mu\cdot d\mu\cdot d\phi}{\int_0^{2\pi}\int_0^{1} I_s^{\downarrow}(\theta_s,\theta_v,\phi)\cdot\mu^*\cdot d\mu^*\cdot d\phi^*}$$

$$I_s^{\uparrow} = \frac{1}{\pi}\int_0^{2\pi}\int_0^{1} r_s(\theta_s,\theta_v,\phi) I_s^{\downarrow}(\theta_s,\theta_v,\phi)\mu^* d\mu^* d\phi^*$$

$$\alpha_s = (1-s)\cdot\alpha_{black} + s\cdot\alpha_{white}$$

MODIS albedo algorithm

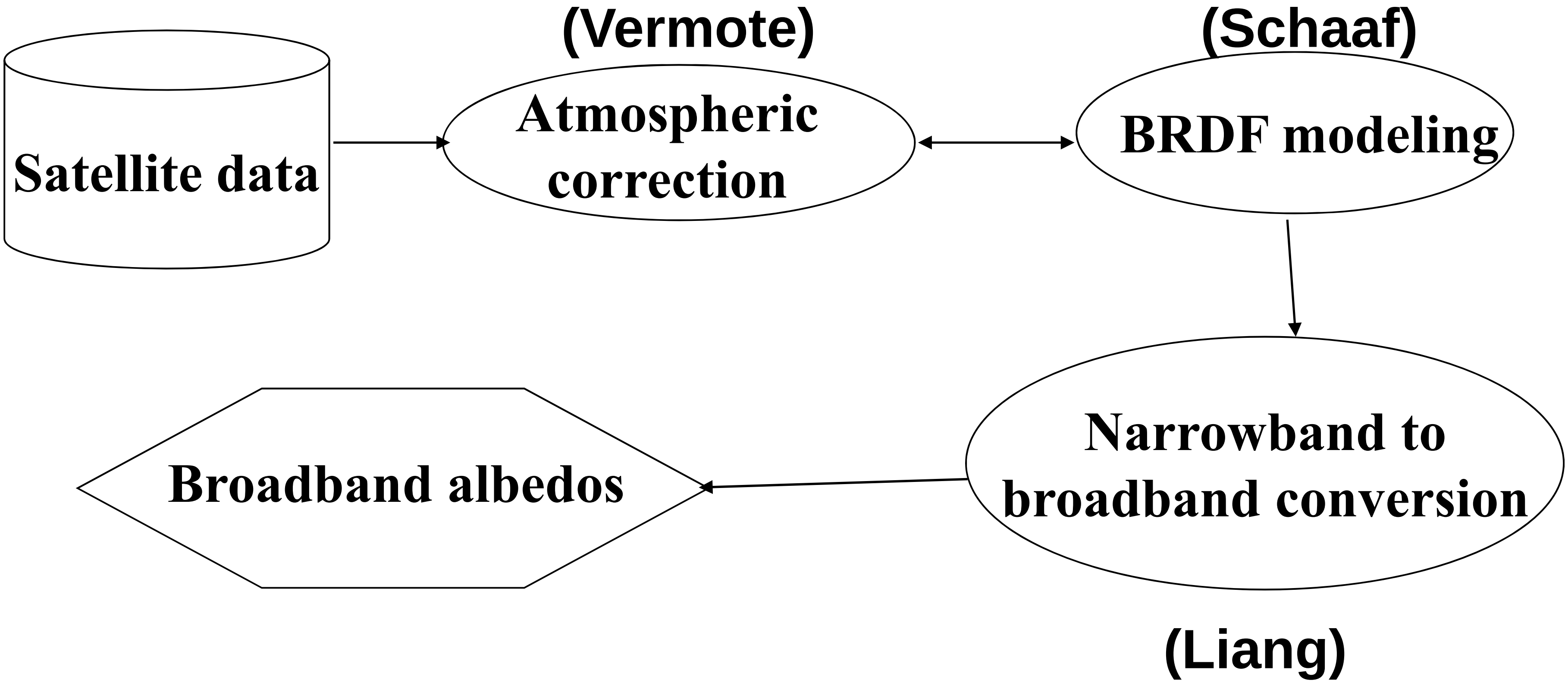

Satellite data

(Vermote)

Atmospheric correction

(Schaaf)

BRDF modeling

Narrowband to broadband conversion

(Liang)

Broadband albedos

MODIS aerosol over the land

- Derive apparent reflectance (normalized radiance at the top of the atmosphere) at 2.2 μm, $\rho^*_{2.2}$
- Assume that aerosol is transparent at 2.2 μm, thus: $\rho^s_{2.2} = \rho^*_{2.2}$ where $\rho^s_{2.2}$ is the surface reflectance.
- Determine surface reflectance at 0.47, and 0.66 μm:

$$\rho^s_{0.47} = 0.5\rho^s_{0.66} = 0.25\rho^*_{2.2}$$

- Determine the aerosol type (e.g. smoke or dust) from the excess radiance:

$$\Delta\rho^*_{0.47} = \rho^*_{0.47} - \rho^s_{0.47} \quad \Delta\rho^*_{0.66} = \rho^*_{0.66} - \rho^s_{0.66}$$

$$\Delta\rho^*_{0.47} / \Delta\rho^*_{0.66} ==> \text{aerosol type}$$

- Determine the optical thickness from the excess radiance:

$$\Delta\rho^*_{0.47} => \tau_{0.47} \, , \, \Delta\rho^*_{0.66} => \tau_{0.66}$$

λ(μm)

0.47

0.55

0.66

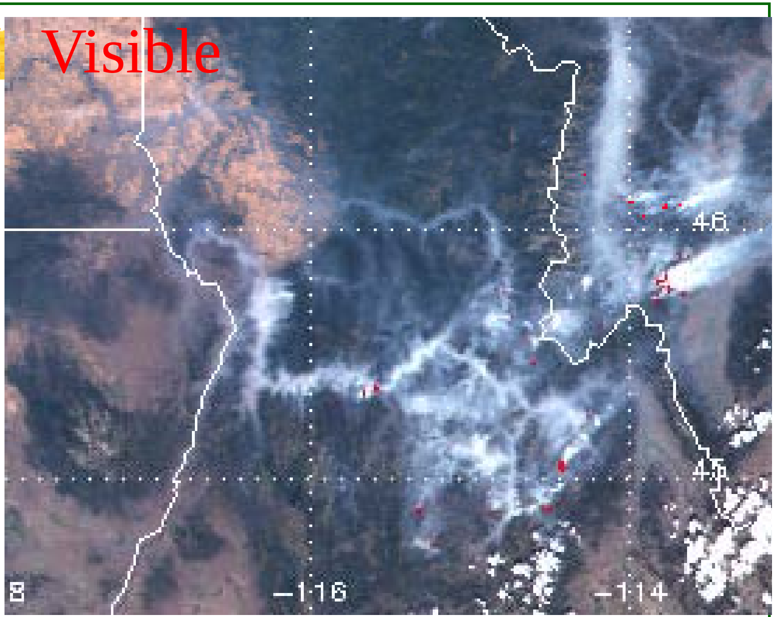

1.2

1.6

2.1

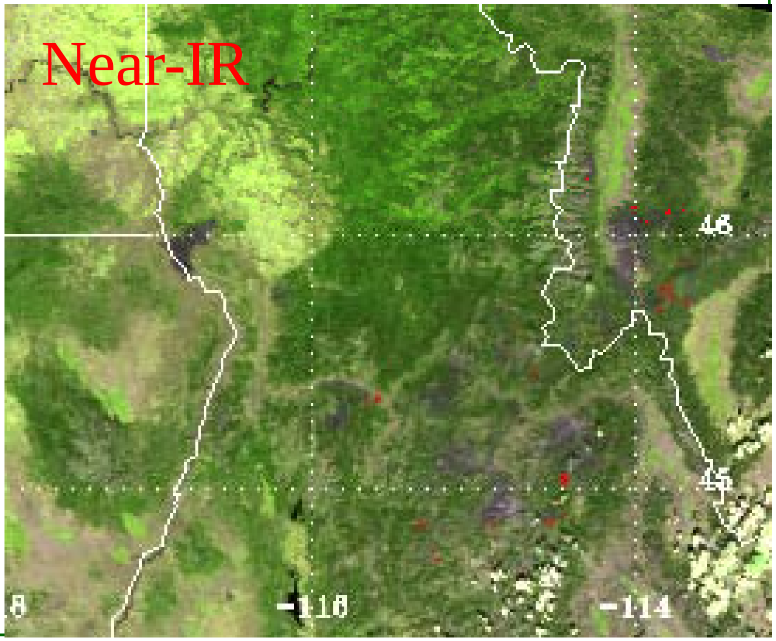

The modified three-parameter linear surface BRF kernel model:

$$r_s(\theta_s,\theta_v,\phi)=f_{iso}+f_{vol}\cdot K_{vol}(\theta_s,\theta_v,\phi)+f_{geo}\cdot K_{geo}(\theta_s,\theta_v,\phi)$$

Where: the volumetric and geometrical kernel function has the following form:

$$K_{vol}=K_{RT}=\frac{(\pi/2-\xi)\cos\xi+\sin\xi}{\cos\theta+\cos\vartheta}\left(1+\frac{1}{1+\xi/\xi_0}\right)-\frac{\pi}{4}$$

$$K_{geo}=K_{LSR}=O(\theta_s,\theta_v,\phi)-\sec\theta'-\sec\vartheta'+0.5(1+\cos\xi')\sec\theta'\sec\vartheta'$$

$$O=(t-\sin t\cos t)(\sec\theta'+\sec\vartheta')/\pi$$

$$\cos t=\frac{h\sqrt{D^2+(\tan\theta'\tan\upsilon'\sin\phi)^2}}{b(\sec\theta'+\sec\vartheta')}$$

$$D=\sqrt{\tan^2\theta'+\tan^2\upsilon'-2\tan\theta'\tan\upsilon'\cos\phi}$$

$$\cos\xi'=\cos\theta'\cos\upsilon'+\sin\theta'\sin\upsilon'\cos\phi$$

$$\theta'=\tan^{-1}(\frac{b}{r}\tan\theta_s)$$

$$\vartheta'=\tan^{-1}(\frac{b}{r}\tan\theta_v)$$

ξ_0=1.5°, $\frac{h}{b}$=2.0 and $\frac{b}{r}$=1.0

Liang, S., (2001), Narrowband to Broadband Conversion of Land Surface Albedo. I. Algorithms, *Remote Sensing of Environment*, 76:213-238.

$$\begin{aligned}\alpha_{\text{short}} &= 0.160\alpha_1 + 0.291\alpha_2 + 0.243\alpha_3 + 0.116\alpha_4 \\ &\quad + 0.112\alpha_5 + 0.081\alpha_7 - 0.0015\end{aligned}$$

$$\alpha_{\text{visible}} = 0.331\alpha_1 + 0.424\alpha_3 + 0.246\alpha_4$$

$$\alpha_{\text{diffuse-visible}} = 0.246\alpha_1 + 0.528\alpha_3 + 0.226\alpha_4 - 0.0013$$

$$\alpha_{\text{direct-visible}} = 0.369\alpha_1 + 0.374\alpha_3 + 0.257\alpha_4$$

$$\begin{aligned}\alpha_{\text{NIR}} &= 0.039\alpha_1 + 0.504\alpha_2 - 0.071\alpha_3 + 0.105\alpha_4 \\ &\quad + 0.252\alpha_5 + 0.069\alpha_6 + 0.101\alpha_7\end{aligned}$$

JPSS (VIIRS) two albedo algorithms

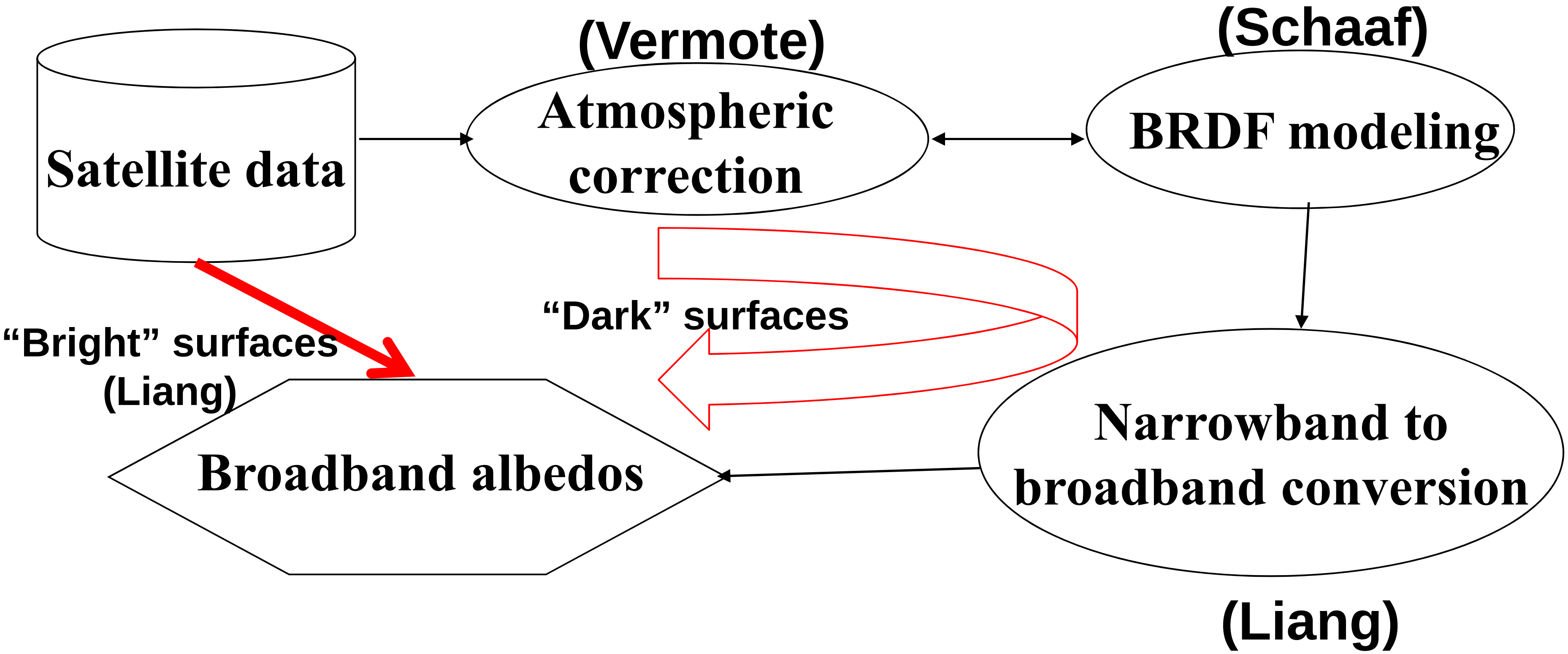

Broadband albedo estimation
Joint Polar Satellite System (JPSS)

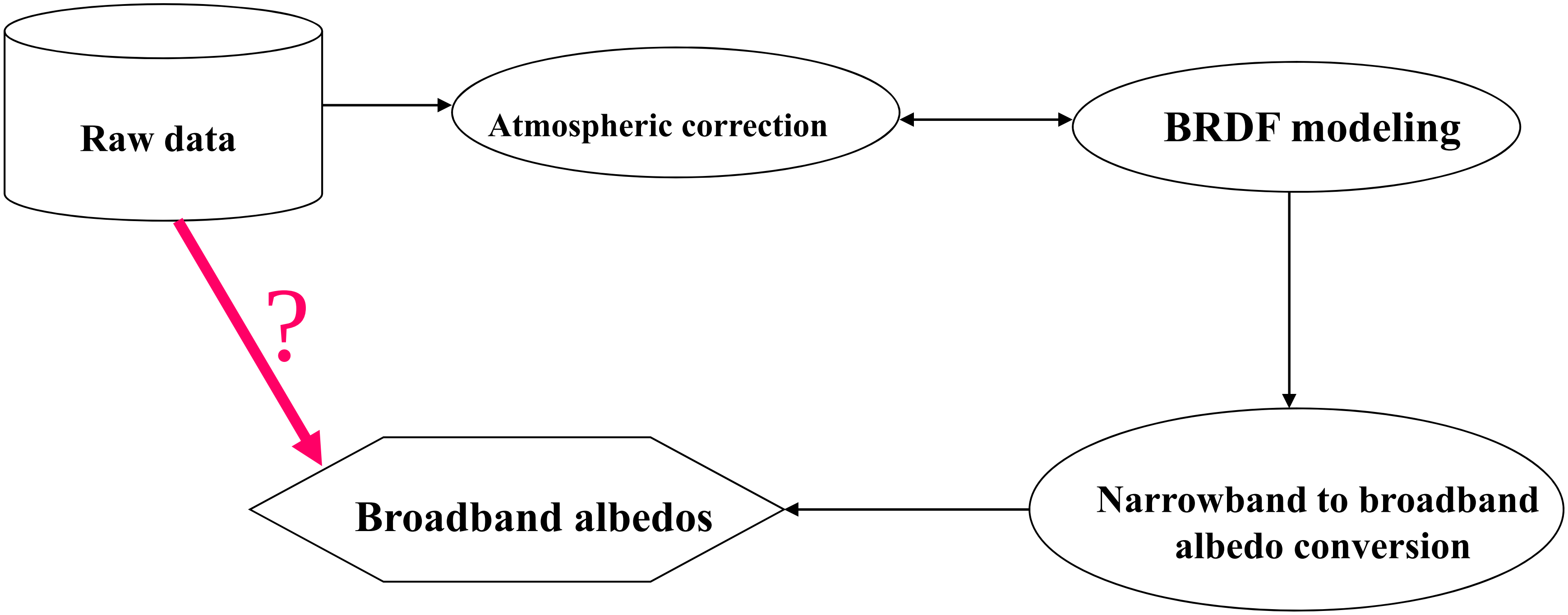

Raw data

Atmospheric correction

BRDF modeling

Narrowband to broadband albedo conversion

Broadband albedos

?

Liang, S., (2003), A direct algorithm for estimating land surface broadband albedos from MODIS imagery, *IEEE Trans. Geosci. Remote Sen.*, 41(1):136-145*;*

Liang, S., J. Stroeve and J. Box, (2005), Mapping daily snow shortwave broadband albedo from MODIS: The improved direct estimation algorithm and validation, *Journal of Geophysical Research.* 110 (D10): Art. No. D10109.

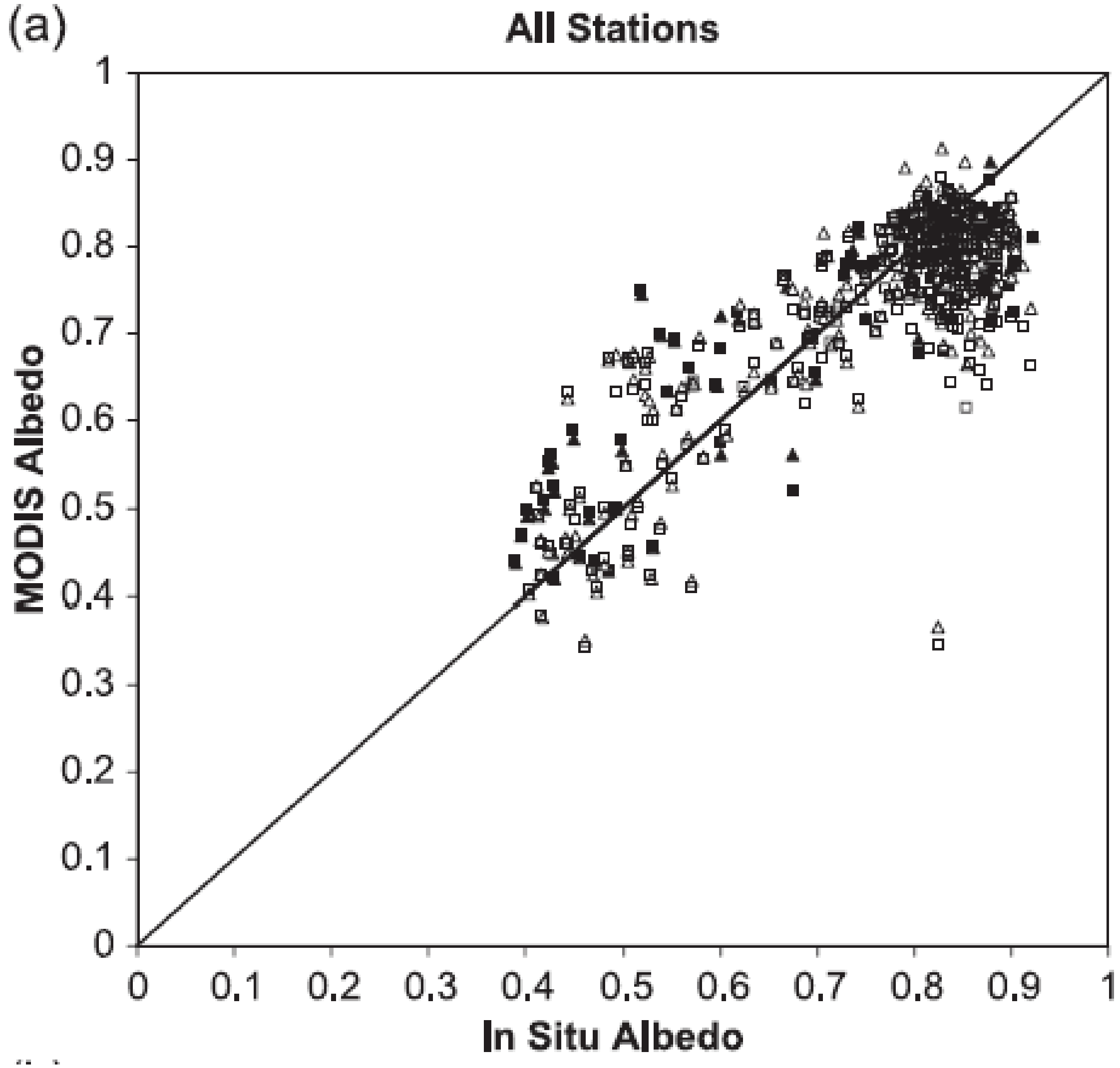

Validation of MODIS shortwave albedo product over Greenland

Stroeve, J., J. Box, F. Gao, S., Liang, A., Nolin, and C. Schaaf, (2005), *Accuracy assessment of the MODIS 16-day snow albedo product: Comparisons with Greenland in situ measurements, Remote Sensing of Environment, 94(1):46-60.*

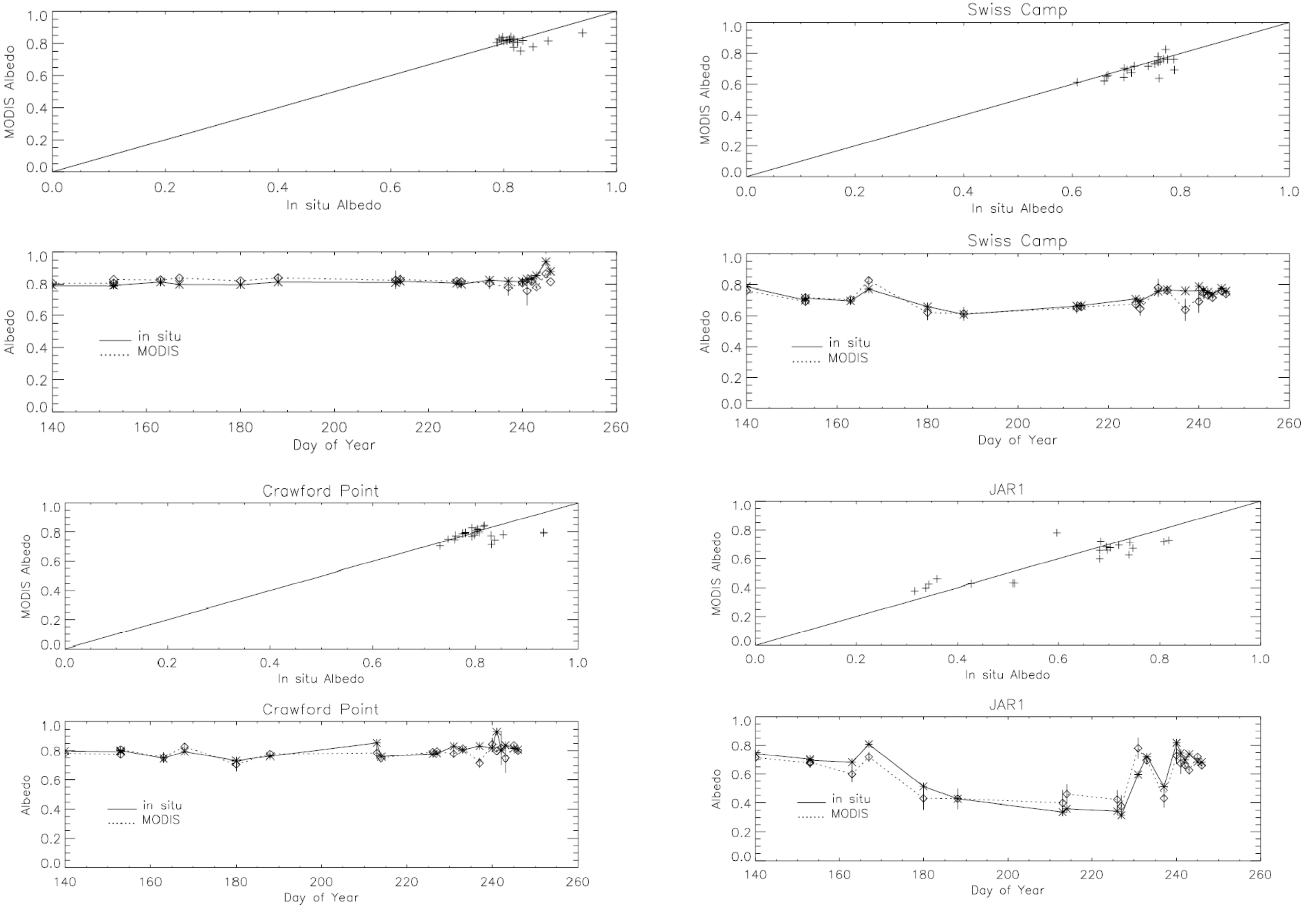

Liang, S., J. Stroeve and J. Box, (2005), *Mapping daily snow shortwave broadband albedo from MODIS: The improved direct estimation algorithm and validation, Journal of Geophysical Research. 110 (D10): Art. No. D10109.*

Global Broadband Albedo

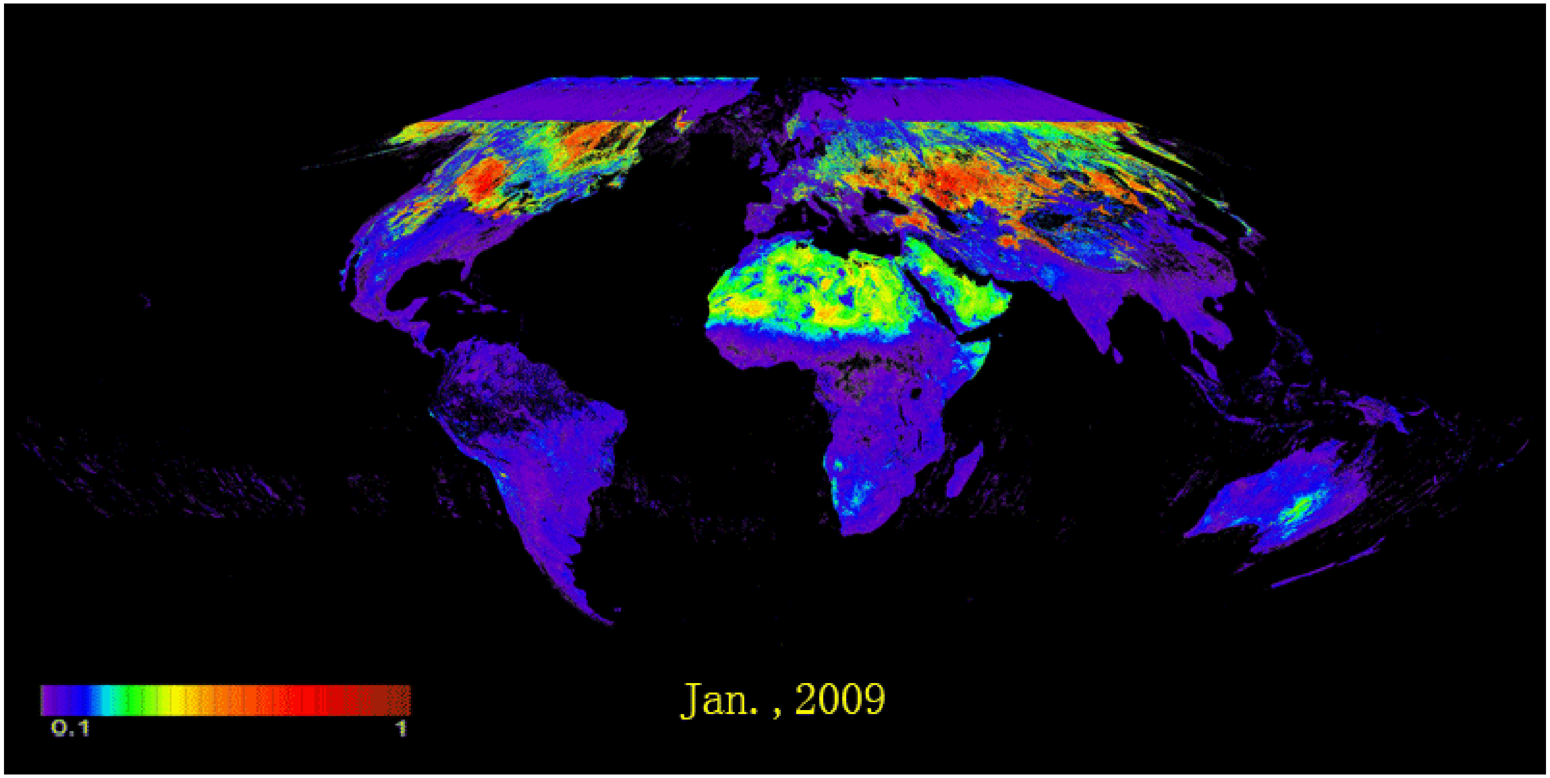

The GLASS project retrieves the daily 1km global albedo from MODIS surface reflectance products
(1984-2010, 5km from 1984-1999; 1km from 2000-2010)

Developing GOSE-R algorithm as a NOAA GOES-R Land Science Team member

Illustration of the proposed GOES-R ABI albedo algorithms

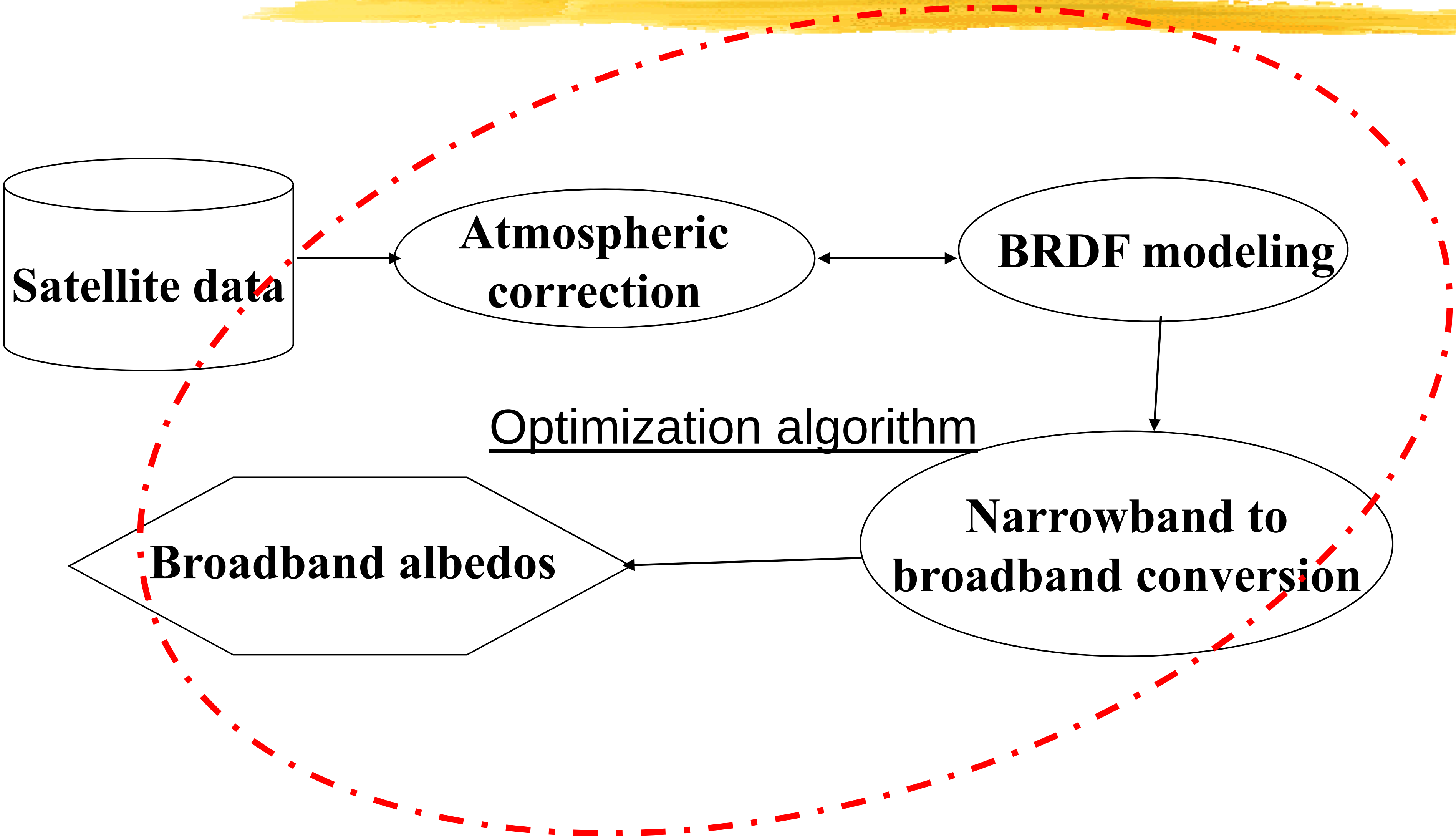

Satellite data

Atmospheric correction

BRDF modeling

Optimization algorithm

Narrowband to broadband conversion

Broadband albedos

Minimizing the cost function:

$$J(x) = \sum_{i=1}^{NO} \left(A_i^{Clm} - A_i^{Est}(x)\right)^2 + \sum_{i=1}^{NO} \sum_{j=1}^{NB} \left(R_{i,j}^{Obs} - R_{i,j}^{Est}(x)\right)^2$$

$$+ J_c = J_b + J_o + J_c$$

Where x are the coefficients of the surface BRDF model and aerosol optical depth (AOD), $A_i^{Est}(x)$ is the calculated surface albedo using the BRDF model, A_i^{Clm} are the background values of albedo from albedo climatology, $R_{i,j}^{Obs}$ and $R_{i,j}^{Est}$ refer to the observed and modeled top-of-atmosphere (TOA) reflectance. J_c is the cost function to account for various constrains (physical meanings of BRDF parameters and AODs, etc.)

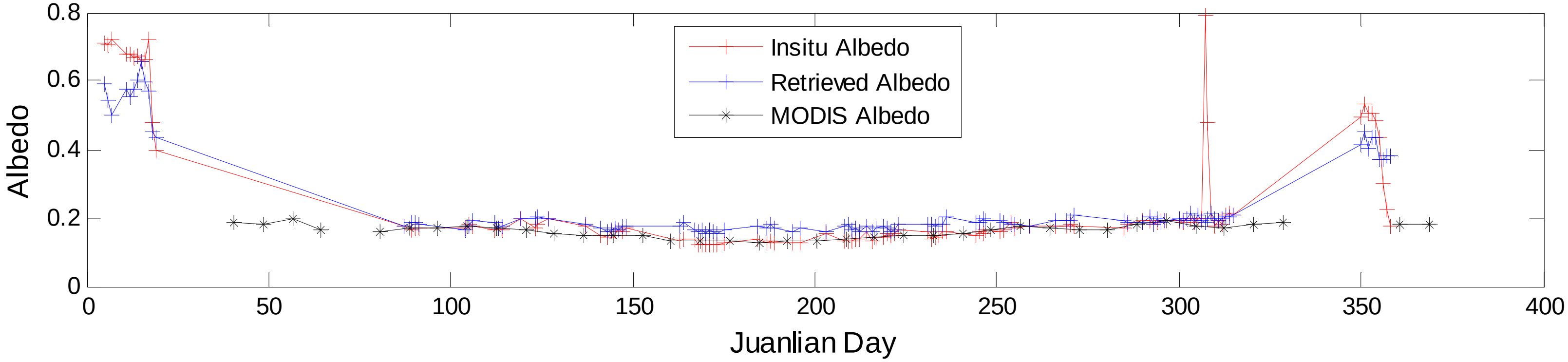
Fort Peck (48.31N,105.10W) Valid Obs=4

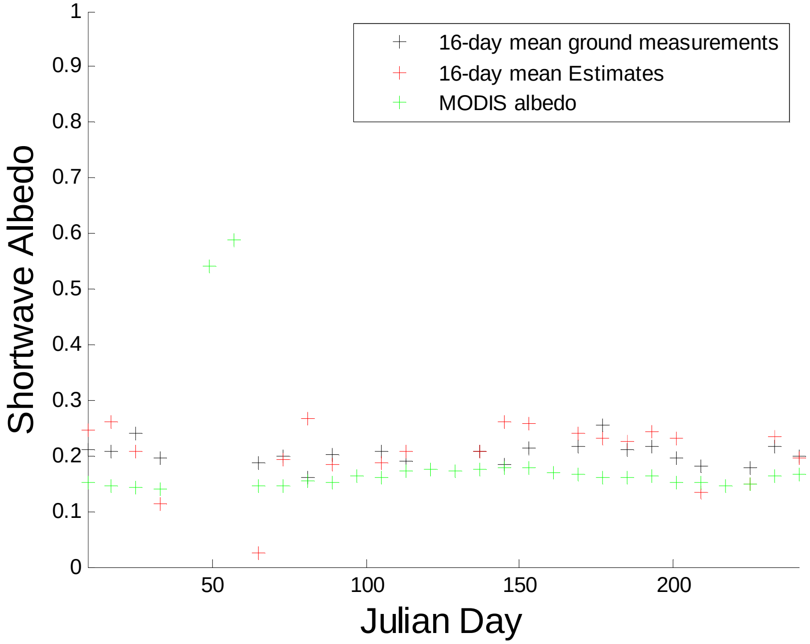
DE-Geb(Daily) Lat:51.1001 Lon:10.9143

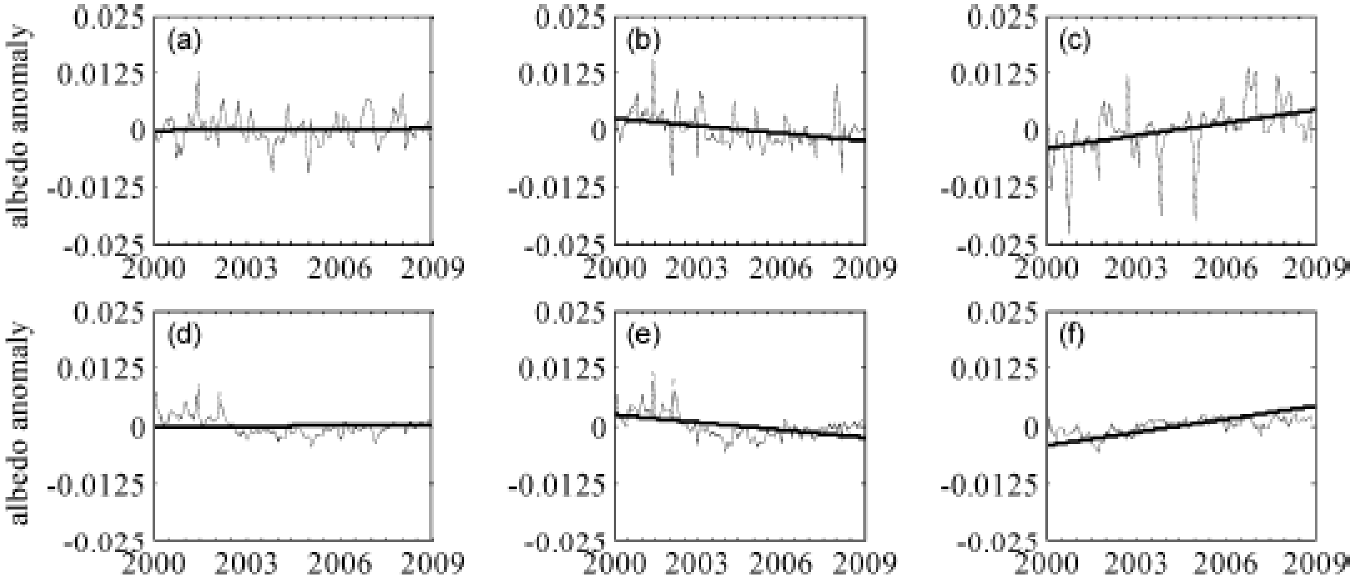

Fig. 2. Global, Northern Hemisphere, Southern Hemisphere land surface shortwave albedo anomalies under snow-covered and snow-free conditions. (a) Global albedo anomaly under snow-covered condition. (b) NH albedo anomaly under snow-covered condition. (c) SH albedo anomaly under snow-covered condition. (d) Global albedo anomaly under snow-free condition. (e) NH albedo anomaly under snow-free condition. (f) SH albedo anomaly under snow-free condition.

Zhang, X. **S. Liang**, K. Wang, L. Li, and S. Gui, (2010), A climatological analysis of global land surface shortwave broadband albedo from MODIS, *IEEE Journal of Special Topics in Applied Earth Observations and Remote Sensing*, 3:296-305

Outlines

- Background
- Insolation/PAR
- Albedo
- Longwave net radiation
- Evapotranpiration
- Summary

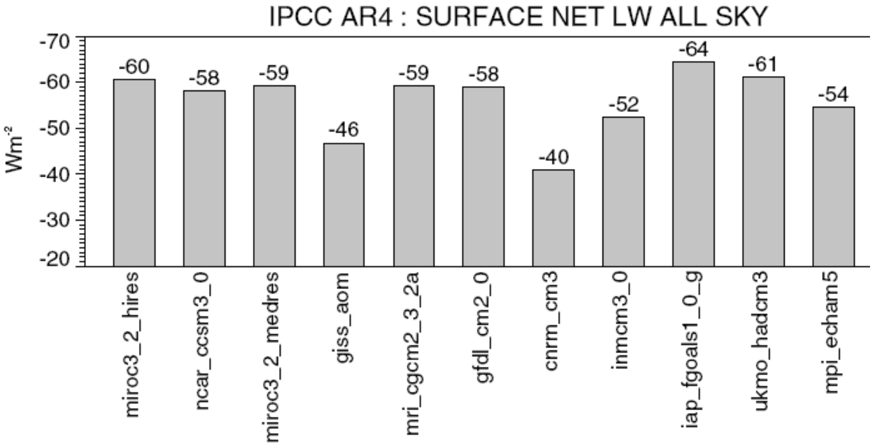

Radiation budgets by IPCC

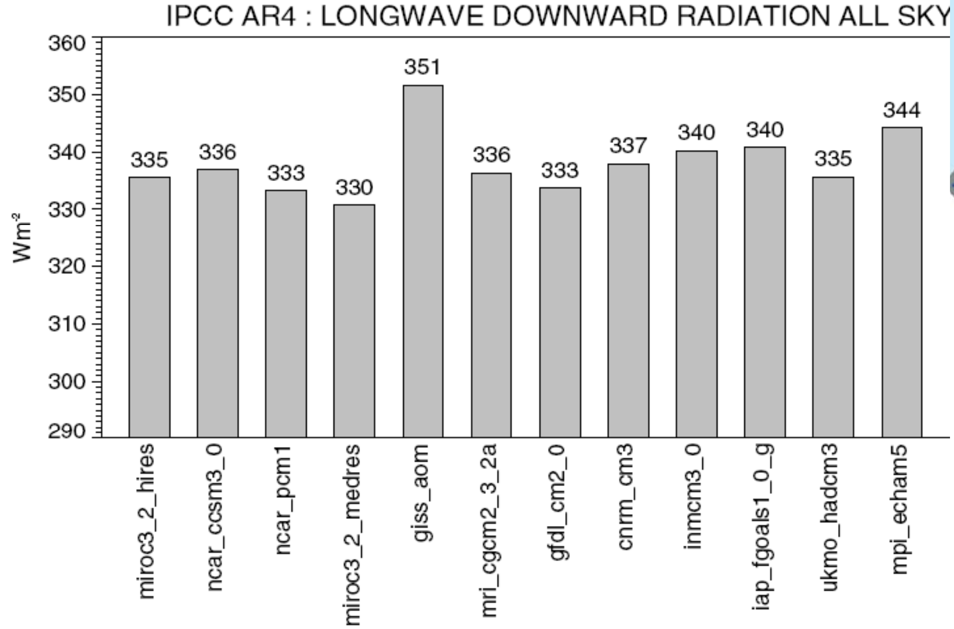

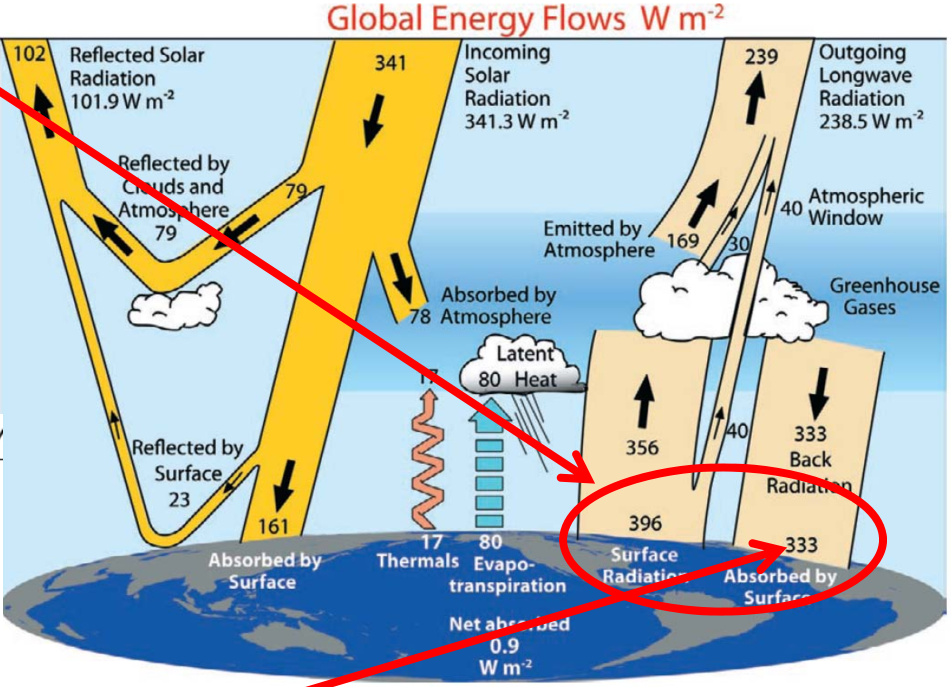

Fig.1 Monthly averages of longwave downward radiation from two satellite products (ISCCP and GEWEX) and different GCMs in the IPCC AR4.

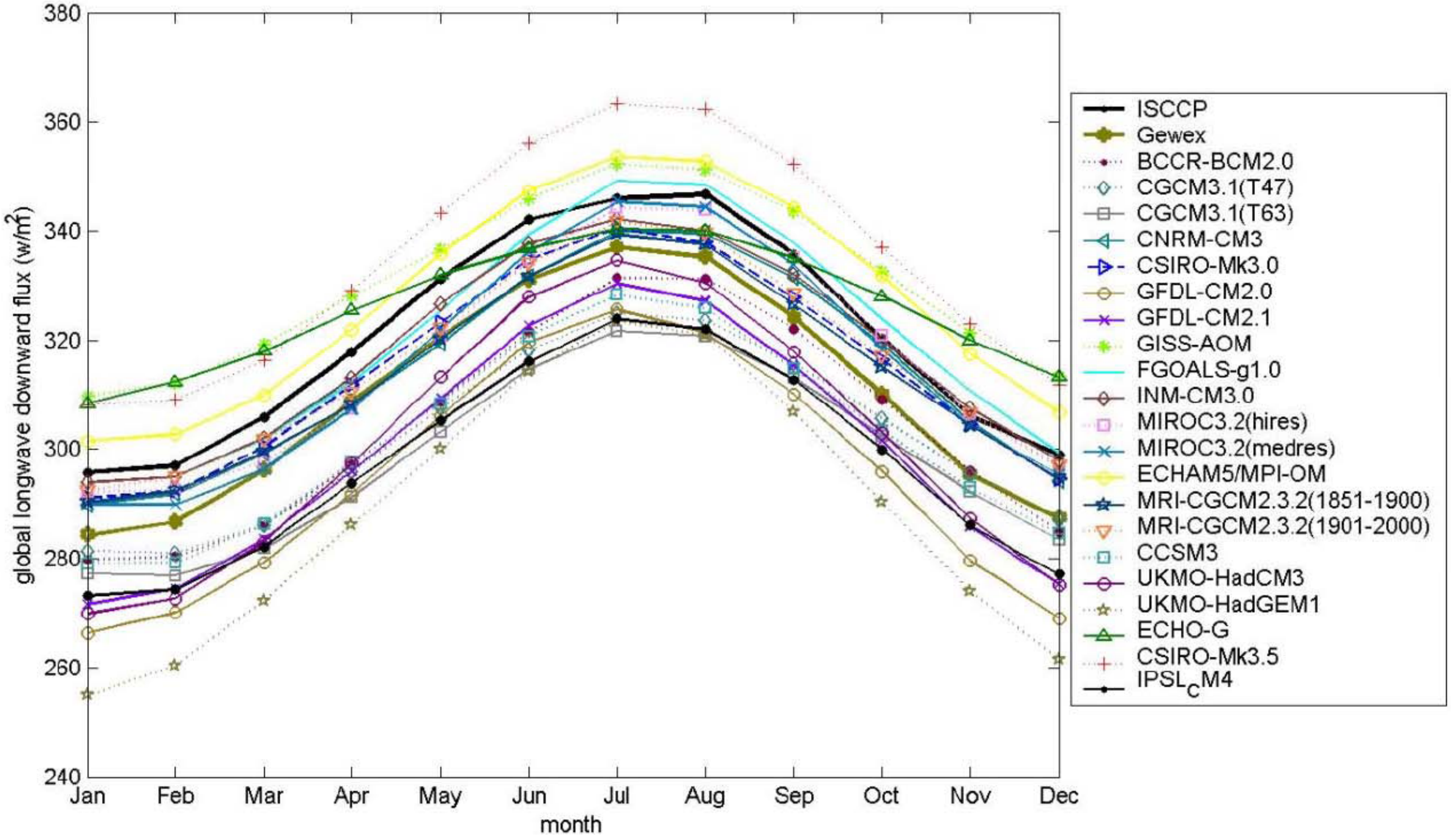

Estimation of downward longwave radiation

1). Empirical methods

2). Calculating downward flux using atmospheric profiles

3). Calculating downward flux from TOA radiance directly

Wang, K., and **S. Liang**, (2009), Global atmospheric downward longwave radiation under all-sky conditions from 1973 to 2008, *Journal of Geophysical Research*, 114, D19101, doi:19110.11029/12009JD011800
Wang, W. & **S. Liang,** (2009), Estimating High-Spatial Resolution Clear-Sky Land Surface Downwelling and Net Longwave Radiation from MODIS Data, *Remote Sensing of Environment*, 113:745-754
Wang, W., & **S. Liang**, (2010). A Method for Estimating Clear-sky Instantaneous Land Surface Longwave Radiation from GOES Sounder and GOES-R ABI Data. *IEEE Geoscience and Remote Sensing Letters*, 7, 708-712

Trend in Downward Longwave Radiation (W m^{-2} ya^{-1})

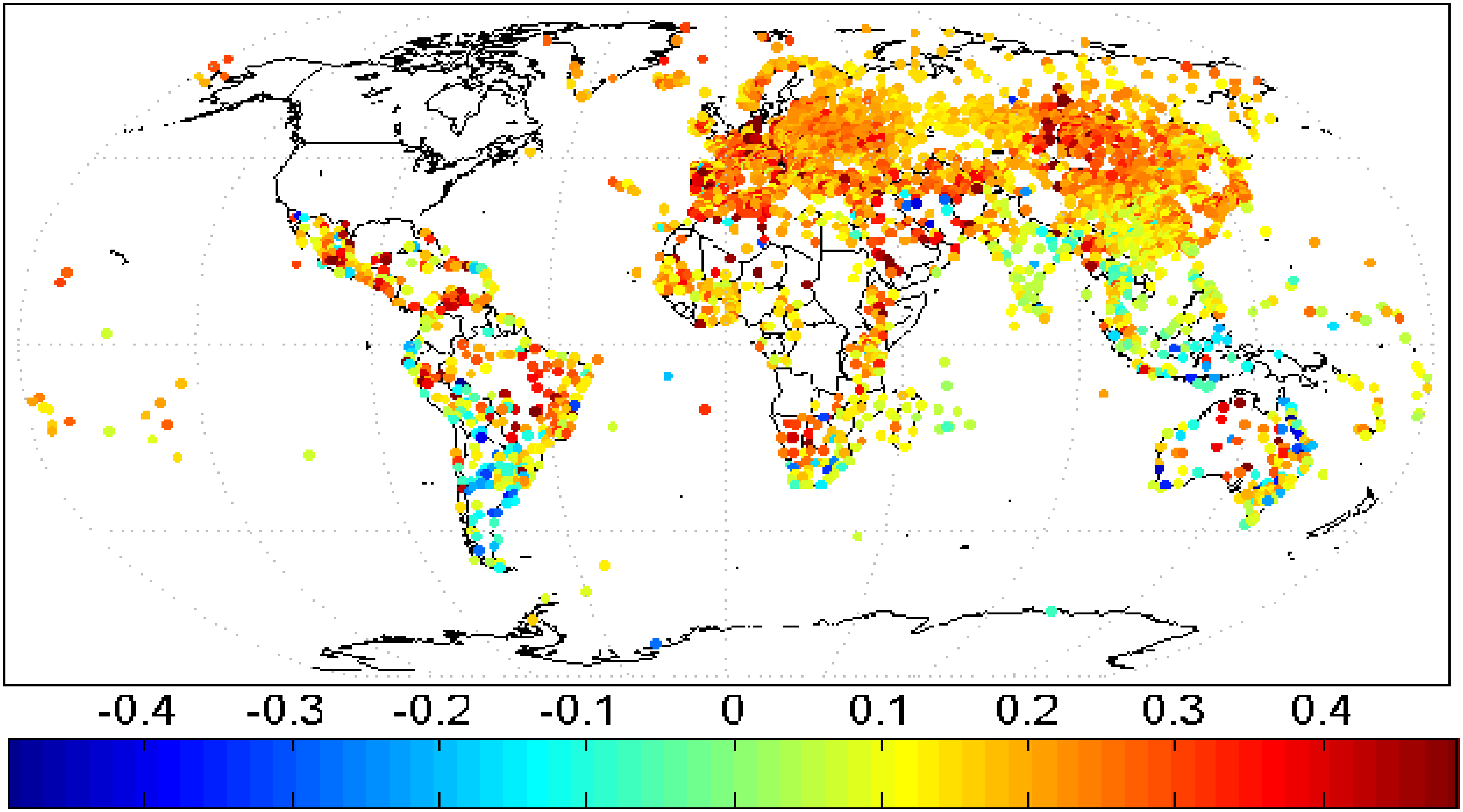

Linear trend of daily (L_d) over 3200 global weather stations where data are available for at least 300 months (25 years) during the period of 1973-2008.

Wang, K., and **S. Liang**, (2009), Global atmospheric downward longwave radiation under all-sky conditions from 1973 to 2008, *Journal of Geophysical Research*, 114, D19101, doi:10.1029/2009JD011800

- Using MODIS Profiles & MODTRAN4
- Problems:
  - LWDN dominated by near surface temp. & moisture
  - MODIS profiles are coarse (20 levels)
    - 1000, 950, 920, 850, 800, 700, 620, 500, 400, 300, 250, 200, 150, 100, 70, 50, 30, 20, 10, 5 hPa
  - Large errors, especially over high elevation sites

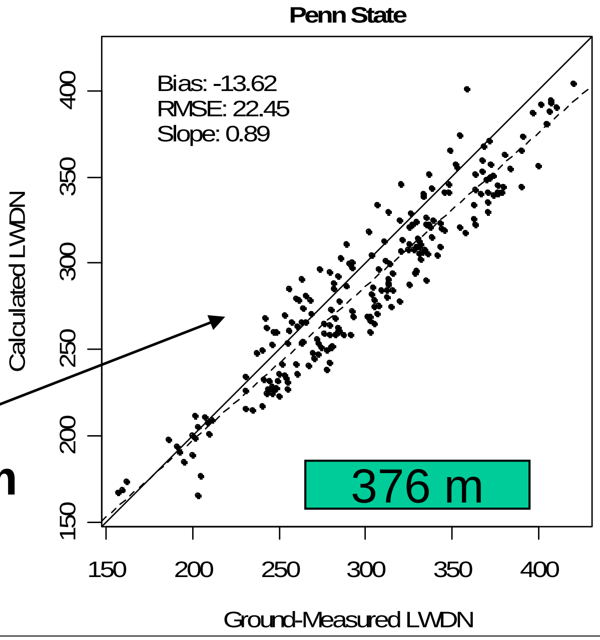

~4 layers below 500 m

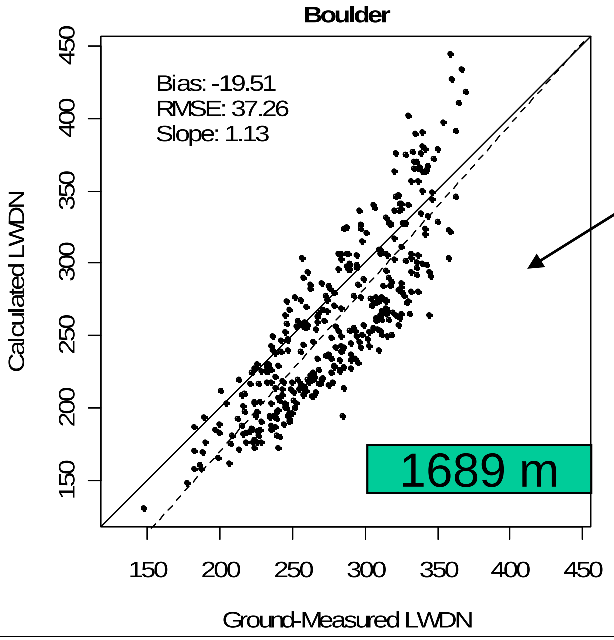

~3 layers below 500 m

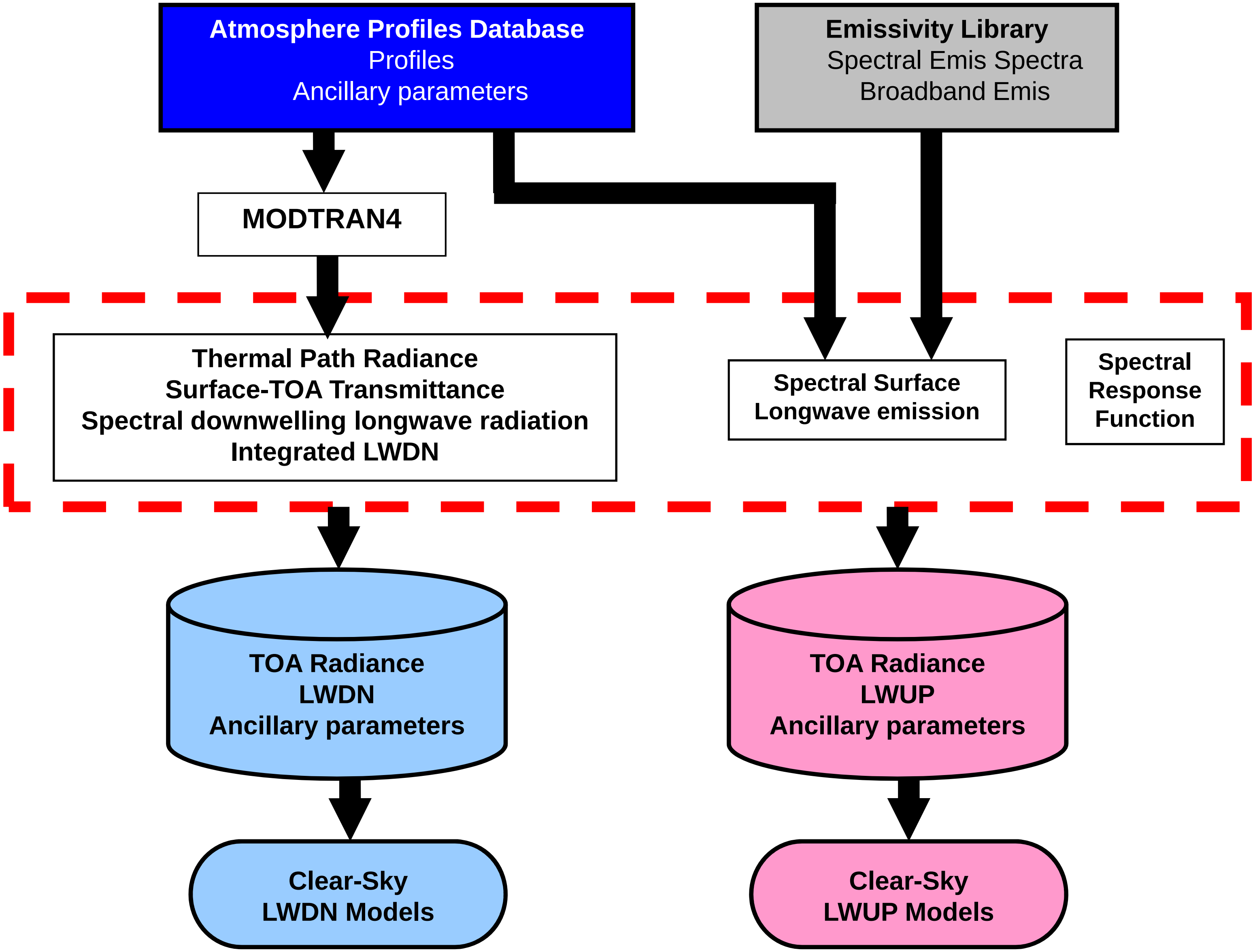

Atmosphere Profiles Database
Profiles
Ancillary parameters

Emissivity Library
Spectral Emis Spectra
Broadband Emis

MODTRAN4

Thermal Path Radiance
Surface-TOA Transmittance
Spectral downwelling longwave radiation
Integrated LWDN

Spectral Surface
Longwave emission

Spectral
Response
Function

TOA Radiance
LWDN
Ancillary parameters

TOA Radiance
LWUP
Ancillary parameters

Clear-Sky
LWDN Models

Clear-Sky
LWUP Models

Framework of Hybrid Methods

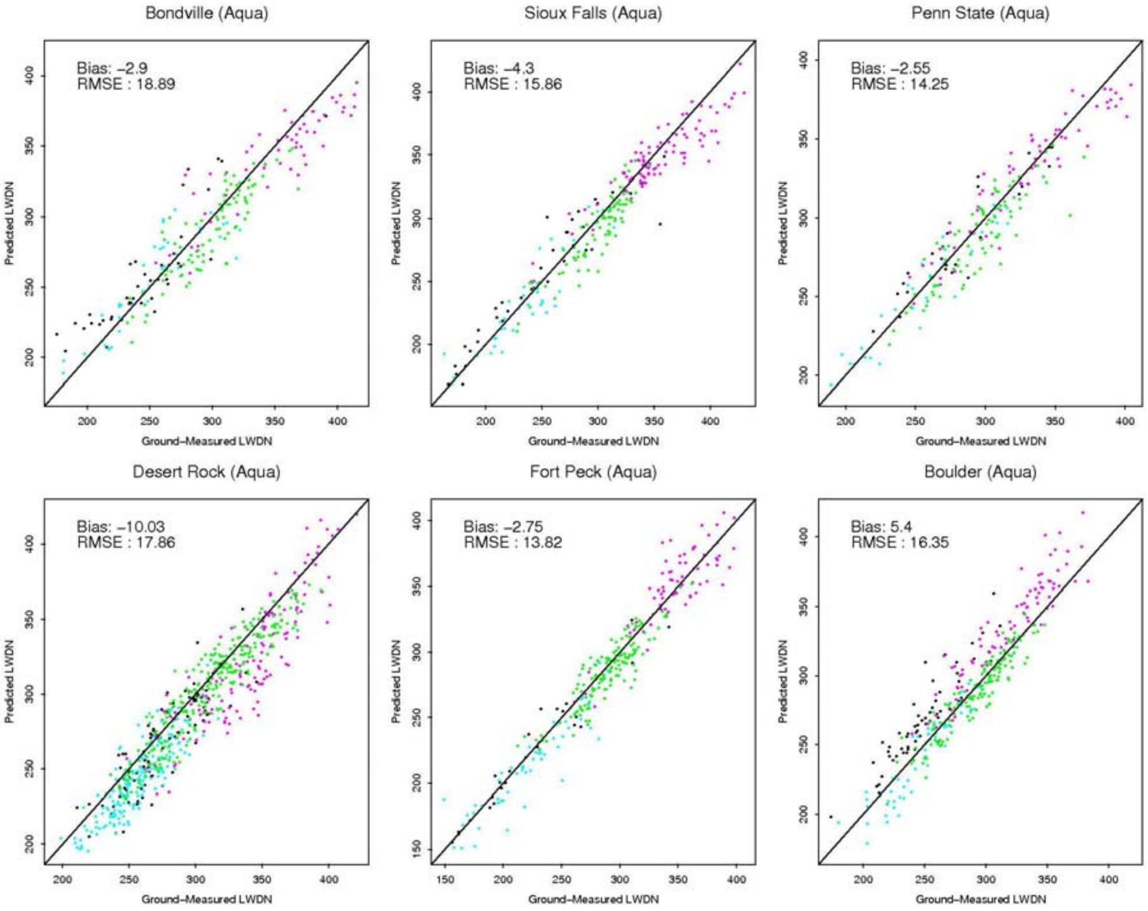

Nonlinear Models

- ♣ Results similar to Terra
- ♣ Smaller RMSEs in Aqua-derived LWDN
  - ✈ Smaller systematic errors in Aqua *(Liu et. Al, 2006)*
  - ✈ *Diff. overpass times → diff. atmospheric conditions*

Avg. RMSE: 17.60 W/m2
Avg. Bias: -0.40 W/m2

day/fallwinter
night/fallwinter
day/springsummer
night/springsummer

Estimating longwave upwelling radiation (LWUP)

(1)Temperature-Emissivity Method

$$F_u = \varepsilon \int_{\lambda_1}^{\lambda_2} \pi B(T_s) d\lambda + (1-\varepsilon) F_d$$

T_s MODIS LST (MOD11_L2)

ε Broadband emis (derived from MOD11B1)

(2) Hybrid Method

- Following the framework for hybrid methods
  - Emissivity Effect
    - UCSB Emissivity Library (59 spectra)
    - ~2000 MODIS Profile
- Statistical Analysis
  - Linear SULR Models (R^2: 0.990, RMSE< 5.42 W/m^2)

$$F_u = a_0 + a_1 L_{29} + a_2 L_{31} + a_3 L_{32}$$

  - Artificial Neural Network (ANN) Models (R^2: 0.996 RMSEs<3.7 W/m^2)

5 Models in total

θ	Model
0°	
15°	
30°	
45°	
60°	

Representative thermal space-borne RS systems

sensors	**Wavebands (μm)**	# of bands	**Spatial resolution**
AVHRR	3.55 – 3.93 10.30 –12.50	1 2	1.1km
MODIS	3.66 – 4.08 8.400 – 13.48	3 4	1km
ATSR/ATSR–2/AASTR	3.55 –3.93 10.4 – 12.5	1 2	1km
ASTER	8.125 – 11.65	5	90m
TM/ETM+	10.00 –12.90	1	120m/60m
MSG–SEVIRI	8.30–13.0	3	3km at nadir
FY–3	3.7 – 4 9.59 – 13.49	2 4	1.1km
GOES	10.2 – 12.5	2	4km at nadir
GMS(Geostationary Meteorological Satellite)	3.5 – 4.0 10.3 – 12.5	1 1	4km at nadir
HJ–1B	3.50 – 3.90 10.5 – 12.5	1 1	150m 300m
METOP–IASI	3.2–15.5 (645–2760 cm^{-1})	8461	12km

Estimating LWUP: validation

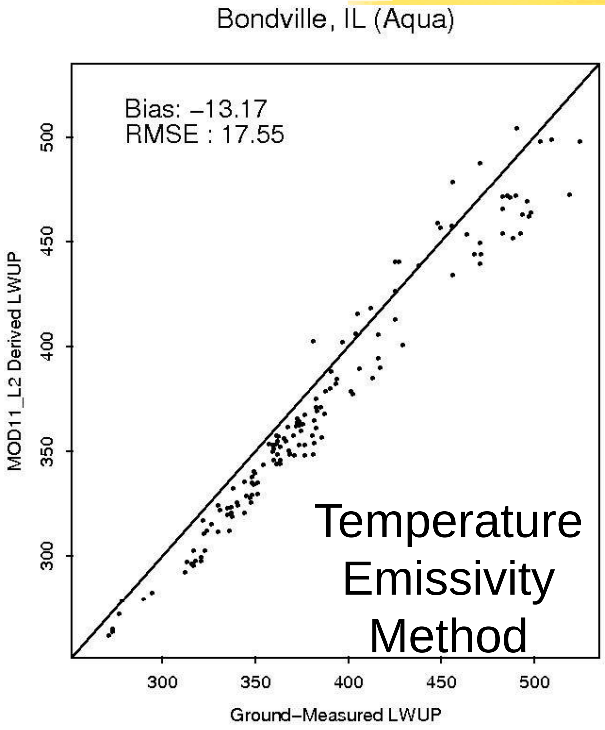

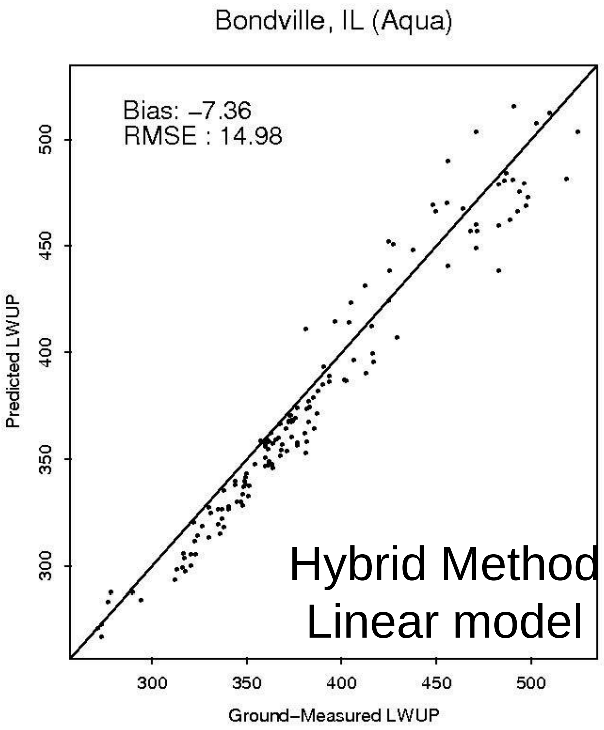

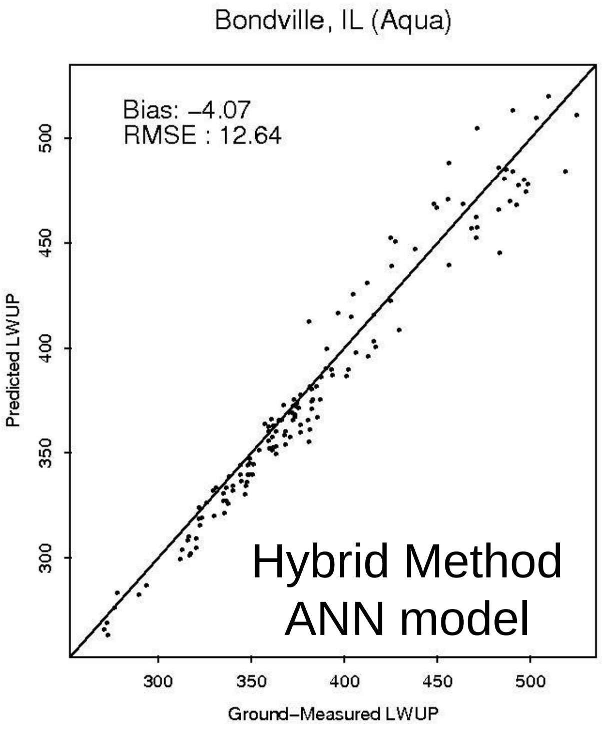

Bondville, IL (cropland, elevation 213 m)

- Smaller RMSEs in Aqua
- Hybrid method outperforms temperature-emissivity method
- ANN model outperforms linear model

Wang, W., **S. Liang** & J. A. Augustine, (2009), Estimating Clear-Sky Land Surface Upwelling Longwave Radiation from MODIS Data. *IEEE Trans. Geosci. and Remote Sens.* 47(5):1555-1575

MODIS LST validation

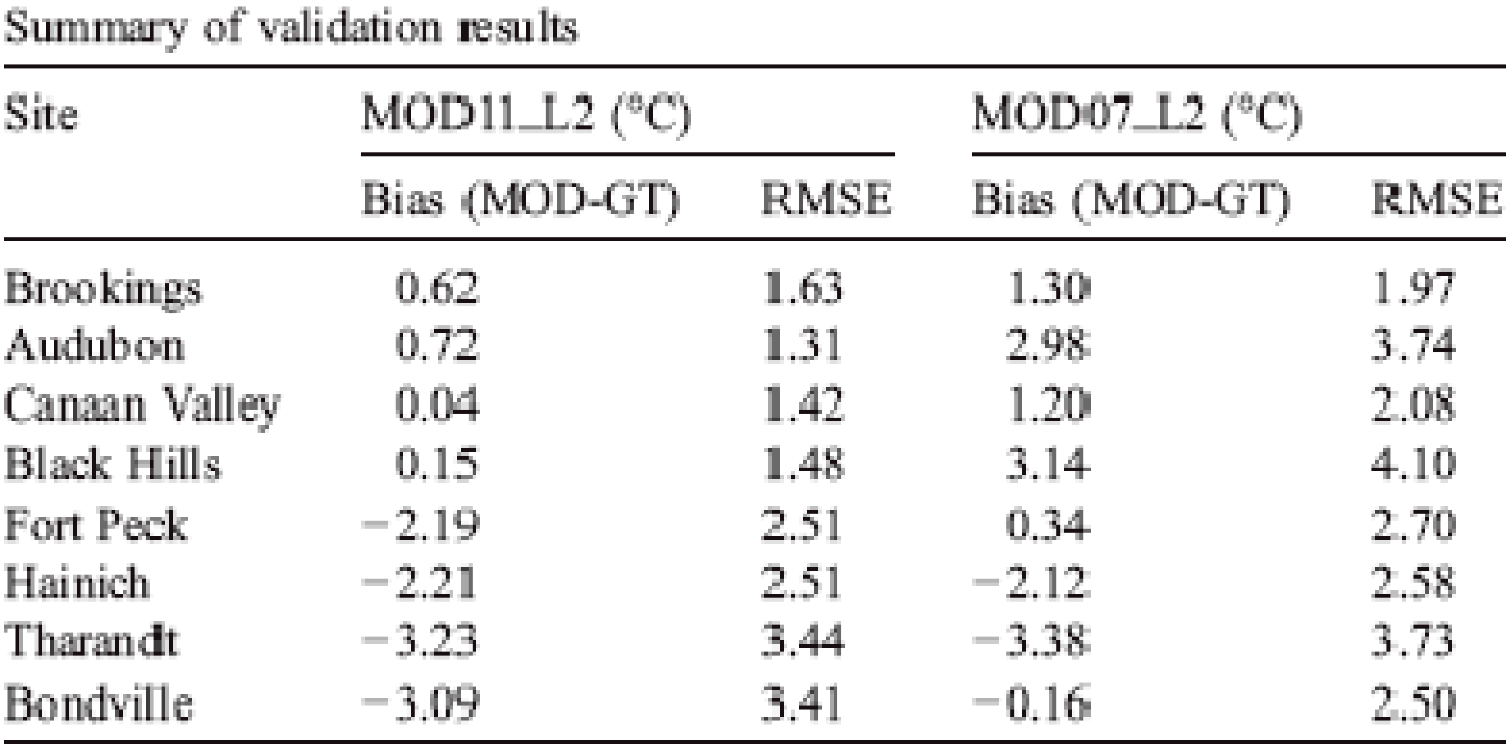

Summary of validation results

Site	MOD11_L2 (°C)		MOD07_L2 (°C)	
	Bias (MOD-GT)	RMSE	Bias (MOD-GT)	RMSE
Brookings	0.62	1.63	1.30	1.97
Audubon	0.72	1.31	2.98	3.74
Canaan Valley	0.04	1.42	1.20	2.08
Black Hills	0.15	1.48	3.14	4.10
Fort Peck	−2.19	2.51	0.34	2.70
Hainich	−2.21	2.51	−2.12	2.58
Tharandt	−3.23	3.44	−3.38	3.73
Bondville	−3.09	3.41	−0.16	2.50

Wang, W., **S. Liang**, and T. Meyer, (2008), Validating MODIS land surface temperature products, *Remote Sensing of Environment*,112:623-635

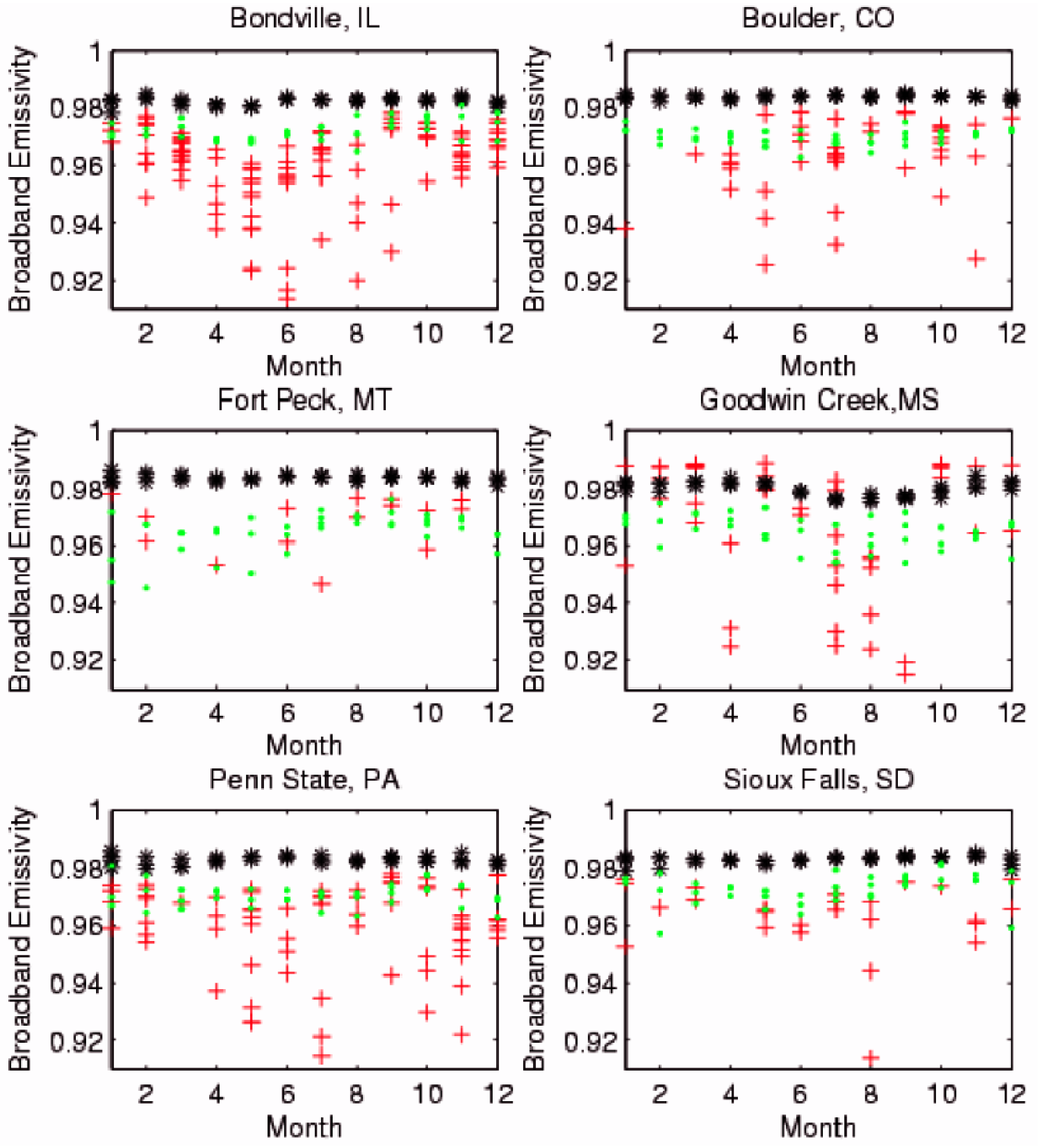

Broadband emissivity calculated from MODIS Collection 4 (green dot) and Collection 5 (black star) monthly emissivity products and ASTER daily emissivity products (red plus sign) at a resolution of 0.05° at six SURFRAD sites.

Wang, K., and **S. Liang**, (2009), Evaluation of ASTER and MODIS land surface temperature and emissivity products using surface longwave radiation observations at SURFRAD sites, *Remote Sensing of Environment*, 113:745-754

The emissivity impact on ground temperature in the coupled CAM2/CLM2 model, control run minus sensitivity run. Unit is K.

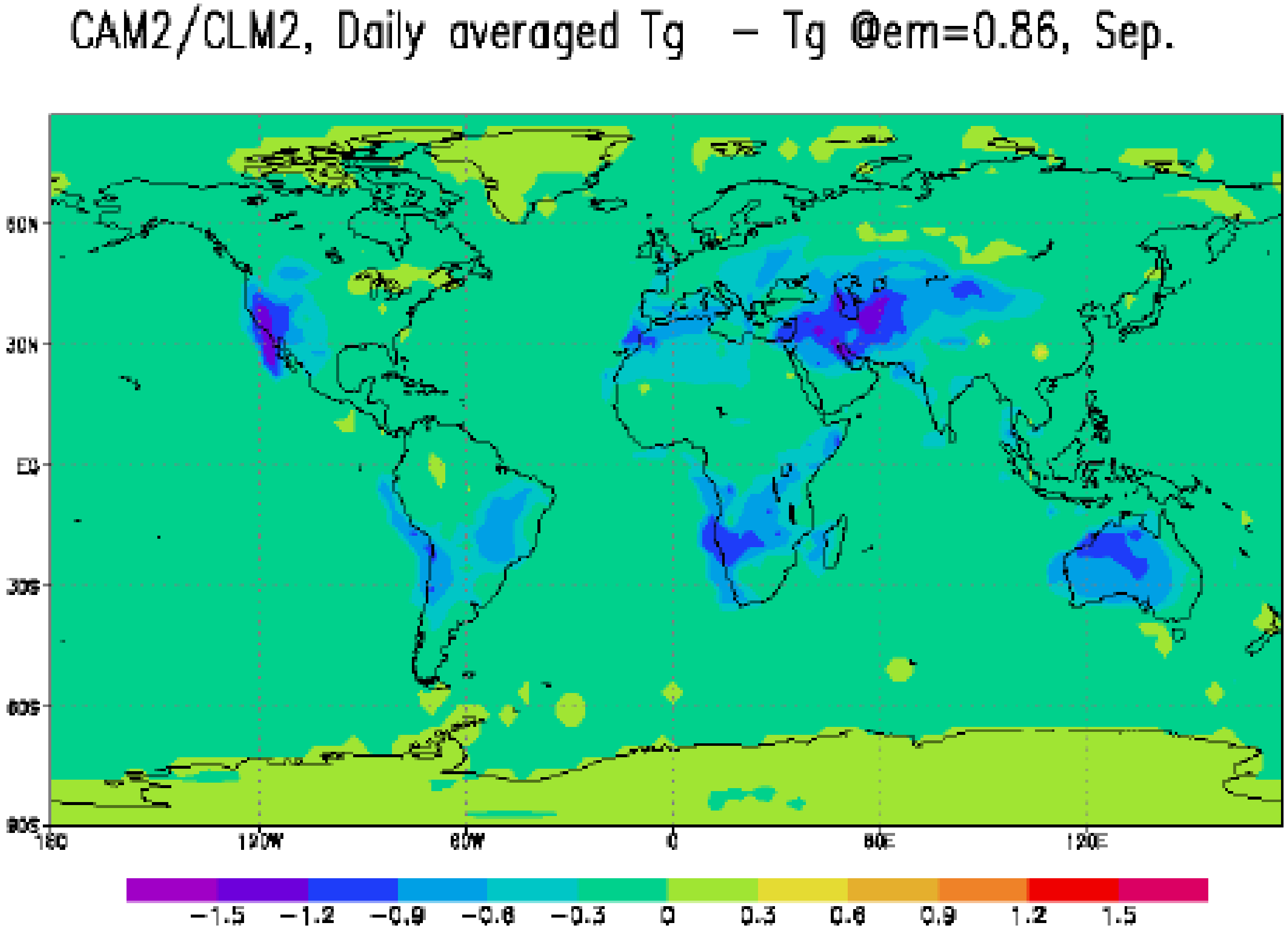

Jin, M., and S. Liang, (2006), Impacts of the MODIS broadband emissivity on GCM simulation, *J. Climate*, 19:2867-2881.

Chinese GLASS Broadband Emissivity Product

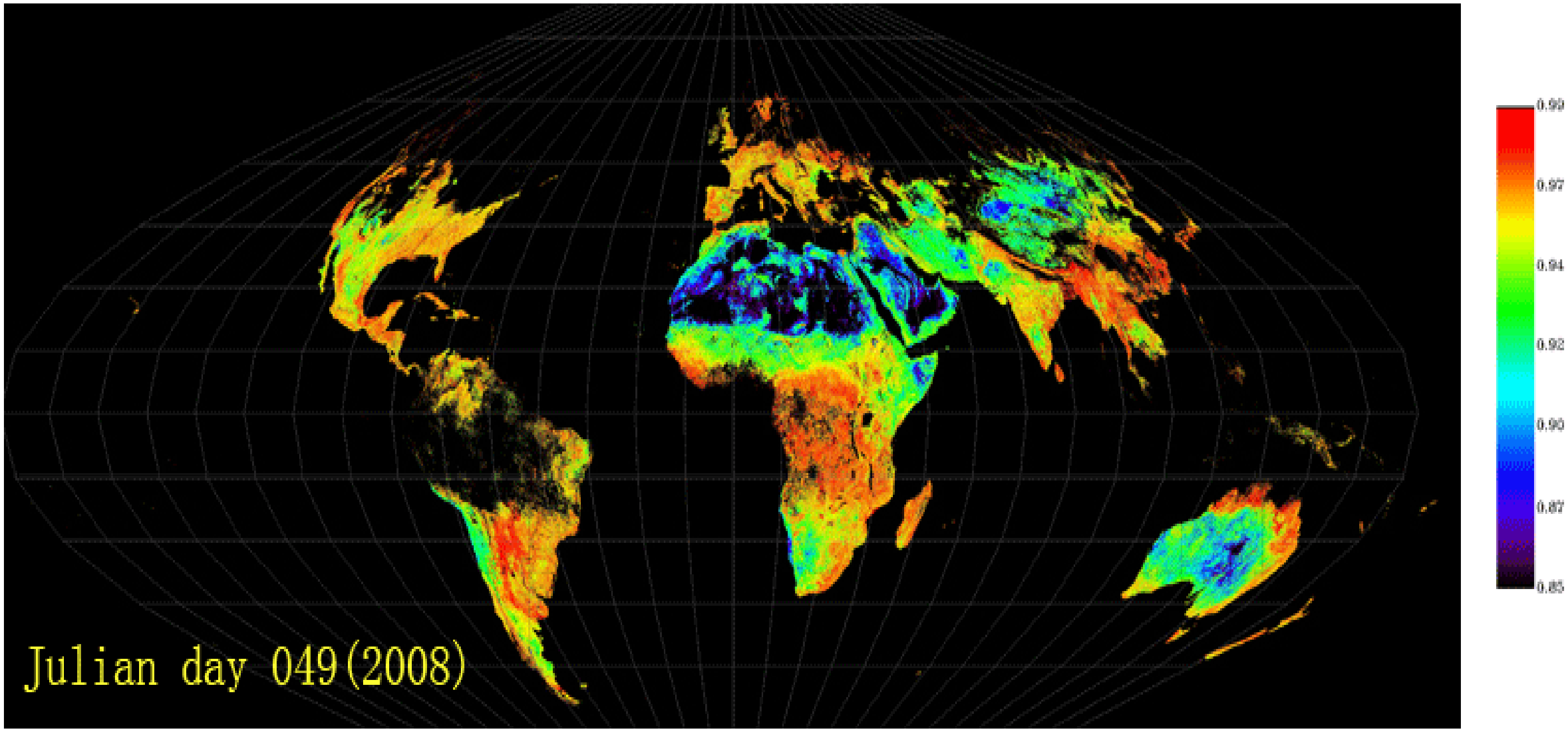

Global eight-day 1-Km land surface broadband emissivity retrieved by our new algorithm using MODIS albedos.

(5km from 1984-1999, 1km 2000-2010, 8day)

Outlines

- Background
- Insolation/PAR
- Albedo
- Longwave net radiation
- Evapotranpiration
- Summary

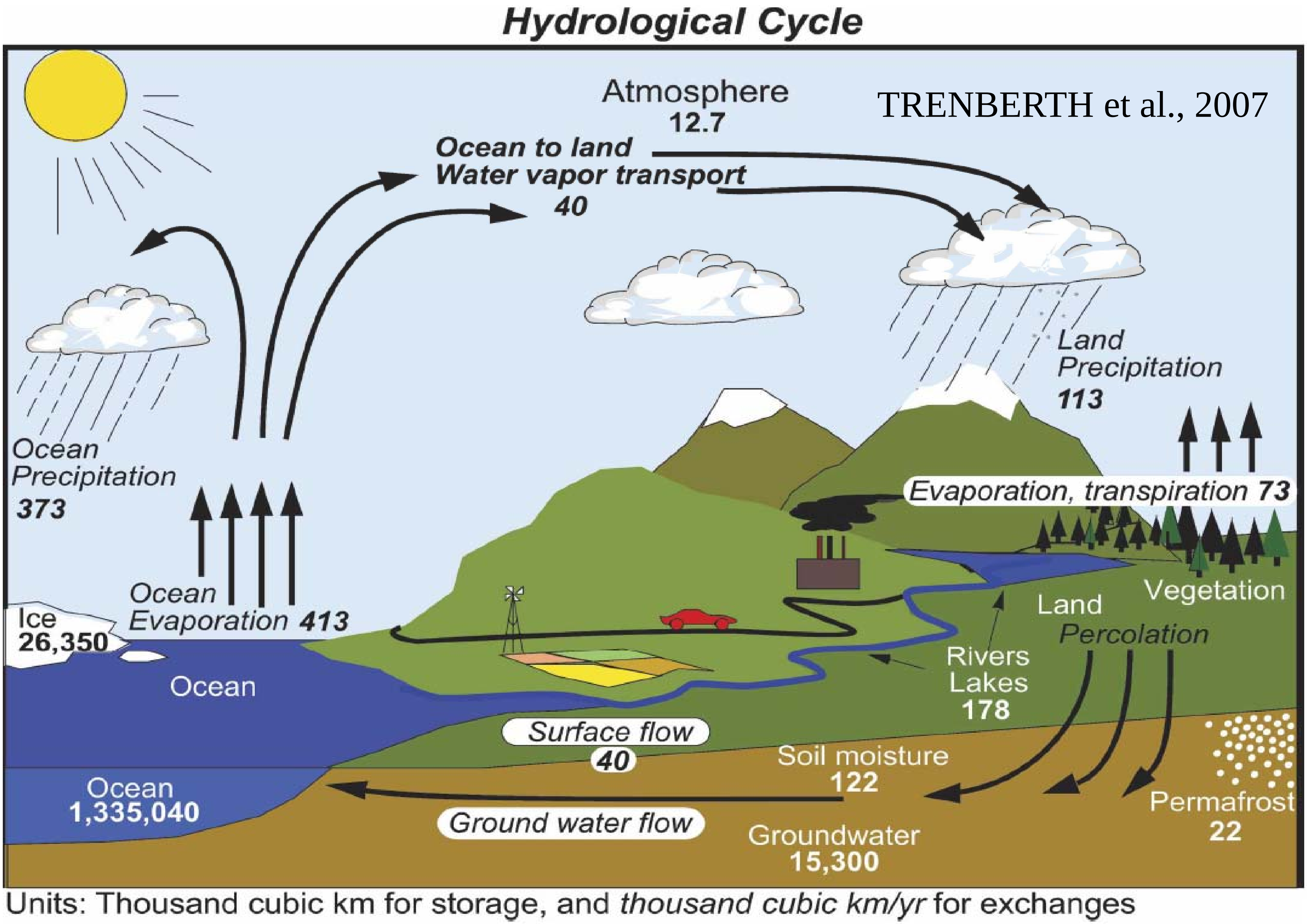

TRENBERTH et al., 2007

FIG. 1. The hydrological cycle. Estimates of the main water reservoirs, given in plain font in 10^3 km^3, and the flow of moisture through the system, given in slant font (10^3 km^3 yr^{-1}), equivalent to Eg (10^{18} g) yr^{-1}.

- Qin, J., **S. Liang**, R. Liu, H. Zhang, and B. Hu, (2007), A Weak-Constraint Based Data Assimilation Scheme for Estimating Surface Turbulent Fluxes, *IEEE Geoscience and Remote Sensing Letters*, 4(4):649-653
- Wang, K. and **Liang, S**. (2008), An improved method to estimate evapotranspiration from a combination of net radiation, vegetation index and temperature: Influence of soil moisture. *Journal of Hydrometeorology 9, 712-727*
- Yiao, Y. **S. Liang**, Q. Qin, and K. Wang, (2010), Monitoring Drought over the Conterminous United States from MODIS and NCEP Reanalysis-2 Data, *Journal of Applied Meteorology and Climatology*, 49(8), 1665-1680
- Yiao, Y. **S. Liang**, Q. Qin, and K. Wang, S. Zhao, (2010), Monitoring Global Land Surface Drought Based on an Improved Evapotranspiration Model, *International Journal of Applied Earth Observation and Geoinformation*, 12(6): S266-S776
- Galleguillos, M., F. Jacob, L. Prévot, P. Lagacherie, **S. Liang**, (2010),Spatializing and validating daily evapotranspiration over a Mediterranean vineyard watershed, *IEEE Geoscience and Remote Sensing Letters*, in press
- Wang, K., B. Dickinson, M. Wild, **S. Liang**, (2010),Evidence for Decadal Variation in Global Terrestrial Evapotranspiration between 1982 and 2002, Part 1: Model Development", *Journal of Geophysical Research - Atmospheres* , 115
- Wang, K., B. Dickinson, M. Wild, **S. Liang**, (2010),Evidence for Decadal Variation in Global Terrestrial Evapotranspiration between 1982 and 2002, Part 2: Results", *Journal of Geophysical Research – Atmospheres* , 115
- Xu, T., S. Liu, **S. Liang**, & J. Qin, (2010), Improving Predictions of Water and Heat Fluxes by Assimilating MODIS Land Surface Temperature Products into Common Land Model, *Journal of Hydrometeorology* , in press

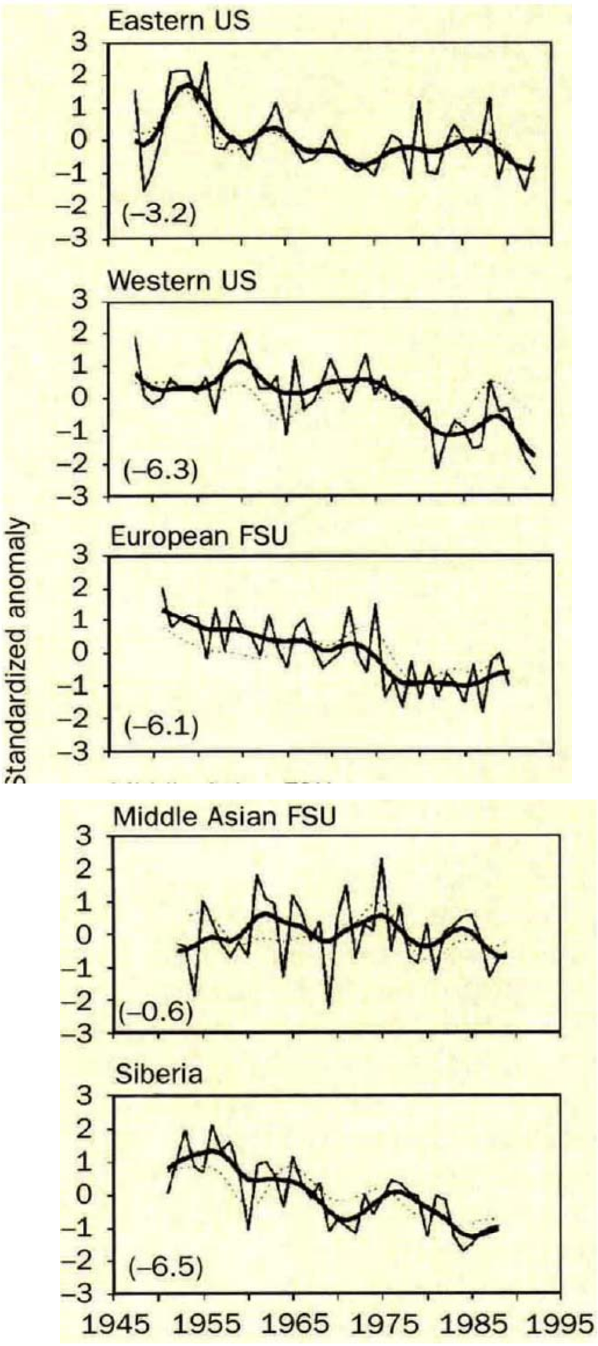

Peterson, T.C., Golubev, V.S. and Groisman, P.Y.
1995: EVAPORATION LOSING ITS STRENGTH.
Nature 377, 687-688.

Farquhar 2002 *Science;*
Ohmura and Wild 2002 *Science*

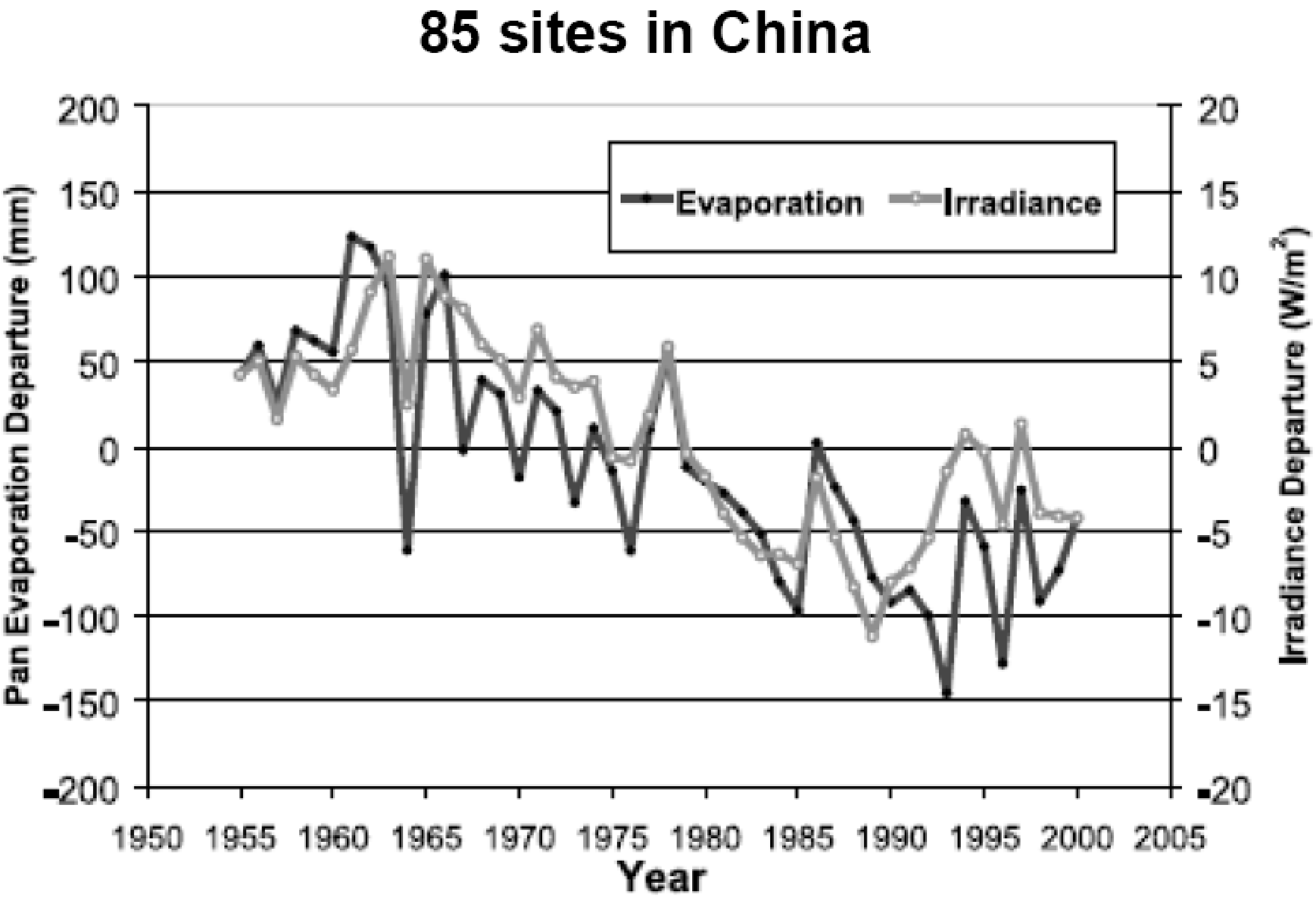

Qian et al. 2006 GRL

Impact on pan evaporation

$$ET_E = \frac{\Delta}{\Delta + \gamma} \cdot R_s \cdot [a_1 + a_2 \cdot VI + RHD \cdot (a_3 + a_4 \cdot VI)], \qquad (8)$$

$$ET_A = \frac{\gamma}{\Delta + \gamma} \cdot WS \cdot VPD \cdot [a_5 + RHD \cdot (a_6 + a_7 VI)], \qquad (9)$$

$$ET = a_8 \cdot (ET_E + ET_A) + a_9 \cdot (ET_E + ET_A)^2, \qquad (10)$$

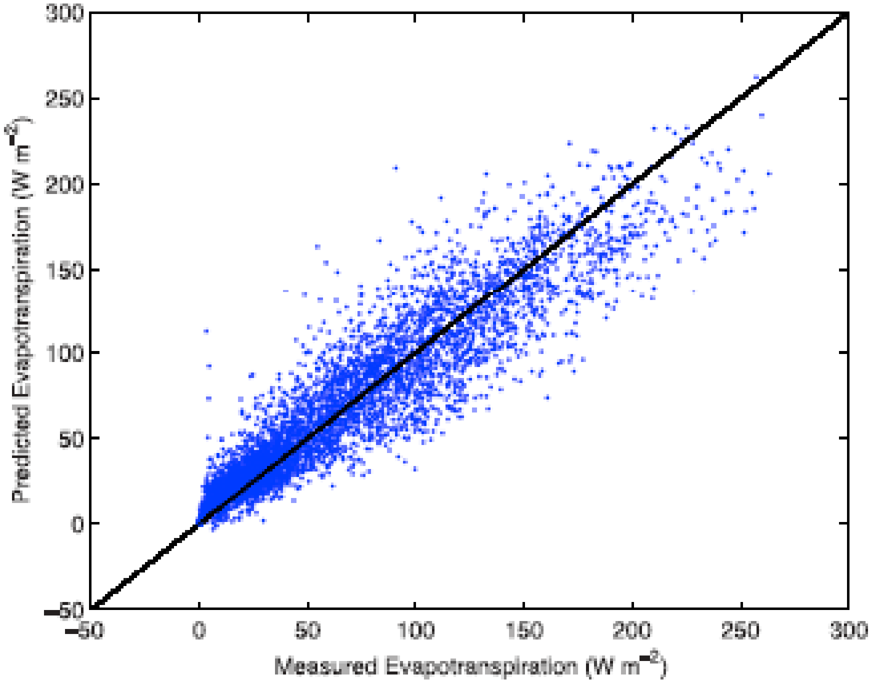

Figure 3. Comparison of the 16 day average predicted and ground-measured ET collected at all 64 sites shown in Table 1 when EVI is used. We used a 16 day average because the MODIS EVI data are available for a 16 day interval.

Wang, K., R. E. Dickinson, M. Wild, S. Liang (2010). "Evidence for decadal variation in global terrestrial evapotranspiration between 1982 and 2002: 1. Model development." Journal of Geophysical Research-Atmospheres **115.**

Wang, K., R. E. Dickinson, M. Wild, S. Liang (2010). "Evidence for decadal variation in global terrestrial evapotranspiration between 1982 and 2002: 2. results" Journal of Geophysical Research-Atmospheres **115.**

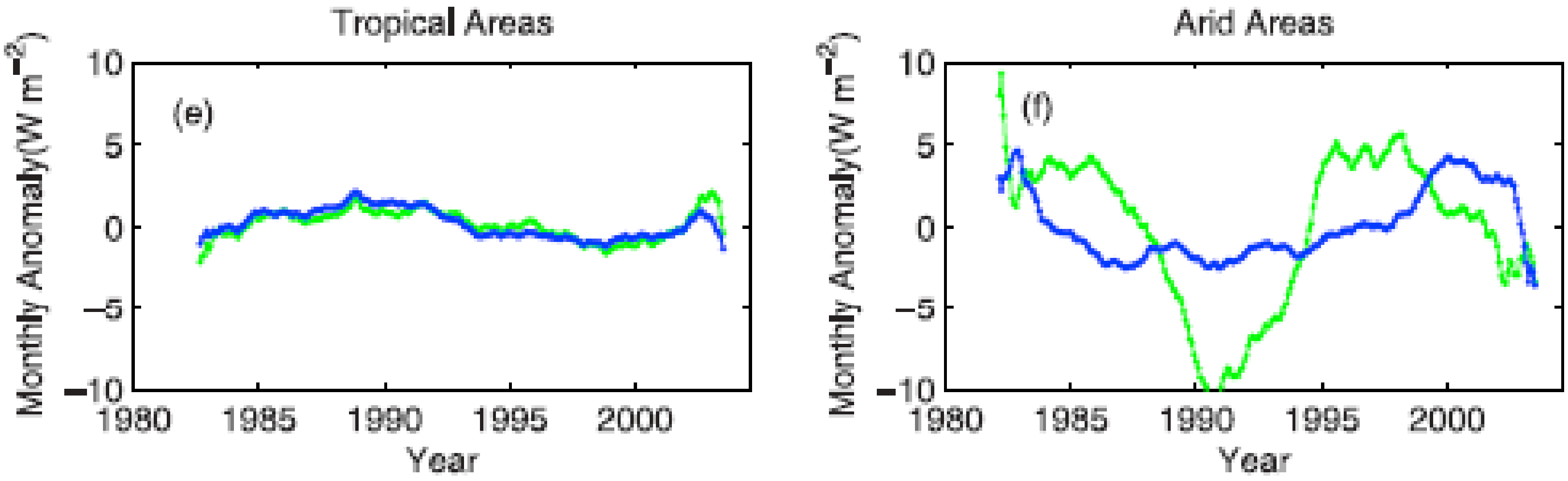

Figure 3. The times series of 5 year smoothed ET (blue line) and R_s (green line) anomalies for (a) Europe, (b) Asia, (c) North America, (d) the Southern Hemisphere, (e) tropical areas, and (f) arid areas. Tropical areas refer to regions where latitude is between 20°S–20°N, and arid areas refer to regions where multiyear average relative humidity is less than 50%. ET and R_s demonstrate significant decadal variation in all the regions.

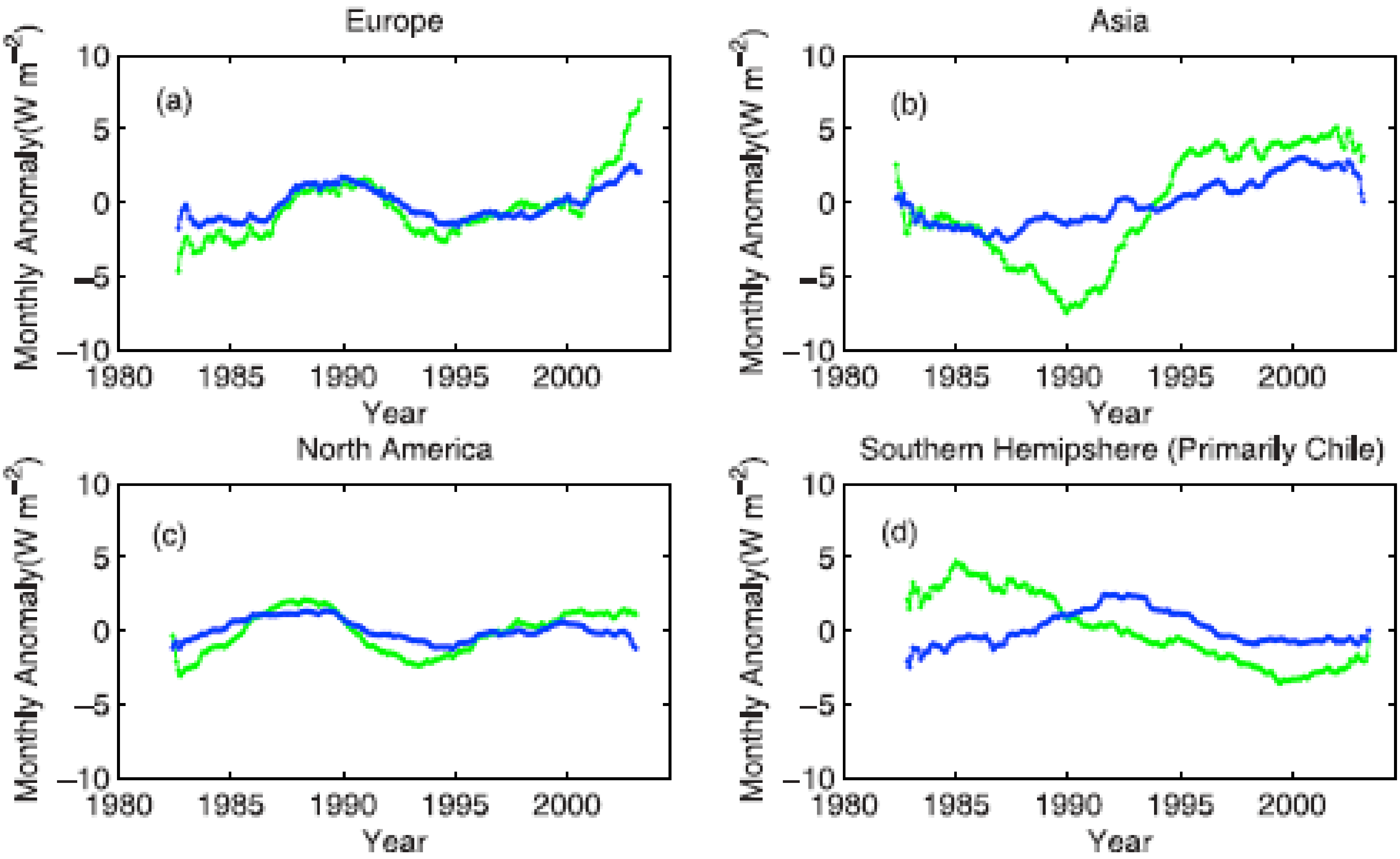

Global ET over land increased by 0.6 W m (2) per decade equal to 1.2W m (2) (about 2.2% in relative value) or 15 mm yr (1) in water flux from 1982-2002

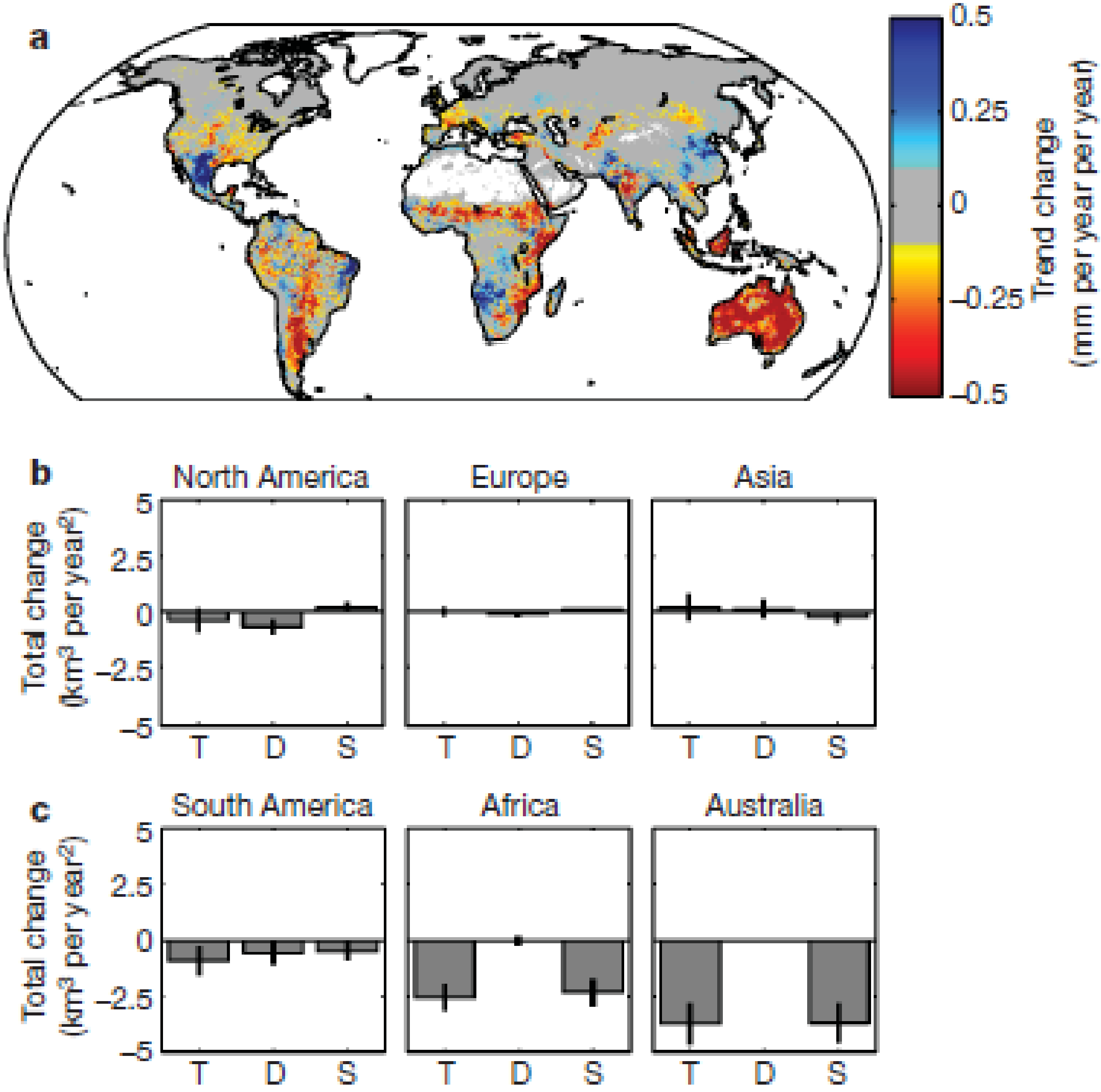

Figure 3 | ET trend changes. a, Map of the change in ET trend between 1982–1997 and 1998–2008 in millimetres per year per year. Small trend changes of ±0.1 mm per year per year are shown in grey to enhance clarity. Total

Jung, et al.,
Nature, 2010

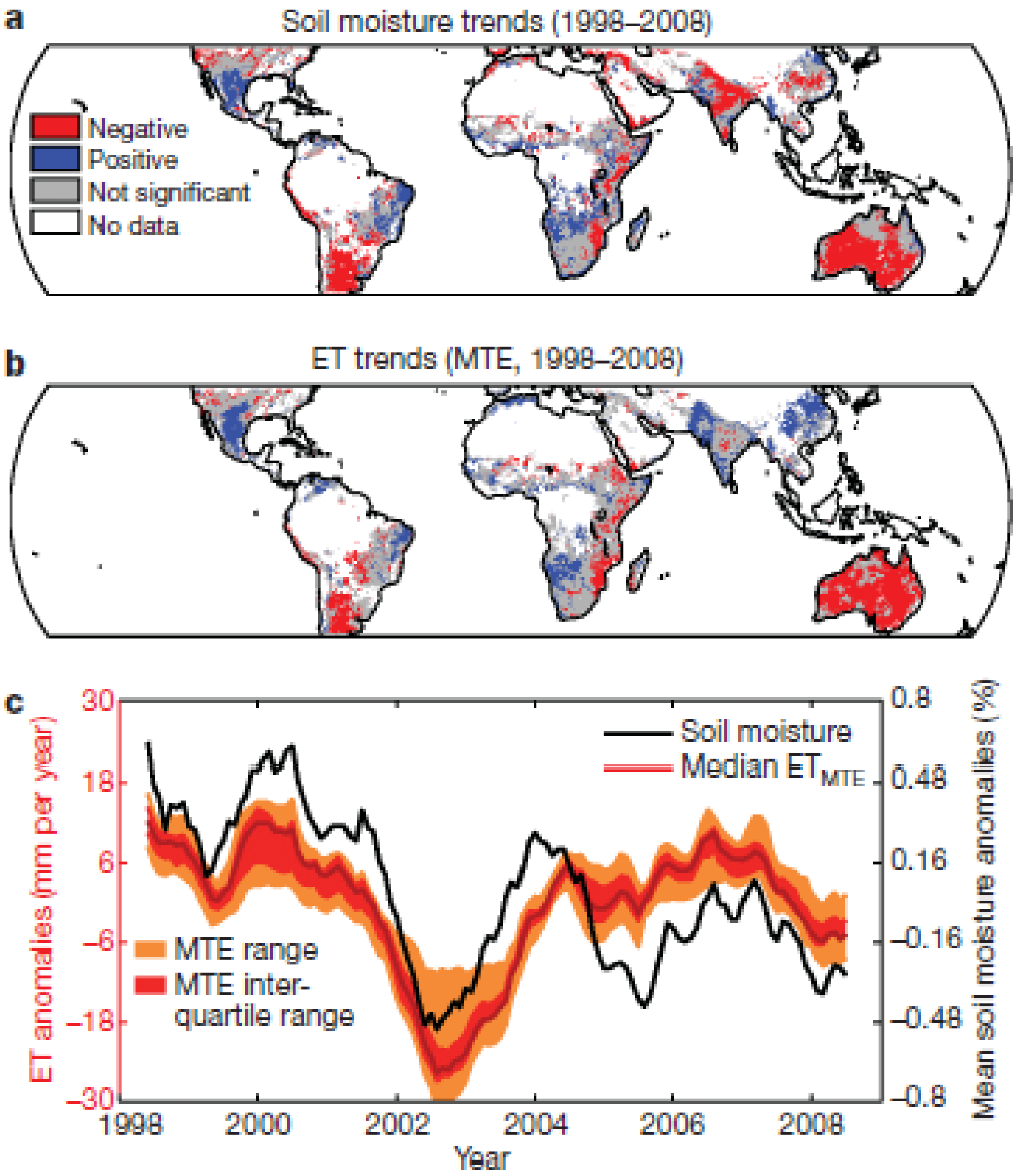

Figure 4 | Soil-moisture and ET trends. Significant ($P < 0.1$) soil-moisture trends derived from TRMM (**a**), significant ($P < 0.1$) ET trends from MTE (**b**) and mean ET and soil-moisture anomalies (seasonal cycle subtracted and filtered with an 11-month running mean) of all valid pixels of the TRMM

Summary

- Climate change and human activities have greatly impacted land surface radiation and energy budgets
- Many feedbacks and impacts have not been fully understood
- Satellite remote sensing can accurately map high-resolution land surface radiation and energy budgets and thus be greatly valuable for various applications

Thank you !